博士論文

HUMAN-FRIENDLINESS OF ROBOTS IN HUMAN ENVIRONMENTS:

MOBILITY, MANIPULATION, AND REHABILITATION PERSPECTIVES

（人間環境で働くロボットの人間親和性に関する研究：

モビリティ、マニピュレーション、リハビリテーションの観点から）

YUNHA KIM

金　潤河

HUMAN-FRIENDLINESS OF ROBOTS IN HUMAN ENVIRONMENTS: MOBILITY, MANIPULATION, AND REHABILITATION PERSPECTIVES

by

Yunha Kim

A dissertation submitted in partial satisfaction of the
requirements for the degree of
Doctor of Philosophy

in

Electrical Engineering and Information Systems

in the

Graduate School of Engineering

of

The University of Tokyo

Supervisor:

Professor Yoichi Hori

Summer 2014

HUMAN-FRIENDLINESS OF ROBOTS IN HUMAN ENVIRONMENTS: MOBILITY, MANIPULATION, AND REHABILITATION PERSPECTIVES

Abstract

HUMAN-FRIENDLINESS OF ROBOTS IN HUMAN ENVIRONMENTS: MOBILITY, MANIPULATION, AND REHABILITATION PERSPECTIVES

by

Yunha Kim

Doctor of Philosophy in Electrical Engineering and Information Systems

The University of Tokyo

This dissertation presents a novel definition, an evaluation criterion, requirements, and design suggestions for the human-friendliness of robots of the immediate future in human environments, from mobility, manipulation, and rehabilitation perspectives. Securing human-friendliness is an essential prerequisite for the realization of the human-robot coexisting society.

With cutting-edge technologies being implemented, robots have increasingly been commercialized and launched onto the market. The demands for robots, who can help, for example, clean the house, communicate with people, carry heavy things, and work in dangerous environments with or instead of humans, are expected to increase rapidly in the immediate future, given the fact that the average population of many societies is getting old, and the working conditions and perimeters of human activities are changing and expanding.

These robots of the near future greatly differ from the ones that we have known so far in terms of that they share the same time and space with humans, and continuously interact with them in physical, psychological, or other ways. As they are coming into our society, guidelines regarding safety for robots and ourselves must be set to prevent problems of any kind. However, the main stream of the robot research and development has been mostly focused on, and dedicated to improving the performance of the conventional robots. Consequently, most endeavor has been given to making robots stiffer, faster, more efficient, more precise, and more robust, while paying relatively little attention to the human-friendliness of robots.

Ever since Asimov first devised the Three Laws of Robotics in 1942, the guidelines regarding human-robot relationship have been discussed and amended over the last seventy years in sociological domains. And finally in 2006, the British government sponsored a speculative paper suggesting that robots one day might demand equal rights to humans, which marked the first government-level action on the issue. In the following year, also the government of the Republic of Korea came to announcing that it would draft a Robot Ethics Charter to address and prevent "robot abuse of humans and human abuse of robots." However, in contrast to the development of the argument in sociological domains, the discourse concerned with human-robot interactions and safety in the engineering domain still stays local and in its infancy.

To our relief, recently in 2014, a new international standard (ISO) governing the safety issues of the service robots has been published to catch up with the changes of demands and expectations. However, it is no more than setting a foundational guideline in human-robot interactions, barely mentioning that "robots should be inherently safe." One can also find a

few research works on the issue only to find that each of them postulates different conditions and concepts, and that the discourse has not reached any consensus yet, despite its importance. That being said, now it is timely and significant to address how robots should treat humans and vice versa – the human-friendliness of robots in engineering terms.

A wide spectrum of issues involving robots' body and mind has to be addressed for safe and dependable human-robot interactions. Among many, in this dissertation, the body components which involve robot design and control, concerned with the physical portion of the interactions, are mainly focused on and dealt with, based on the fact that the supreme priority falls on the physical aspects of the safety. And the principle that this dissertation makes is simple and clear: "Robots have to be compliant."

In this work, the human-friendliness of robots is newly defined by adopting the concept of the lumped compliance. Then, a criterion to evaluate the human-friendliness is formulated. And while answering the questions such as how should robots be designed, how should they be controlled, and what human aspects should be considered, the requirements and suggestions that lead to improvements of the human-friendliness are provided and verified theoretically and experimentally. Three laboratory-made robots are used for the experiments, to postulate, respectively, mobility, manipulation, and rehabilitation, which form the basis of most of the robotic applications we expect to face in the near future.

In Chapter 1, an overview of the history involving robots and humankind is given. From the overview, the relationship between humans and robots and, the trends in it with regard to the physical distance and interactions are explained. Based on the aspects of the change and the forecast demands and expectations, we will see the problems that we are facing now in preparation for the human-robot coexisting society, where we find the motivation and justification of this work. Based on it, three robotic applications are introduced in the following three chapters, to specify the requirements and conditions that robots of the near future should meet, and eventually to draw a conclusive philosophy in Chapter 5.

Firstly in Chapter 2, a future mobility platform, CIMEV, is introduced. By adopting compliant mechanical elements – caster wheels here – in the system, it is clearly shown that the lumped compliance (the human-friendliness) of the whole robot improves. In addition, it is also shown that introducing compliant control algorithms, such as a disturbance observer, helps robots to perceive and adapt themselves to the changes of the surrounding environments. Moreover, mobile robots working in human environments are required to have high maneuverability and controllability, which are realized by utilizing the characteristics of caster wheels in CIMEV.

In Chapter 3, biologically inspired manipulators, including JUMPBiE, are introduced. The systems' high compliance, that animal's musculo-skeletal structures (in this dissertation, to be specific, the bi-articular muscles) provide, enables safe and human-/environment-friendly motion in robot manipulation. The homogeneity in stiffness distribution and output force characteristics of the bi-articular actuation helps to improve the performance of the robots in human environments. It is also shown that the use of compliant mechanical elements (springs, here) also helps to enhance the human-friendliness of robot manipulators.

In Chapter 4, a novel type exoskeleton for rehabilitation, H-FEX, is introduced after a thorough consideration on the human bio-mechanical characteristics. Based on a study on human body kinematics and muscle activation, a novel algorithm to estimate the muscle group activation rates during gait is formulated. Then, the estimation result leads us to the implementation of an advanced design and control for exoskeletons for rehabilitation, by specifying the dete-

riorated muscle groups, where to assist. Moreover, the viscoelastic characteristics of human muscles opens a way to the extensive use of springs and dampers, which eventually enhance the human-friendliness of the devices.

In Chapter 5, based on the findings and observations from the robotic applications introduced in the previous chapters, a novel definition and a criterion are formulated to tell how human-friendly a robot is. The new definition of human-friendliness, in this dissertation, adopts the concept of the lumped compliance, whose derivation and application methods are also elaborated. Then, the design requirements and suggestions for enhancing the human-friendliness are provided both hardware-wise and software-wise, which are implemented in designing and controlling the robots introduced in Chapter 2, 3, and 4.

Finally in Chapter 6, the findings and contributions of this work and, some open issues for future work are explained and discussed.

Now we are entering a new era of the human-robot coexistence. Many robotic applications are working together with us already, and in the immediate future, we will see many more robots sharing our daily lives together with us. In this dissertation, robots' human-friendliness itself is extensively studied. A novel definition of it, requirements for it, and suggestions to enhance it are given, and they are backed by theoretical and experimental verifications using laboratory-made robots, from mobility, manipulation, and rehabilitation perspectives. Regarding that those three applications are the basis for most robotic systems, the findings and suggestions provided in this work must be helpful and inspiring the next 'human-friendly' robots of the future.

To my family and friends,

I cannot thank you enough.
Live long and prosper.

Contents

List of Figures

List of Tables

Acknowledgments

I would like to express my deep-felt gratitude to my supervisor, Professor Yoichi Hori, for his advice, encouragement, patience and constant support. He always provided me with energy and clear explanations when I was lost, tired, or even doubting in my abilities. When discouraged I was always able to get refreshed by following his prescription: "Go get drunk." I wish all students the honor and opportunity to know him and drink with him.

I also want to thank Professor Hiroshi Fujimoto at the Department of Advanced Energy of The University of Tokyo and Dr. Sehoon Oh at the Department of Mechanical Engineering of Sogang University, for their suggestions, comments and academic guidance. They were extremely helpful in providing expertise I needed in order to complete this work. Indeed, they are not only good instructors but also great mentors.

And I truly appreciate the invaluable help of all the supervising committee members — Professor Hiroyuki Ohsaki, Professor Takashi Kubota, Professor Takafumi Koseki, Professor Tatsuaki Hashimoto, Professor Akihiko Yokoyama, and Professor Katsushi Ikeuchi. Their profound knowledge and practical insights led me to improve and complete this work.

Oh, I cannot forget Dr. Kanghyun Nam at Samsung Electronics, Co., Ltd., Dr. Hongzhong Zhu and Dr. Valerio Salvucci at The University of Tokyo, my friends. I thank them for their sincere help and warmest encouragements. Without their support, I would not have been able to complete this work.

Additionally, I wish to thank all the professors and staff of The University of Tokyo for their hard work and dedication, providing me the means to complete my course works and degree. Especially, I thank Mr. Toshiyuki Uchida at the Department of Electrical Engineering of The University of Tokyo, for providing technical suggestions and support, and Ms. Yoko Hiromori at the Department of Advanced Energy of The University of Tokyo for her sincere support for administrative affairs.

For the financial support, I must thank the Ministry of Education, Culture, Sports, Science and Technology (MEXT) of Japan, who enabled me to concentrate on this work without worrying about self-preservation issues during the whole period of my stay (Five years and a half! Wow!) in Japan.

And finally, I would like to thank my family for their continuing, loving support. Mom, dad, and Saerom, I will never be able to express my feelings enough, only that I love you.

NOTE: This dissertation was submitted to the supervising committee on June 2, 2014.

Chapter 1

Introduction

Robots have been around us in conceptual and physical forms for a long – much longer than anyone can imagine – time. To begin a long story about robots and humankind, firstly in this chapter, robots, humans and their interaction in the past, now, and in the future are described and discussed. At the other end of the thread, we will have insights to see problems that robots and humankind are currently facing, and that must be solved in order to open a new chapter of the story of the two species. Eventually, this long story about robots and humankind is intended to provide solutions to those problems. At the end of this chapter, an overview of this dissertation is given.

1.1 Robots and Humankind

The term 'robot' was first used in a play, Rossum's Universal Robots (R.U.R.), composed by a Czech writer, Karel Čapek, in 1921, where the robots were organic beings, not mechanical, however worked the same as modern robots do (Fig. 1.1). By the 1960s, engineers began to use the term to refer to reprogrammable industrial machines, and many writers borrowed the term to name the mechanical creatures in their science fiction stories, which made everyone familiar with the term regardless of different definitions. The term is quite new from historical perspective, however, the concept is far older than that.

If we define a robot as 'a machine capable of automatically carrying out a complex series of movements' according to the Oxford English Dictionary, one of the first concepts of robot appeared in a Homeric oral epic, the Iliad, in the 8th century B.C.E., where robot-like machines, e.g. Talos (Fig. 1.2), were mentioned. Likewise, many other ancient Greek and Roman mythologies have robotic characters in the stories although their forms and types vary. On the other hand, when it comes to the early forms of real machines, Babylonians' water clock, the clepsydra (422 B.C.E.), must be one of the first robotic devices in history. Then in around 400 B.C.E., an ancient Greek philosopher, Archytas, is known to have built a pulley-driven wooden dove automaton, which was powered by compressed air. Later in 16th century C.E., Leonardo da Vinci drew many schematics for robots and demonstrated a lion automaton to King Francis I of France (Fig. 1.3). In 17th century, hundreds of Karakuri automata (Fig. 1.4) started to appear in Japanese Edo period to entertain people. Besides, there have been so many other robotic machines and concepts that can be found in history and literature; we cannot name them all.

Figure 1.1: A scene from a 1938 TV production of “Rossum’s Universal Robots” (Photo: BBC)

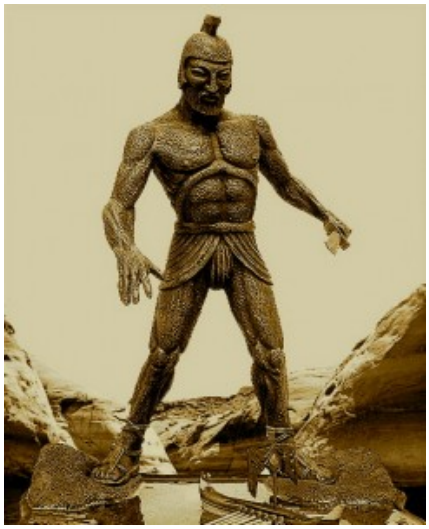

Figure 1.2: The World’s First Robot: Talos (Photo: Vanderbilt University)

These all are the ancestors of modern robots.

They were conceived over 4,000 years ago in ancient rituals and myths, and given shape to in forms of early mechanical toys and automata. These ancient robots had no apparent purpose other than amusement. Nevertheless, the mechanical principles on which they were based were derived from improvements in these mechanical toys, and the clock and automata makers made great contributions to mechanization of factories. The trigger was the Industrial Revolution, which took place in many European countries and the U.S. in around the 18th and 19th century. During this period, improvements in regulators for steam engines enabled people to think of automatic machines not just as entertaining devices, but as the basis of profitable businesses [1].

Around the same time, the importance of the training of technicians and engineers began to be recognized, which led to the establishments of engineering schools in many countries, for instance, British “Red Brick” schools (1850s), German polytechnics (1870s), the faculty of

Figure 1.3: A replica of Leonardo da Vinci's mechanical lion (Photo: AP)

Figure 1.4: A Karakuri automaton (Photo: Steven Sentosa, MyCorner)

engineering of the University of Tokyo (1886), and the Massachusetts Institute of Technology (1876). Consequently, the mechanical engineering profession was transformed from one run by self-taught mechanics to a group of college-educated specialists. During the 19th and 20th centuries, these newly emerging engineer groups dedicated themselves to the improvements in general level of engineering, together with the availability of materials, the installation of electricity, and the increased manufacturing capacity of products for export, domestic, and military purposes, which provided a great incentive to develop automatic machines, and eventually motivated improvements in control engineering in a bid to reduce the involvements of human operators in factories to move toward the full automation of the machines.

Robots, having their ancestors in the rituals, myths, and amusement, have evolved following the accumulation and integration of technical innovations and social transformations with the emergence of the highly educated group of technicians and engineers. Robots have been in fictional and mythological stories; they have been around or in theaters to entertain people; and with the technological explosion they stepped into factories.

1.2 Industrialization to Robotization

By the mid-20th century, two world wars which accompanied the rapid industrialization and the spread of mass-production, accelerated the development of robots. In 1947, Del Harder, an executive officer at Ford used the term 'automation' to refer to the increased use of electro-mechanical, hydraulic, and pneumatic production and part-handling machines, which were fixed to one certain task and partially automated. Before long, the invention of transistor and modern computers in the 1950s enabled computerized control of robots, which made robots reprogrammable – flexible – to adapt to changing tasks. Computerized controllers created the demands for robots in industry, and also the demands for companies to produce them. By the 1970s, computer controlled robot arms began to face intense competition. In 1973, the first commercially available microcomputer-controlled robotic arm, The Tomorrow Tool (T3) was launched onto the market. In 1974, the Swedish IRB-6 was introduced, and the STANFORD ARM successfully assembled an automobile part in an experiment. This STANFORD ARM, then, greatly affected the birth of the well-known robot, the Programmable Universal Machine for Assembly (PUMA, Fig. 1.5), which was successfully and widely adopted in factory production lines and, is still in use on many industrial and educational sites around the world [1].

After the successful introduction of PUMA, factory automation by introducing robots has explodingly expanded in numbers and geographically worldwide. By the end of the 1980s, the International Federation of Robotics (IFR), which administers worldwide affairs of the robot industry, had its member organizations in Germany, Sweden, Japan, Korea, the U.S., and etc., and now the members are scattered in 14 countries of 3 continents. Among them, Swiss-based ABB, who started robot production in 1974, was the first to sell 100,000 robot units on to the market in 2002 [2]. Nowadays, robots play important roles in industrial fields, and they became indispensable in most automobile factories, food manufacturing lines, semiconductor fabrication processes, and etc. (for instance, Fig. 1.6).

Ever since they began in earnest to be used on industrial sites, industry has been the only field where robots can play such important roles, and consequently industrial robots have

Figure 1.5: Unimate Industrial Robots, PUMA 700 (Photo: Academy of Media Arts of Cologne)

Figure 1.6: Modern industrial robots in an automobile manufacturing line (Photo: YTN)

formed the most portion of the entire robot population worldwide. And as a matter of course, modern robot research works and their orientation have been closely connected to the demands of the industry, which can be implied from the following '10 good reasons' robots are used on industrial sites. Robots can [2]:

- reduce operating costs;
- reduce capital costs (e.g. inventory, work in progress);
- reduce material waste and increase yield;
- reduce employee turnover and improve recruitment;
- save space in high value manufacturing areas;
- increase production output rates;
- increase product manufacturing flexibility;
- improve product quality and consistency;
- improve quality of work environment for employees; and
- comply with safety rules and improve workplace heath and safety.

To meet the demands — in order to reduce production costs and improve product quality — robot research has been focused on and oriented towards better precision and efficiency. Thus modern robots have become more powerful, stronger, faster, and stiffer. So now modern robots can lift tons of steel plates with no sweat, work for a long consecutive time without a break or complaining, and even tell a sub-micron difference in what they see or touch. Moreover, keeping pace with continuously evolving computer science and many other related engineering technologies, the performance of modern industrial robots is ceaselessly being improved with more accurate sensors, more powerful and efficient actuators, and smarter brains.

1.3 Robots in the Immediate Future

The technological explosion related to robots worked not only for industry, but also for many applications in other fields. In addition, the socio-economic transition — such as the aging of the population — of many societies is provoking the demands for robots. Robots now can assist people by augmenting human motor and sensory powers, doing household choirs for them, or entertaining and communicating with them. Also, there are robots that fight on the battle fields instead of human soldiers, or explore the solar system and the outer space without humans accompanied. Indeed, robots now can do everything ranging from vacuuming floors to exploring Mars.

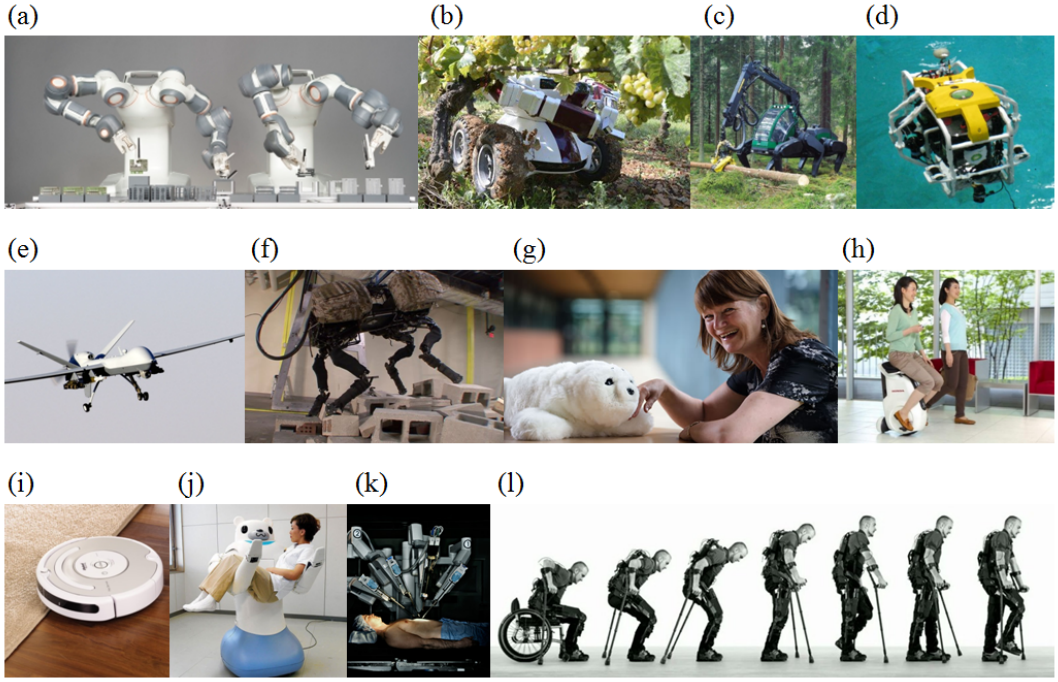

Figure 1.7: Various robots that we see now or will probably see in the near future: (a) future industrial robots (Photo: ABB); (b) robots in agriculture (Photo: AFP); (c) robots in forestry (Photo: PlusTech); (d) underwater robots (Photo: CoralBots); (e) drones (Photo: USAF); (f) porters (Photo: Boston Dynamics); (g) companion robots (Photo: Northumbria University); (h) personal mobility (Photo: Honda); (i) cleaning robots (Photo: iRobot); (j) welfare robots (Photo: RIKEN); (k) surgical robots (Photo: Max Aguilera-Hellweg); (l) rehabilitation robots and exoskeletons (Photo: TIME)

Yet, only a limited number of these non-industrial robots — except for the exceptional robot vacuum cleaners — are in use currently, mainly due to high costs and price, that hinder the growth of the market. However, the threshold is near, and we will see more and more robots with various types and functions around us in the immediate future. For instance, in Fig. 1.7, some of the promising robots are introduced. Industrial robots will be more dextrous and do more sophisticated jobs in the factories. Other robots will work for humans in the farms and the forests, relieving humans of heavy labor and enhancing the productivity, and at the same

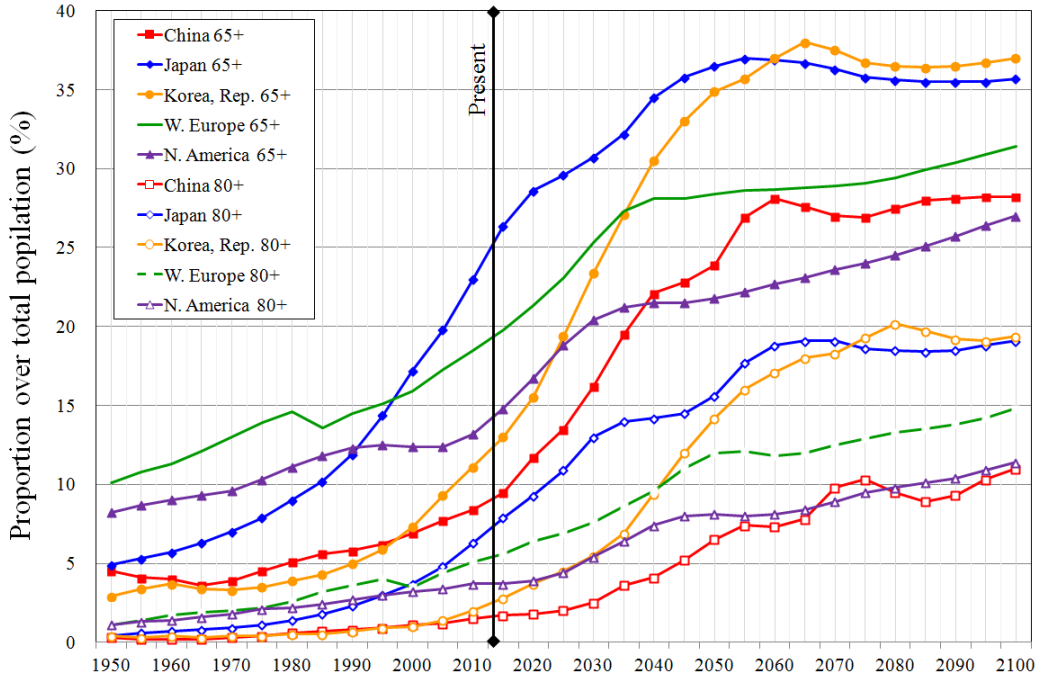

Figure 1.8: Aged population proportion trends in major countries and regions from 1950 to 2100 [3].

time, reducing environmental load. Underwater robots will go deeper into the ocean to provide knowledge about our planet, or save lives in case of maritime accidents. Military robots such as drones and porters will change the future of war. Lastly but most importantly, service robots including companion robots, personal mobility, housekeeping robots, and robots for medical and rehabilitation purposes will greatly improve our quality of life in many ways.

In the background of this increasing demands for robots, is a huge transformation going on in our societies. That is, increasing life expectancies and decreasing birth rates in many countries are provoking the demands for robots to fill the lack of human labor power. As shown in Fig.1.8, in 2013 one Japanese person out of four is already 65 years old or older, and the proportion is forecast to rise up to 37% by the year of 2050. Korea, one of the most quickly aging countries, is expected to overtake Japan in 50 years [3]. Consequently, many issues regarding aging are rising in importance around the world. Robots now are perceived as a part of solution to the issues, regarding that they can augment the lacking human labor power.

These promising robots of the near future are here to be categorized, for further discussion, according to their field of use as in Table 1.1. Also, they are mapped as shown in Fig. 1.9, according to their degree of physical distance and interaction with regard to humans. In both Table 1.1 and Fig. 1.9, robots that work in human environments are marked with an asterisk (*), which we want to talk about in this long story. From the map, we can get one important idea that “robots are coming into our daily lives.” This new breed of robots will touch us, talk to us, cooperate with us, and vice versa, hanging around in our homes. Robots of this kind are particularly important due to the fact that they share the same time and space, and continuously interact with humans in physical, psychological, or other ways. This aspect of the new breed

Table 1.1: Robots we see now, or will see in the immediate future. Robots marked with an asterisk (*) work in human environments where humans and robots share the same time and space interacting with each other.

Category	Applications	Remarks
Manufacturing	Robot arms, Food handling, Cosmetics, Medicine, and etc.	Industrial robots
Field	Agriculture, Forestry, Fishery, Underwater, Construction, Inspection, and etc.	
Military and Aerospace	Drones, Combatants, Non-combatants, Rovers, and etc.	
Service	*Housekeeping, *Attendant, *Amusement, *Toys, *Rescue, *Companion, and etc.	Service robots
Medical	*Surgery, *Welfare, *Rehabilitation, *Monitoring, *Diagnosis, and etc.	Service robots
Mobility platforms	*Personal mobility, Logistics, Porters, and etc.	Service robots
Other robotic machines	Home appliances, Automobiles, Vessels, Areal vehicles, Trains, and etc.	

makes a significant difference from the robots which we have known so far.

Looking into statistical data might help us to deepen our insights into the situation we are currently facing. Fig.1.10$\sim$1.14, for example, show the robot sales and forecasts in industrial and non-industrial domains, from a report issued by the International Federation of Robotics (IFR), recently [4]. The statistics data tells us that the demands for industrial robots have been steadily increased, and will do for the time being. More important part is the appearance of the new breed, and their expected explosion in numbers. It is obvious and encouraging that both the old breed – industrial robots, and the new breed – robots in human environments, will support our society.

As seen in Fig.1.10, more than a hundred thousand of industrial robots are being sold annually, and the market is expected to grow steadily as many developing countries are advancing their industry automation. Although the demands for industrial robots at present are mainly concentrated (70% sales in 2012) in a few industrialized countries such as Germany, the United States, Japan, and Korea, many countries and regions with great potentials such as Brazil, China, and India are expected to raise the market (at 6% growth rate on average) in the following years [4]. Not to mention that industrial robots have successfully accomplished their missions for the past decades, they are expected to continue their jobs as long as we need them.

More importantly, the demands for robots in other categories are growing, and growing fast as inferred from the sales data shown in Fig.1.11 and 1.12, although the number of units is still by far smaller than that of industrial robots for the moment. While robots for military and field use account for a considerable portion of the numbers for now, the growth of the others, including mobile platforms and cleaning robots, is notable considering that they have just appeared. As further explained later, these new breed robots are expected to overtake the

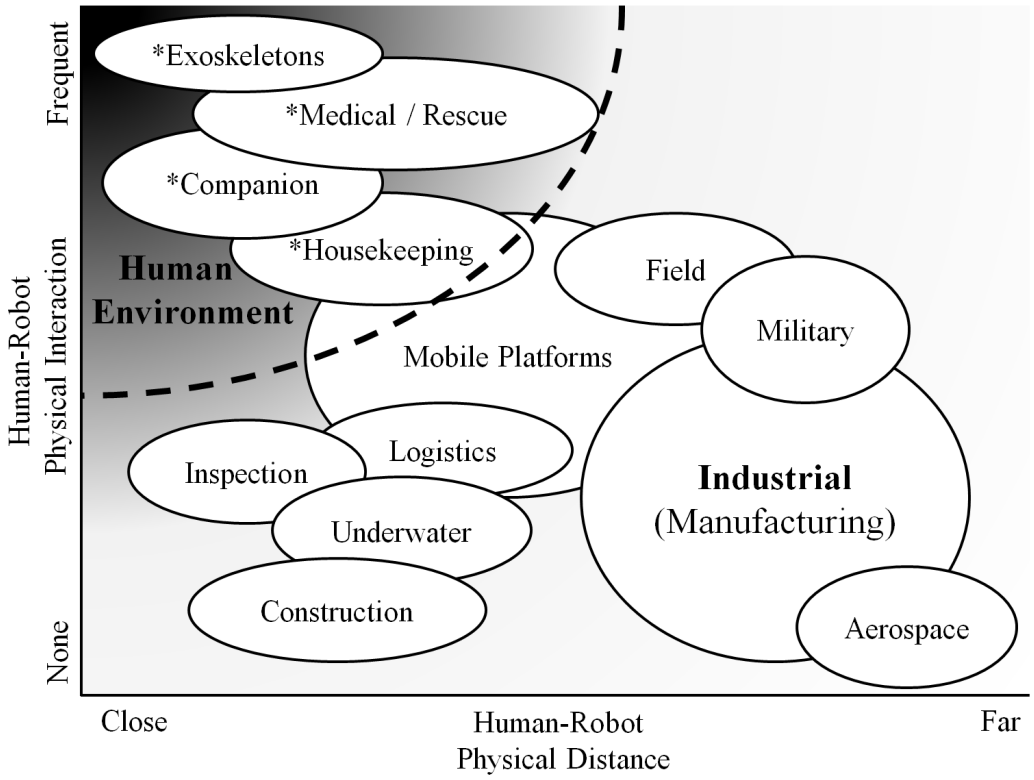

Figure 1.9: Types of robots mapped with regard to human-robot physical distance and human-robot physical interaction. Robots marked with an asterisk (*) work in human environments where humans and robots share the same time and space interacting with each other.

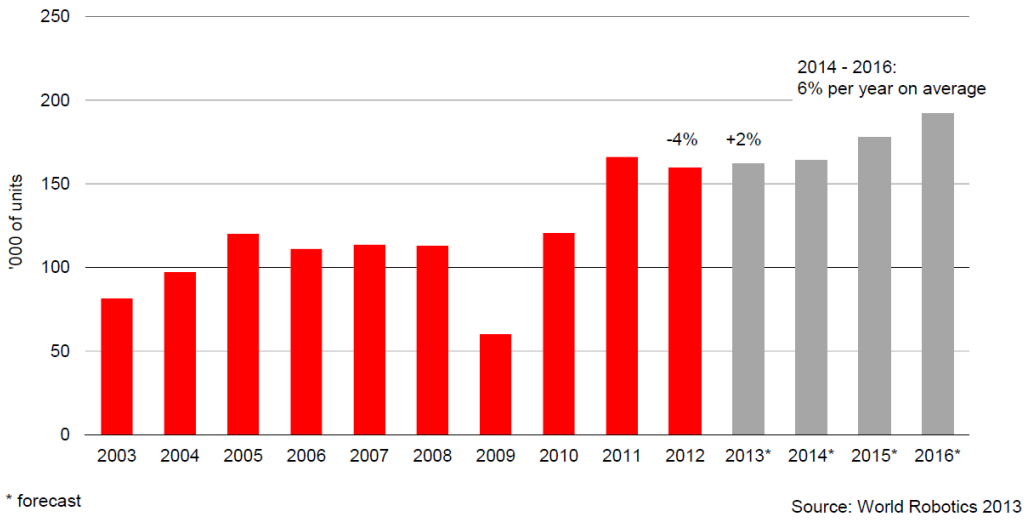

Figure 1.10: Worldwide annual supply of industrial robots from 2003 to 2016. (Graph: IFR [4])

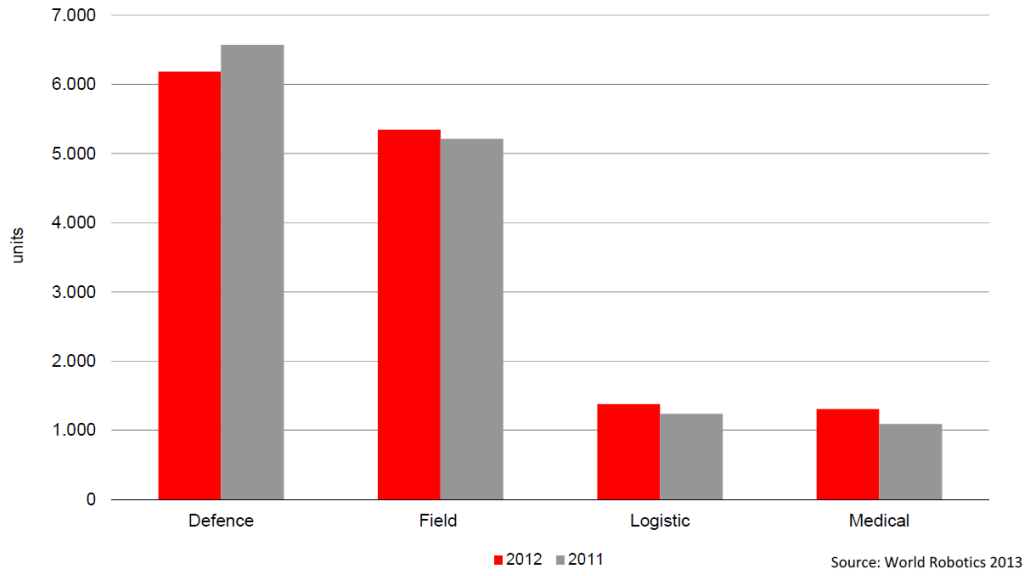

Figure 1.11: Robot sales for professional use for major applications from 2011 to 2012. (Graph: IFR [4])

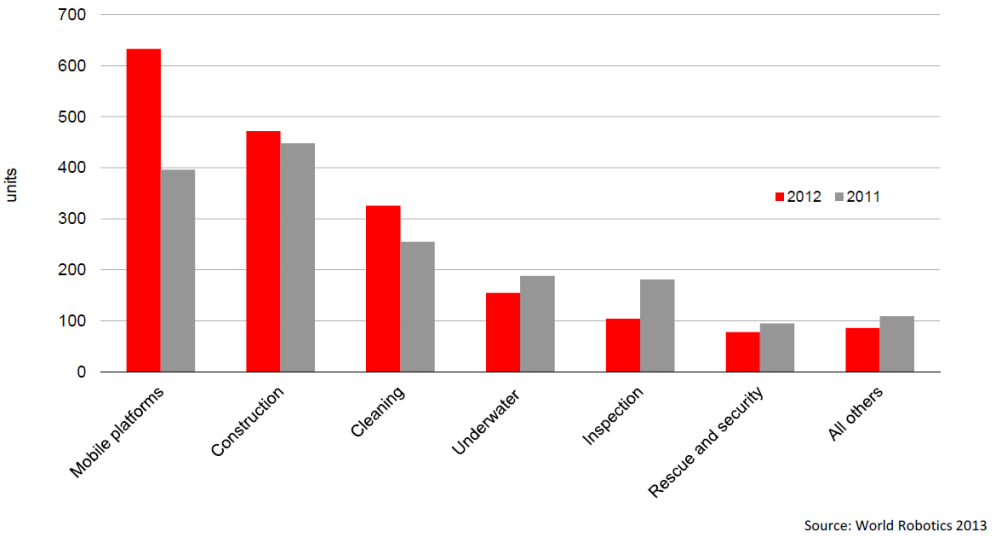

Figure 1.12: Robot sales for professional use for other applications from 2011 to 2012. (Graph: IFR [4])

old breed in a few decades in both numbers and the size of the market.

Fig.1.13 and 1.14 show the sales and forecast of the robots in non-industrial sector. While robots for field and military use are still expected to dominate the market for a few following years, the household robots and robots for amusement are forecast to show rapid increase in sales. Millions of household robots, such as robotic vacuum cleaners, floor-washing robots, and attendant robots, are being sold annually, and companion robots and robotic toys that can communicate, entertain and play with the users will largely increase in only a few years. Again,

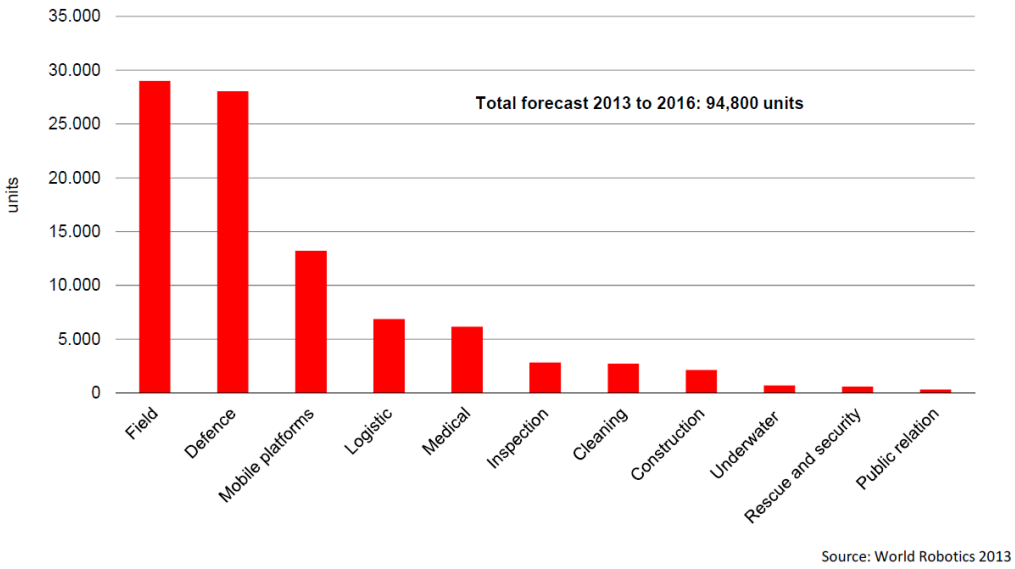

Figure 1.13: Robot sales forecast professional use from 2013 to 2016. (Graph: IFR [4])

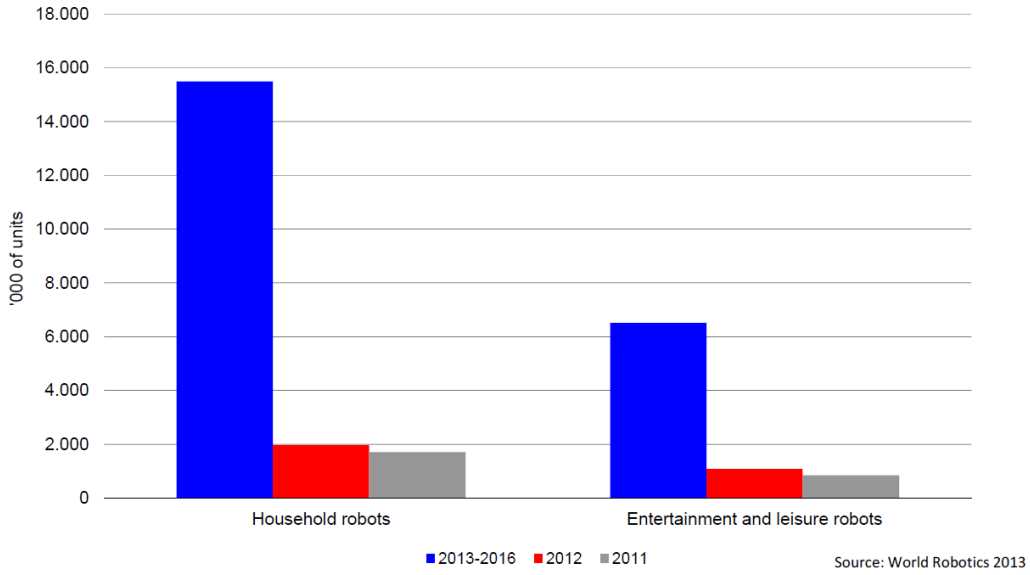

Figure 1.14: Robot sales and forecast for personal/domestic use from 2011 to 2016. (Graph: IFR [4])

they are coming into our daily lives.

From another statistical report, it gets more obvious. Fig.1.15 shows the estimates of the market size of the Japanese robot industry for the upcoming 20 years [5]. The most striking point of it is that service robots are predicted to overtake the others combined in only 20 years. Service robots here exclude defense and field robots, and include medical robots, welfare and rehabilitation robots, household robots, mobility platforms, logistic robots, robots for amusement, rescue and security robots, and etc., which are all the new breed robots that share the same time and space with human users in physical and psychological terms. It is saying that

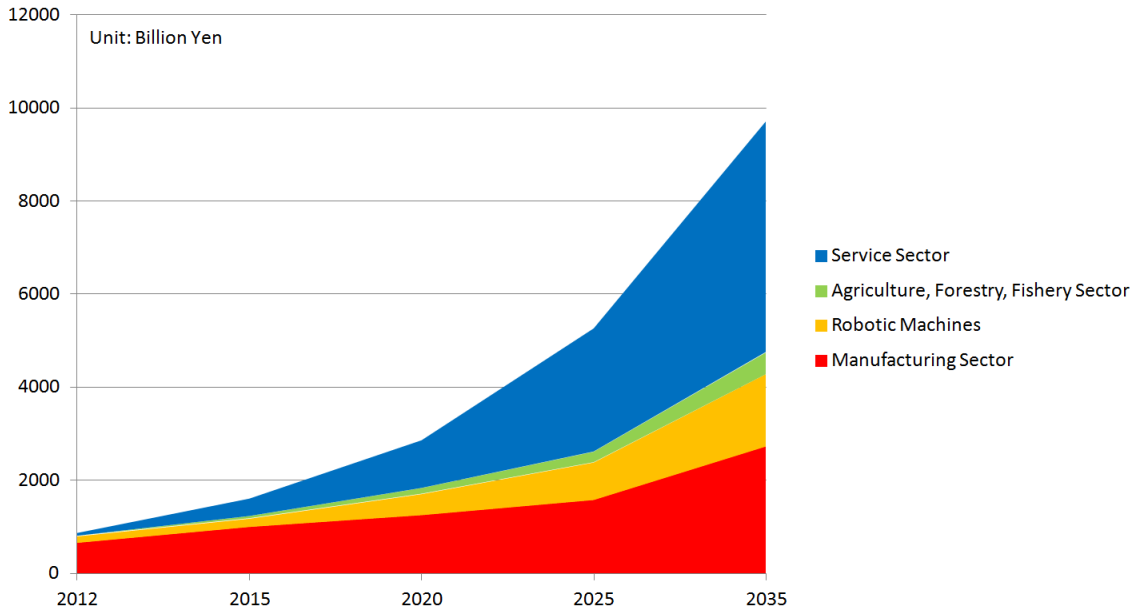

Figure 1.15: Estimates of the current and future robot industry market size of Japan from 2012 to 2035 [5].

we will see 80 times more service robots — in monetary terms — around us in 20 years than we do now in Japan, assuming that the robot price stays still. But what if the price of the robots goes down? Yes, we are now entering the new era of human-robot coexistence, and thus we have to be prepared.

1.4 Paradigm Mismatch

From the historical background, the motivation and the orientation of the robot research and development so far have been boiled down to cost, quality, and safety issues. And that is, robots have to be fast, precise, and consistent in performing tasks, and they should never complain or get ill if proper maintenance provided. For these reasons, robots have been designed and controlled to meet the requirements that fundamentally increase production efficiency, excluding and/or replacing humans from the system. Consequently, robots today have become stronger, powerful, more precise, stiffer, and heavier. This paradigm is simply expressed by 'the stiffer the better.' Human-robot safety in this context refers to eliminating human-related factors from the time and space in which robots operate. It seems to have been worked well so far and will do forever for industrial robots. But the problem is that, this paradigm and the concept of safety don't hold for the new breed robots.

As robots are coming into our daily lives, guidelines for robots and ourselves must be set to prevent problems of any kind, and it is definite that the guidelines must be human-centered ones. One can find a few research works on the issue, however, the discourse has not reached any consensus yet. Still, most robots are designed and controlled to have improved precision and robustness with high stiffness without seriously taking humans into account.

Fortunately, robots living with us today are not so big, heavy, or powerful. No today's

robotic vacuum cleaner can hurt humans. However, what if they become bigger, heavier, and stronger? For example, Honda's Asimo can definitely hurt people if it blunderingly interacts with them. Being one of the most advanced humanoid robots ever developed in history, it can walk, run, jump, and talk, and even serve drinks, however, no one is allowed to touch Asimo while it is in motion. Asimo's sophisticated system works fine only when excluding human factors from the system; in other words, it is still one of the old breed robots – industrial ones. It is hard to think that 'untouchable' robots help with laundry, wash dishes, clean toilets and bathtubs, and help with moving heavy objects in our homes. It is rather easier to imagine they hurt people by punching in the chest, pinning on the wall, or smacking on the head just like their relatives do. If the paradigm mismatch remains unresolved, the human-robot coexistence must never happen.

Another statistical data tells us why. Each year many lives are lost and a number of disabling injuries occur through robot-related accidents and incidents around the world. In Japan, 28 lives were killed in industrial-robot-related accidents during 13 years from 2000 to 2012 as shown in Table 1.2 [6], which may seem very few compared to the numbers in other industrial disasters, but even one accident is one accident too many, and we are expecting them to live with us.

Table 1.2: Annual fatalities in robot-related accidents in Japan [6]

Year	2000	2001	2002	2003	2004	2005	2006
Fatalities	1	1	2	6	1	1	4
Year	2007	2008	2009	2010	2011	2012	Total
Fatalities	4	1	2	2	1	2	28

Here are some descriptions of real-life robot accidents selected from [7] and [8].

- A repairman climbed over a safety fence without shutting off the power to the robot and worked in its area while it was temporarily stopped. When the robot resumed movement, it pushed him into a grinding machine and, consequently, he died.

- A robot stopped because one of the parts did not make a locating switch. The victim entered the cell and attempted to locate the part. The robot activated and crushed the employee to death.

- Four workers entered the restricted space to troubleshoot a robot with power on. One worker decided to put the part back onto the fixture and the robot assumed it was time to go. The worker was pinned to the fixture.

- A technician was working on a robot-conveyor arm. The machine dips parts into solutions and cycles every 15 minutes. The victim forgot about the 15-minute cycle and was caught between the robot arm and the conveyor.

- Two electricians entered a cell which had two robots that load two assembly fixtures. A yellow caution light was on indicating that it was safe to enter the cell. Apparently while the electricians were checking the equipment one of them hit a limit switch which caused one of the robots to move quickly to the fixture to remove a panel. One of the

electricians was standing in front of the assembly machine and was pinned by the robot and end-effector.

As inferred from the descriptions, accidents involve human errors: humans do things that they are not supposed to do. However, robots should take full responsibility for the safety involving humans in living with us, since we humans are forgetful, careless, neglectful, and, at the same time, fragile animals. Time is running out. Now it is time to solve the paradigm mismatch problem, and this work is dedicated to provide hints and inspiration for the next.

1.5 For Human-Robot Coexistence

This work addresses the 'human-friendliness' of robots that will work in human environments in the immediate future. Based on the fact that we are entering a new era of the human-robot coexistence, where robots are coming into our homes and work places to share the same time and space with humans.

Ever since Asimov first devised the Three Laws of Robotics in 1942 [9], the guidelines regarding human-robot relationship have been discussed and amended over the last seventy years in sociological domains. And finally in 2006, the British government sponsored a speculative paper suggesting that robots one day might demand equal rights to humans, which marked the first government-level action on the issue. In the following year, also the government of the Republic of Korea came to announcing that it would draft a Robot Ethics Charter to address and prevent "robot abuse of humans and human abuse of robots [10]." However, in contrast to the development of the argument in sociological domains, the discourse concerned with human-robot interactions and safety in the engineering domain still stays local and in its infancy.

To our relief, recently in 2014, a new international standard (ISO) [11] governing the safety issues of the service robots has been published to catch up with the changes of demands and expectations. However, it is no more than setting a foundational guideline in human-robot interactions, barely mentioning that "robots should be inherently safe." One can also find a few research works on the issue only to find that each of them postulates different conditions and concepts, and that the discourse has not reached any consensus yet, despite its importance. That being said, now it is timely and significant to address how robots should treat humans and vice versa – the human-friendliness of robots in engineering terms.

A wide spectrum of issues involving robots' body and mind has to be addressed for safe and dependable human-robot interactions. Among many, in this dissertation, the body components which involve robot design and control, concerned with the physical portion of the interactions, are mainly focused on and dealt with, based on the fact that the supreme priority falls on the physical aspects of the safety. And the principle that this dissertation makes is simple and clear: "Robots have to be compliant." It is essential for **Safety**, **Reliability**, and **Adaptability** of the robots. The key aspect of these is compliance of the system. Compliance in this context means both mechanical and virtual ones. By using compliant actuators and passive compliant elements, and by using control algorithms that provide robots with sensitivity, the human-friendliness — safety, reliability, and adaptability — of robots will be improved. Before drawing the conclusive philosophy, first we start with thorough observations and contemplation using three robotics applications from mobility, manipulation, and rehabilitation perspectives,

which are respectively introduced in the following three individual chapters. These three basic functions are particularly important, since they are the basis of most robot applications as it can be inferred from Fig. 1.7. Based on the results of each, the argument of this work is made in Chapter 5.

1.6 Overview of the Thesis

This dissertation is organized as follows. In Chapter 2, firstly a future mobility platform, CIMEV, is introduced. By adopting compliant mechanical elements – caster wheels here – in the system, it is clearly shown that the lumped compliance (the human-friendliness) of the whole robot improves. In addition, it is also shown that introducing compliant control algorithms, such as a disturbance observer, helps robots to perceive and adapt themselves to the changes of the surrounding environments. Moreover, mobile robots working in human environments are required to have high maneuverability and controllability, which are realized by utilizing the characteristics of caster wheels in CIMEV.

In Chapter 3, biologically inspired manipulators, including JUMPBiE, are introduced. The systems' high compliance, that animal's musculo-skeletal structures (in this dissertation, to be specific, the bi-articular muscles) provide, enables safe and human-/environment-friendly motion in robot manipulation. The homogeneity in stiffness distribution and output force characteristics of the bi-articular actuation helps to improve the performance of the robots in human environments. It is also shown that the use of compliant mechanical elements (springs, here) also helps to enhance the human-friendliness of robot manipulators.

In Chapter 4, a novel type exoskeleton for rehabilitation, H-FEX, is introduced after a thorough consideration on the human bio-mechanical characteristics. Based on a study on human body kinematics and muscle activation, a novel algorithm to estimate the muscle group activation rates during gait is formulated. Then, the estimation result leads us to the implementation of an advanced design and control for exoskeletons for rehabilitation, by specifying the deteriorated muscle groups, where to assist. Moreover, the viscoelastic characteristics of human muscles opens a way to the extensive use of springs and dampers, which eventually enhance the human-friendliness of the devices.

In Chapter 5, in order to resolve the problems found in this chapter, a novel definition and a criterion are formulated to tell how human-friendly a robot is, based on the observations and contemplation made through the experiments and discussion using three robotic applications. The new definition of human-friendliness, in this dissertation, adopts the concept of the lumped compliance, whose derivation and application methods are also elaborated. Then, the design requirements and suggestions for enhancing the human-friendliness are provided both hardware-wise and software-wise, which are implemented in designing and controlling the robots introduced in this work.

Finally in Chapter 6, the findings and contributions of this work and, open issues for future work are explained and discussed.

Chapter 2

CIMEV: A Future Mobility Platform

In this chapter, a future mobility platform, CIMEV, is introduced. By adopting compliant mechanical elements – caster wheels here – in the system, it is clearly shown that the lumped compliance (the human-friendliness) of the whole robot improves. In addition, it is also shown that introducing compliant control algorithms, such as a disturbance observer, helps robots to perceive and adapt themselves to the changes of the surrounding environments. Moreover, mobile robots working in human environments are required to have high maneuverability and controllability, which are realized by utilizing the characteristics of caster wheels in CIMEV.

2.1 Introduction

Utilizing the advantages of electric motor described below [12], many motion control strategies for electric-motor-driven mobility such as anti-slip traction control, running stability control, and range extension control, have been introduced in recent years [13][14][15]. These control methods are effective hence electrified vehicles can run more safely and energy-efficiently than conventional Internal Combustion Engine Vehicles (ICEVs). TORQ Roadster, electric vehicles from Arcimoto, and many other concept electric vehicles from many manufacturers around the world are the icons symbolizing the vitality of the field.

- Torque generation of an electric motor is very quick and accurate.
- A motor can be attached to each wheel.
- Motor torque can be measured easily.

In addition to aforementioned properties, mobility electrification helps to excel ICEVs in terms of two-dimensional motion control, by assigning two inputs - the steering and the direct yaw moment - while the conventional platforms have only the steering input. The torque vectoring technology for ICEVs [16][17] seems to be similar to the direct yaw moment input, however it is obvious that the controllability and the system response become much better than ICEVs due to the reasons listed above.

However, most of these research works are based on the four-wheeled platform with the conventional mechanical steering system, which has not changed from the beginning of the

mass production of the Ford Model T in 1908. It was originally designed and has been optimized for an internal combustion engine to transmit power to each of the driving wheels. Consequently it is clear that to use the conventional platform for the independent motor driven mobility is a waste of ability, hence motivates this work.

Despite the underlying importance, it seems that there have been only a few attempts to provide a new platform for the independent motor driven mobility. In 1968, Slay [18] invented an electric-motor-driven mobility that could change direction at right angles using powered caster wheels. Similarly, Lam et al. designed a novel type all wheel driven and steered mobility [19]. These systems imply a number of possibilities of what mobility electrification can bring about. Yet such systems are still too expensive in terms of the number of actuators and control efforts. Slay's system needs analyses on stability and maneuverability. Lam's work is rather focused on the driver interface, thus the vehicle dynamics itself has to be investigated more in various speed ranges. Another design proposed by Ebihara et al. [20] gives some hints for the new design of micro mobility. It uses only the moment steering showing that the performance is good enough to deal with given tasks. The free rotating casters work well on the irregular terrain — a grass field. However, it still needs improvements, if postulating personal mobility applications, in high speed running performance considering the lateral forces when cornering.

Besides, some other attempts to provide high agility for mobility platforms can also be found. Swisher's invention of 1952 [21] contributed to the mobility of lawn mowers which require quickness in their motion due to the fact that their operation space is usually restricted, and has obstacles and ditches. Brienza's work on a novel steering linkage [22], and Borenstein's mobile robot platform [23] are highly applicable and useful to the vehicles in the field of welfare and social security. All three of them, however, operate in a relatively low speed range where controllability and stability problems of vehicle dynamics can be neglected, hence they are not taken into account. As for future personal mobility solutions, the dynamics of the vehicle in the high speed range such as steering and cornering characteristics becomes important, because it is deeply related to the safety issues. The authors present considerations on these issues, which makes a part of contributions of this work.

In this work, a novel mobility platform using caster wheels and independent driving motors is proposed. Provided with four wheels, the system is designed to be structurally stable, and with caster wheels on the front axle the proposed system is able to fully utilize the two inputs – the steering angle and the direct yaw moment – in two-dimensional vehicle motion. The design philosophy and the control strategies are developed and discussed in the following sections.

2.2 Study on Wheel Placements

To seek the most appropriate configuration for an independent-motor-driven mobility, it is necessary to discuss the wheel placements and their effects on the vehicle behavior first. In this section, some general wheel placements and corresponding dynamics are introduced. Then the relevant stability evaluation criteria are shown, and followed by discussion on the compatibility with motion control.

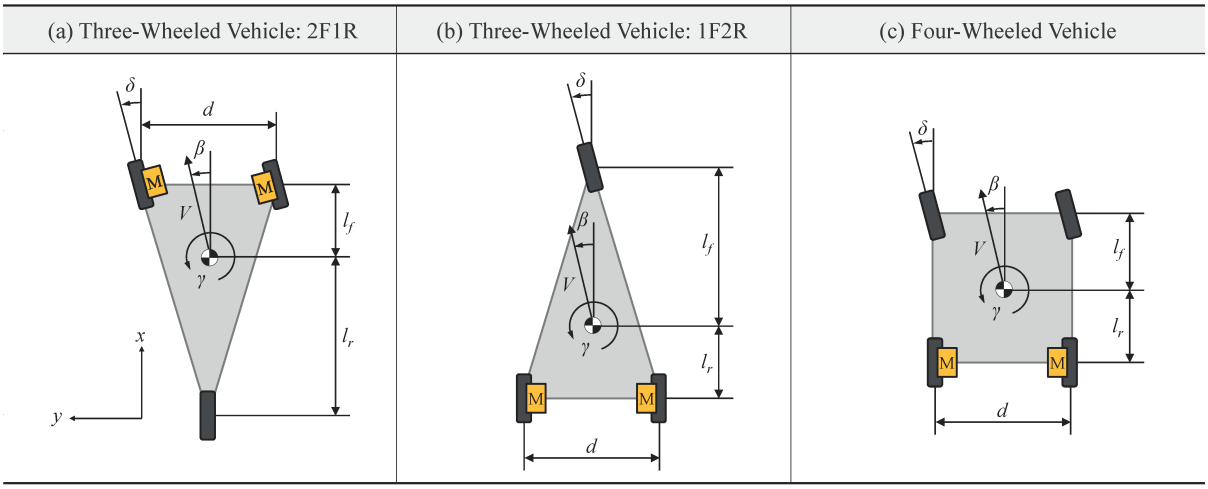

Figure 2.1: Three models used in the analyses. Frame of reference, center of gravity, motor position, and etc. are indicated.

Wheel Placements and Dynamics

Three generally thinkable kinds of vehicle wheel placements and their dynamics are introduced here: three-wheeled vehicle model with one wheel front; three-wheeled vehicle model with one wheel rear; and four-wheeled vehicle model. It is assumed that each of the dynamic models has two independent driving motors in the system for fair comparison. The effect of the suspension system is neglected for simplicity, assuming that the vehicle would mainly run on the paved roads where the tire-ground contact is secured to a certain degree.

Major assumptions for the system analyses are: all vehicle models introduced here share the vehicle parameters shown in Nomenclature, which are equivalent to those of the experimental vehicle CIMEV (Fig. 2.7); each system has two independent driving motors within, and the steering wheels are on the front axle; the effect of the suspension system on the vehicle dynamics is ignored; and the center of gravity of each system is assumed to be located at its geometric center of the base, i.e. each wheel negotiates with equally divided vertical load.

For all systems introduced in the analyses of this section, the state space representation is as expressed below:

$$\dot{\mathbf{x}} = \mathbf{A}\mathbf{x} + \mathbf{B}\mathbf{u} \tag{2.1}$$

$$\mathbf{y} = \mathbf{C}\mathbf{x} + \mathbf{D}\mathbf{u} \tag{2.2}$$

where,

$$\mathbf{x} = \begin{bmatrix} \beta & \gamma \end{bmatrix}^T \tag{2.3}$$

$$\mathbf{u} = \begin{bmatrix} \delta & M_z \end{bmatrix}^T \tag{2.4}$$

$$\mathbf{C} = \mathbf{I} \tag{2.5}$$

$$\mathbf{D} = \mathbf{0} \tag{2.6}$$

for all cases.

Three-Wheeled Vehicle and its Dynamics

Huston, Graves and Johnson first studied three-wheeled vehicle dynamics in 1982 [24]. They made stability comparisons between a three-wheeled vehicle with two wheels on the front axle (2F1R), a three-wheeled vehicle with two wheels on the rear axle (1F2R) and a standard four-wheeled vehicle, and concluded that three-wheeled vehicles can offer safe alternatives to four-wheeled vehicles.

Here, two dynamic models which Huston et al. proposed are introduced with some modifications: it is assumed that two independent driving motors are equipped, and the steering wheels are in the front in both cases.

Three-Wheeled Vehicle (2F1R) and its Dynamics

The schematic of the system is shown in Fig. 2.1(a). Two independent driving motors are attached in the front steering wheels, and a non-driving-nor-steering wheel is in the rear. The governing equations are as below:

$$\mathbf{A} = \begin{bmatrix} -\frac{2C_f+C_r}{mV} & -\frac{2l_fC_f-l_rC_r}{mV^2} \\ -\frac{2l_fC_f-l_rC_r}{I_z} & -\frac{2l_f^2C_f+l_r^2C_r}{I_zV} \end{bmatrix} \tag{2.7}$$

$$\mathbf{B} = \begin{bmatrix} \frac{2C_f}{mV} & 0 \\ \frac{2l_fC_f}{I_z} & \frac{1}{I_z} \end{bmatrix} \tag{2.8}$$

Three-Wheeled Vehicle (1F2R) and its Dynamics

The schematic of the system is shown in Fig. 2.1(b). Two independent driving motors are attached in the rear wheels, and a non-driving steering wheel is in the front. The governing equations are as below:

$$\mathbf{A} = \begin{bmatrix} -\frac{C_f+2C_r}{mV} & -\frac{l_fC_f-2l_rC_r}{mV^2} \\ -\frac{l_fC_f-2l_rC_r}{I_z} & -\frac{l_f^2C_f+2l_r^2C_r}{I_zV} \end{bmatrix} \tag{2.9}$$

$$\mathbf{B} = \begin{bmatrix} \frac{C_f}{mV} & 0 \\ \frac{l_fC_f}{I_z} & \frac{1}{I_z} \end{bmatrix} \tag{2.10}$$

Four-Wheeled Vehicle and its Dynamics

Although the dynamic analyses for four-wheeled ground vehicles are plentiful, most of them are concerning the conventional engine-driven vehicles. Here, a dynamic model for an independent motor driven electric vehicle is introduced. The model is based on the bicycle model. The schematic of the system is shown in Fig. 2.1(c), and the governing equations are as below:

$$\mathbf{A} = \begin{bmatrix} -\frac{2(C_f+C_r)}{mV} & -\frac{2(l_fC_f-l_rC_r)}{mV^2} \\ -\frac{2(l_fC_f-l_rC_r)}{I_z} & -\frac{2(l_f^2C_f+l_r^2C_r)}{I_zV} \end{bmatrix} \tag{2.11}$$

$$\mathbf{B} = \begin{bmatrix} \frac{2C_f}{mV} & 0 \\ \frac{2l_fC_f}{I_z} & \frac{1}{I_z} \end{bmatrix} \tag{2.12}$$

Structural Stability Evaluation

As the first step, vehicle's structural stability, which refers to the tip-over stability in this case, is evaluated. Previous research works have introduced numerous criteria to quantify the vehicle tip-over stability [25], such as Static Stability Factor (SSF) [26], Load Transfer Metric (LTM) [27], Energy Stability Margin (ESM) [28], and Force-Angle Stability Metric (FAS) [29]. By applying each of these criteria to the models introduced above, the structural stability is examined.

Table 2.1: Structural Stability Summary

Criterion	2F1R	1F2R	4W
SSF	0.74	0.74	1.11
LTM	7.26	7.26	10.89
ESM	16.78	16.78	18.63
FAS	poor when accel.	poor when braking	-

Evaluation results are shown in Table 2.1. Numbers are unitless, and the larger number indicates the better stability. Generally, 4-wheeled vehicle is the most structurally stable by all criteria, which can be explained by the fact that 4-wheeled vehicle has the largest base of support which is directly related to the tip-over moment.

Compatibility with Motion Control

In order to see the compatibility of the system with motion control, the controllability and the system response of the vehicle dynamic models are evaluated. Firstly, the controllability of each system is checked. Secondly, yaw rate responses are shown with respect to the steering input and the yaw moment input respectively, since we are dealing with two major inputs which distinguish the proposed platform from conventional engine vehicles from the motion control point of view.

Controllability Study

First of all, using the state equations (2.1)$\sim$(2.12), controllability of each system is checked. Controllability of a system can be clarified by calculating the rank of the matrix $\Gamma_c[A, B]$. The system is controllable if and only if $\Gamma_c[A, B]$ has full rank. This criterion is binary, i.e. it only provides 'YES-NO' answers, and the answers for the given systems are shown in Table 2.2.

Table 2.2: Controllability Check

	2F1R	1F2R	4W
rank($\Gamma_c[A, B]$)/Dimension	2/2	2/2	2/2
Controllability	YES	YES	YES

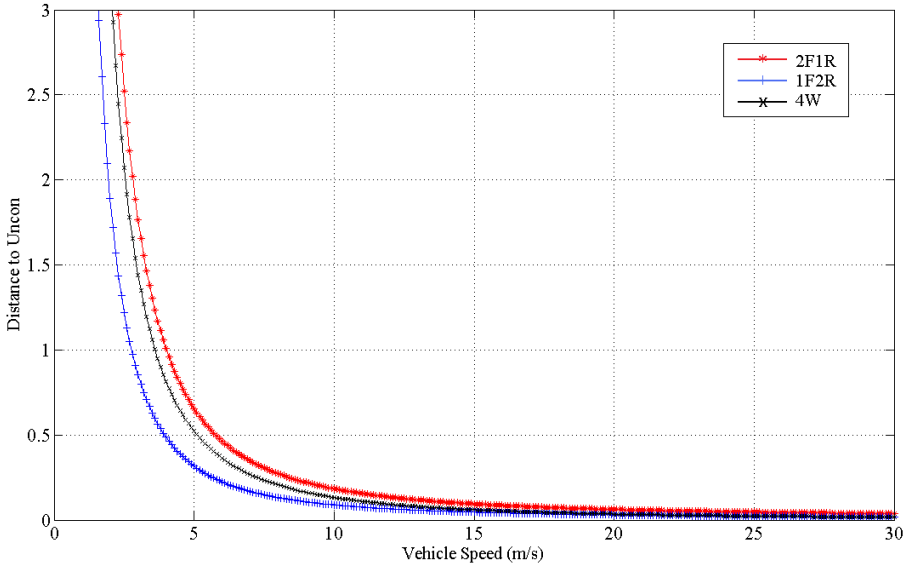

Figure 2.2: Distance to the Uncontrollability

For more in-depth comparison of the controllability of the different systems, a quantitative measurement is needed. In order to meet this demand, the method used is the quantification method introduced by Eising [30], which provides a standard to measure how far a controllable system is from an uncontrollable one. The distance $\mu(A, B)$ between a controllable system from an uncontrollable one is defined as follows:

$$\mu(A, B) \equiv \min \sigma_n(sI - A, B) \tag{2.13}$$

where $\sigma_n(sI - A, B)$ is the smallest singular value of $[sI - A, B]$. This criterion indicates the spacial distance from a system to its nearest uncontrollable point, which means when $\mu(A, B) = 0$, the system becomes uncontrollable if there is any parameter deviation in the system. According to the definition, the distances for the given systems are shown in Fig. 2.2.

All vehicle models are controllable. However, as seen in Fig. 2.2, in terms of robustness the 3-wheeled vehicle with two wheels on the front is the most farthest from the uncontrollability, even farther than the 4-wheeled one. The result shows that the relative controllability of the 3-wheeled vehicle which has two wheels on the front, is higher than that of the 4-wheeled vehicle at any vehicle speed, which implies that the 2F1R vehicles are more robust against parameter variation than the 4-wheeled ones. This can be generalized, because the only parameter that varies in the matrices A and B and affects the result is the vehicle speed V, given that the system inputs remain the same.

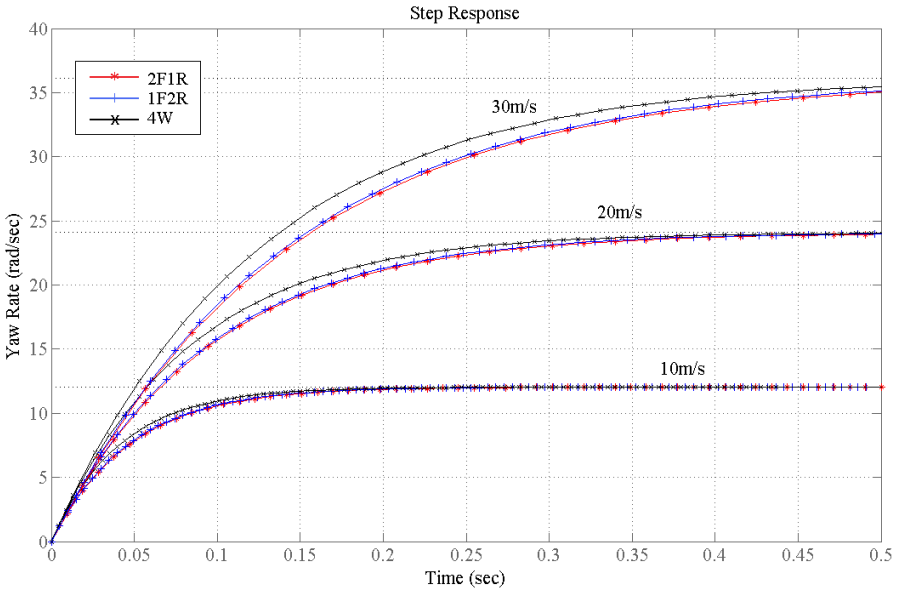

Figure 2.3: Step Steering Input (30 degrees) vs. Vehicle Yaw Response

Vehicle Yaw Response Analyses

For vehicle yaw response analyses, state equations are converted into transfer functions $G(s)$ as:

$$G(s) = C(sI - A)^{-1}B + D \tag{2.14}$$

where, system inputs are defined in (2.4), and common output is the vehicle yaw rate γ, which makes six transfer functions in total for the analyses. The details are omitted, and the results are shown in Fig. 2.3∼2.6.

Figure 2.3 shows the responses of the vehicle models in time domain when given a step steering input whose magnitude is 30 degrees which is usually the maximum value for passenger vehicles at $t = 0$. It can be seen that the 3-wheeled vehicle models are slower in response than the 4-wheeled one, however, the difference is not so significant; the vehicle speed is dominant, not the configuration. It can be confirmed in Fig. 2.4. Thus it can be generally stated that vehicle's yaw response to the steering input is dependent on the vehicle speed.

When there exists the difference between traction forces generated by two driving wheels, yaw moment occurs in the vehicle, which distinguishes the proposed platform from the conventional engine vehicles. This difference is regarded as another input variable: the direct yaw moment input.

Fig. 2.5 shows the yaw responses of the vehicles in time domain when given a step direct yaw moment input whose magnitude is 80% of the vertical load of each case, which is usually the maximum friction on a dry asphalt, at $t = 0$. It can be seen that the response speed of the 3-wheeled vehicles is faster than that of the 4-wheeled one. Moreover, the steady state gain of the 3-wheeled vehicles is remarkably larger than that of the 4-wheeled one at any longitudinal

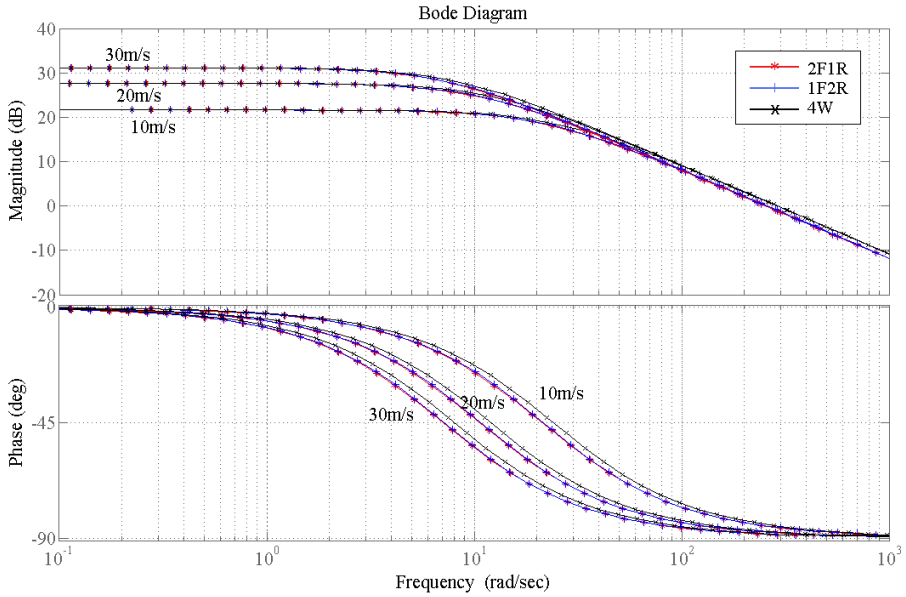

Figure 2.4: Bode Plot: Steering Input vs. Vehicle Yaw Response

speed. This difference in gain can be explained by examining the transfer functions governing the dynamics.

$$G(0)_{\gamma M_z} = \begin{array}{l} \dfrac{V(2C_f+C_r)}{2L^2C_fC_r(1-\frac{m(2l_fC_f-l_rC_r)V^2}{2C_fC_rL^2})} = \dfrac{3V}{8L^2C_0} \\ \dfrac{V(C_f+2C_r)}{2L^2C_fC_r(1-\frac{m(l_fC_f-2l_rC_r)V^2}{2C_fC_rL^2})} = \dfrac{3V}{8L^2C_0} \\ \dfrac{V(2C_f+2C_r)}{4L^2C_fC_r(1-\frac{m(l_fC_f-l_rC_r)V^2}{2C_fC_rL^2})} = \dfrac{V}{3L^2C_0} \end{array} \tag{2.15}$$

where C_0 is an arbitrary coefficient. From this observation, it is obvious that the difference in gain results from the difference of cornering stiffness, which is a mechanical stiffness hindering the direct yaw moment input from turning the vehicle.

Moreover, in Fig. 2.6 it can be seen that the frequency response is almost the same as Fig. 2.4, but there only exists difference in gain. Such relatively small gain makes it difficult for the direct yaw moment input to contribute to motion control. Improvements need to be made here to fully utilize two inputs of the independent motor driven mobility platforms.

To summarize, the three-wheeled vehicles are less structurally stable than the four-wheeled one. They have, however, more larger gains in yaw rate response to the yaw moment step input, which is a desirable property in motion control using independent driving motors. Especially the three-wheeled model with two front wheels has almost the same response to the unit step steering input, compared to the four-wheeled model, whereas it shows better response to the

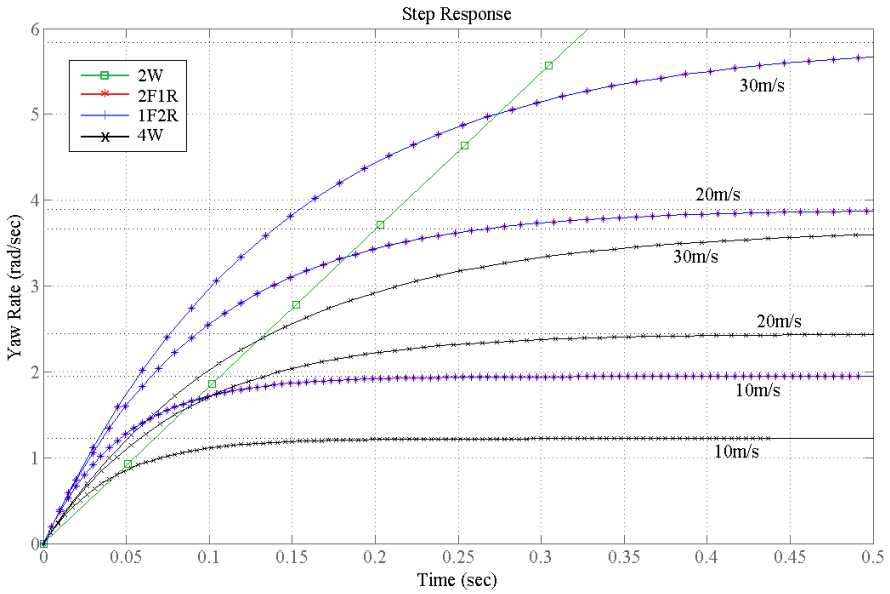

Figure 2.5: Step Direct Yaw Moment Input vs. Vehicle Yaw Response

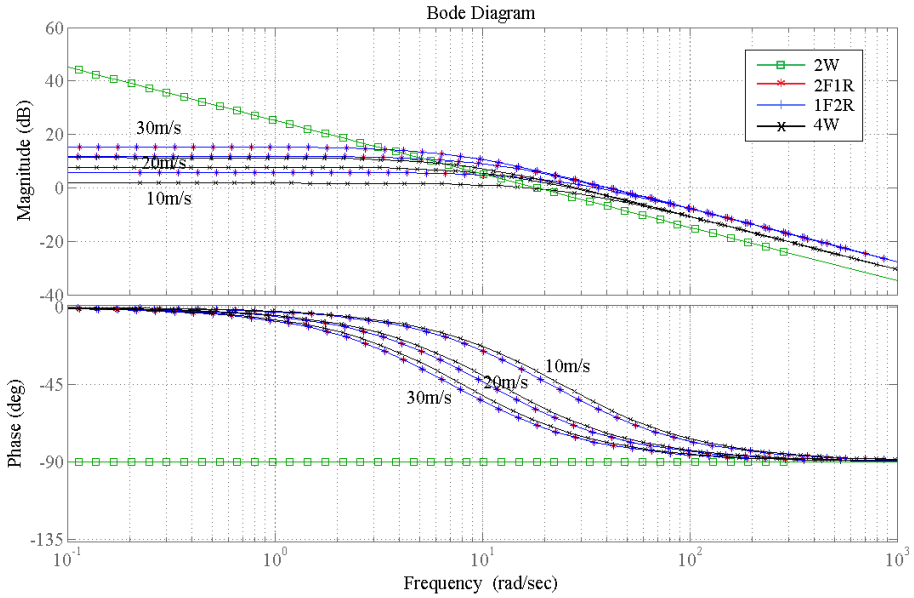

Figure 2.6: Bode Plot: Direct Yaw Moment Input vs. Vehicle Yaw Response

yaw moment input. Thus, considering the vehicle motion control using independent driving motors, the three-wheeled vehicle can be an attractive alternative.

From the observations made here, it is clear that when trying to find a novel platform for the independent motor driven mobility, there are some efforts to be made: to reduce mechanical stiffness hindering the direct yaw moment input from turning the vehicle, and to maintain struc-

tural stability and controllability of the system, which forms the background of the proposed system design.

2.3 CIMEV for Future Mobility Platform

Based on the observations of the previous section, this work proposes a novel structure using caster wheels and independent driving motors, as one of the possible configurations for the future personal mobility solution. The system consists of two independent driving wheels and two caster wheels. This configuration enables the vehicle to have: a low mechanical stiffness against the direct yaw moment input because caster wheels can rotate freely, and a high static stability because the vehicle has four wheels, which showed the highest static stability from the observation in the previous section.

In order to demonstrate the feasibility of the proposed system, an experimental vehicle which has two driving wheels and two caster wheels was fabricated. Before fixing the actual configuration, a contemplation was needed to decide where to put the caster wheels: front or rear.

Vehicles which require high agility such as forklift, whose operational space is restricted, often have steering wheels in the rear, because steering wheels on the rear axle enable high yaw rates to make sharp turns. However, nearly all passenger vehicles have steering wheels on the front for better stability. An obvious difference between these two types of vehicle is the operational speed range.

CIMEV

CIMEV (Caster-wheeled Independent Motor-driven Electric Vehicle) is designed to run unmanned. It is controlled by a digital signal processor (S-BOX) with two input signals transmitted through a radio controller. The PWM signals interpreted by the receiver are sent into the DSP, where they are linearized to drive the motors – both driving and steering – to run the vehicle. Four independently controlled electric motors are used. Two are used for steering and the other two for driving. The vehicle is powered by a 24V Ni-MH battery. System configuration is shown in Fig. 2.8. More details of the experimental vehicle are shown in [98].

Modeling

The dynamic model suggested by G. Somieski [31] seems to be compatible for the system. The system is modeled neglecting the existence of steering motors, and it is assumed that the casters are free to rotate only under the effect of the stiffness K and the damping D about the king pin. The governing equations are written as:

$$I_w\ddot{\delta} + D\dot{\delta} + K\delta = -M_{sa}(\alpha) - eF_y(\alpha) - D_t(V)\dot{\delta} \tag{2.16}$$

$$\alpha = \delta - \theta_V \tag{2.17}$$

Considering the size and the type of the wheel we are dealing with, which is $0.1m$ in diameter and made of hard-rubber, the terms $M_{sa}(\alpha)$ and $D_t(V)\dot{\delta}$ can be neglected. Moreover,

since $F_y(\alpha)$ can be approximated into a linear form of $F_y(\alpha) = C_f\alpha$, we can simplify (2.16) to (2.18) below, where the theoretical backgrounds can be found in [32], [33], [34], and [35]:

$$I_w\ddot{\delta} + D\dot{\delta} + K\delta = -eC_f\alpha \tag{2.18}$$

As the experimental vehicle has been provided with two steering motors, equations can be written as below, considering the torque inputs of the steering motors, and regarding that the liaison moments and the equivalent forces are given by the motors:

$$I_w\ddot{\delta}_L + eC_f\delta_L = eC_f\beta + \frac{el_fC_f}{V}\gamma + T_{mL} \tag{2.19}$$

$$I_w\ddot{\delta}_R + eC_f\delta_R = eC_f\beta + \frac{el_fC_f}{V}\gamma + T_{mR} \tag{2.20}$$

$$I_z\dot{\gamma} = \frac{l_f}{e}(T_{mL} + T_{mR}) - 2l_rC_r(\beta - \frac{l_r}{V}\gamma) + M_z \tag{2.21}$$

$$mV(\dot{\beta} + \gamma) = \frac{1}{e}(T_{mL} + T_{mR}) + 2C_r(\beta - \frac{l_r}{V}\gamma) \tag{2.22}$$

2.4 Advantages of CIMEV

The global control scheme for CIMEV is shown in Fig. 2.9. The upper-level controller computes the direct yaw moment reference and the lateral force reference in the form of the steering angles in order to meet the speed and yaw rate requirements. The lower-level controllers which are the driving controller and the steering controller, assign the motor torques to give the vehicle speed, yaw rate, and the steering angles.

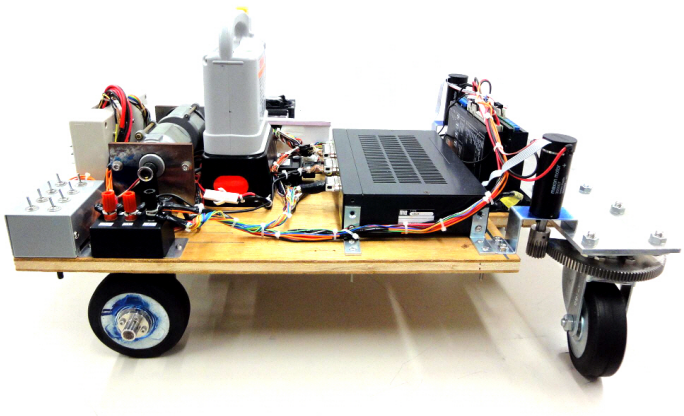

Figure 2.7: Caster wheeled electric vehicle CIMEV: Two rear wheels are driven via belt and pulley by two independent driving motors (90 Watts each). Two front wheels are casters, connected via gears to two independent steering motors (60 Watts each).

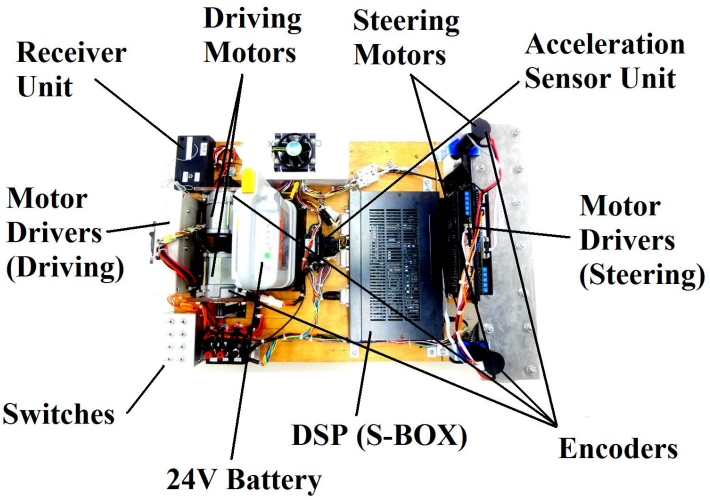

Figure 2.8: System configuration of the experimental vehicle CIMEV: The vehicle is controlled by a digital signal processor (S-BOX) with a remote controller. Its dynamic behavior is monitored and recorded through an acceleration sensor unit and four encoders.

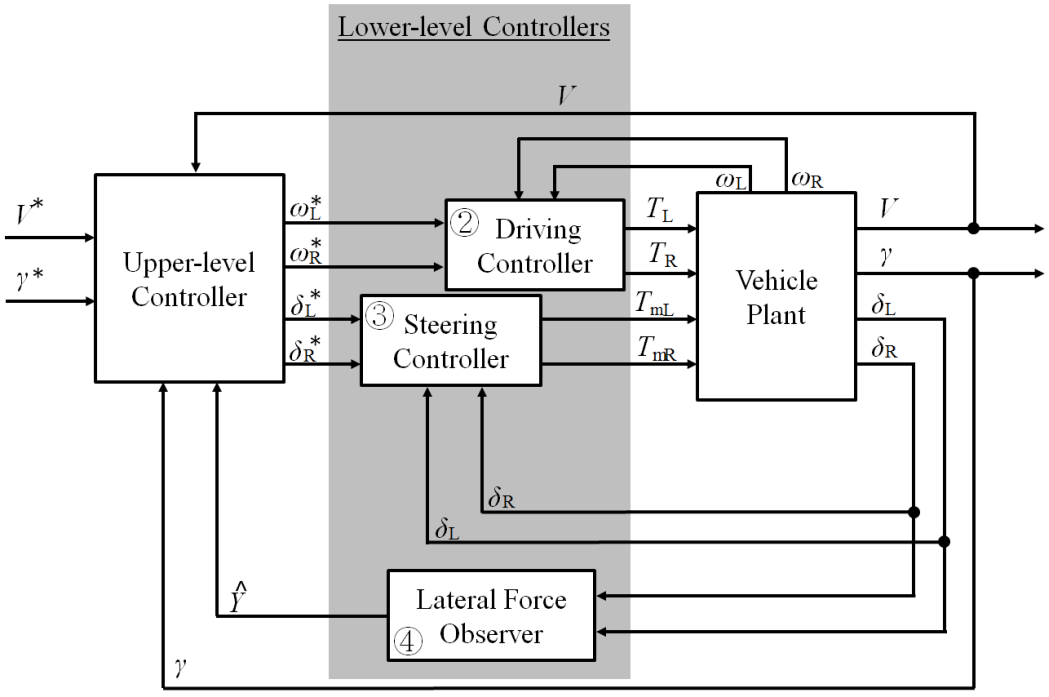

Figure 2.9: Block diagram of the global control scheme for CIMEV.

Experiments were done to show the advantages of the proposed system: high mobility, lateral force observer, load transfer estimation, understeer gradient control, and bank angle estimation. The experiment results are shown, and the corresponding advantages of the system are discussed.

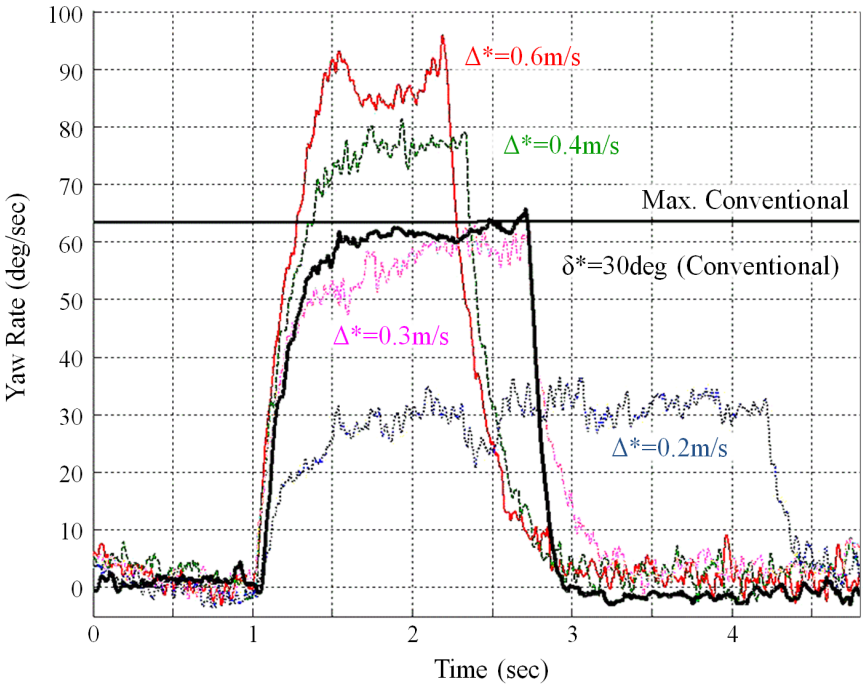

Figure 2.10: Yaw rate responses to the direct yaw moment input versus the conventional steering maneuver at 90 degrees cornering. Vehicle speed is $1m/s$ in all cases. The steering angle is 30 degrees at inner wheel for the conventional steering case. Direct yaw moment is given by wheel speed controller.

High Mobility

Fig. 2.10 shows the experimental result of the vehicle yaw rate responses to the direct yaw moment input versus the conventional steering maneuver at 90 degrees cornering at a low speed of 1m/s. For the conventional steering case, the steering angle was given by Ackermann geometry at 30 degrees which is usually the maximum for passenger vehicles.

It is shown that the yaw rate can go over the maximum rate of the conventional one at a given speed, by applying direct yaw moment to the driving wheels without causing any energy loss from cornering resistance, which is consistent with the observation results from the system analyses. This property enables CIMEV to make a sharper turn than a conventionally steered vehicle, so that CIMEV can move more freely in restricted spaces. This experiment result also can be associated with the ICR location shown in Fig. 2.11. Usually a normal passenger vehicle has the minimum turning radius of 5 meters, meanwhile CIMEV can turn with zero radius.

At low speed, the advantage of using caster wheels is obvious: as the way they are defined, they freely rotate and so does the vehicle. Vehicles with the normal steering system, need to run in order to make turns. CIMEV, on the other hand, can make turns at speed of zero. This property is highly advantageous for the mobile robot applications, since the space in which they work is shared by humans.

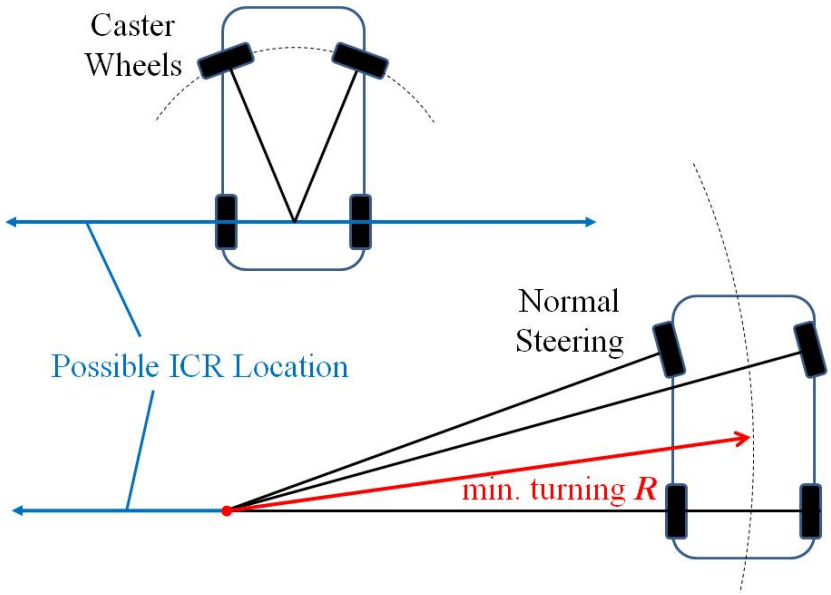

Figure 2.11: Possible location of ICR (Instant Center of Rotation), colored blue. CIMEV (upper) and conventional one (lower). Vehicle with normal steering has usually 5 meters of minimum turning radius, while CIMEV has zero at zero vehicle speed.

Lateral Force Observer

Since CIMEV is equipped with two independent steering motors, it is possible to apply disturbance observers [36] in the control logic of each wheel. From equations (2.19) and (2.20), if we define the disturbance torques for the left and right as:

$$T_{dL} = eC_f\beta + \frac{el_fC_f}{V}\gamma - eC_f\delta_L = eC_f\alpha_L \simeq eY_L \tag{2.23}$$

$$T_{dR} = eC_f\beta + \frac{el_fC_f}{V}\gamma - eC_f\delta_R = eC_f\alpha_R \simeq eY_R \tag{2.24}$$

the lateral force can be simply calculated by dividing the caster length e without using any special sensors to measure it. Moreover, by controlling the steering angles, the vehicle is allowed to have the controlled lateral forces, which gives a number of implications to vehicle motion control field.

Fig. 2.12 compares the lateral forces between the one calculated using disturbance observers and the one using acceleration sensor. Since it is a steady state circle running condition (i.e. $\dot{\gamma} = 0$ and $M_z = 0$), disturbance torques were converted into lateral forces (red and blue dashed lines), and the lateral acceleration was converted into the necessary net lateral force to make the turn (black solid line). Experimental result shows that the lateral force estimation using disturbance observer has reliable accuracy when compared with the calculation using acceleration sensor.

The results are comparable to Yih's work [37] that proposed a novel side-slip estimation method using steering torque information and a disturbance observer. The work provides many

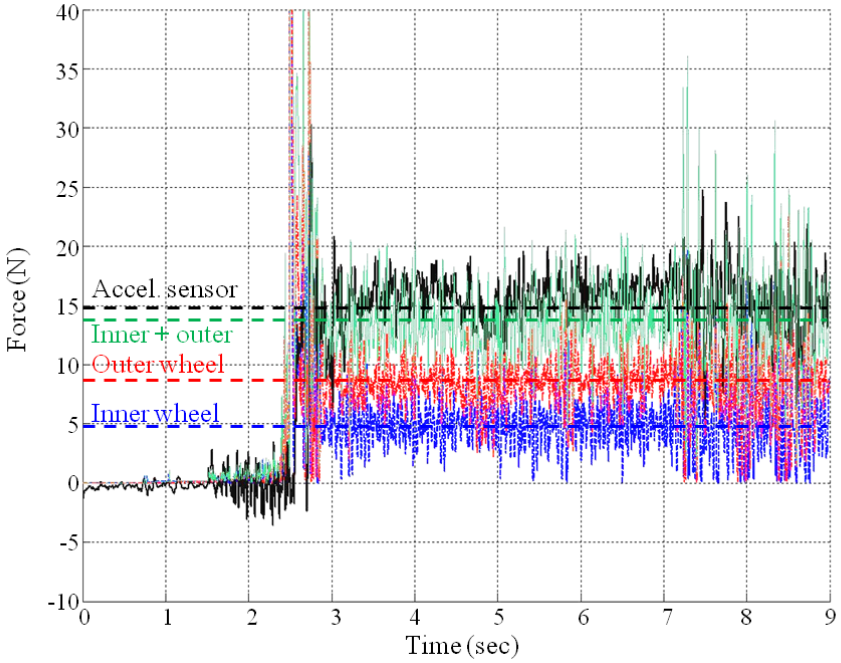

Figure 2.12: Lateral forces calculated by using disturbance observer versus the one calculated by using lateral acceleration sensor during a steady state circle running. Vehicle speed was $2m/s$, and the steering angle was 15 degrees at inner wheel.

practical implications, however, there still remain a number of model uncertainties, or approximated parameters in calculation, which eventually dull down the estimation accuracy, whereas CIMEV consists of a simpler mechanical configuration which imposes less model uncertainties on the estimator — the disturbance observer.

Load Transfer Estimation

As seen in Fig. 2.12, the estimated lateral force has larger value for the outer wheel than the inner one. In this work, it is assumed that the cornering stiffness C_f has a fixed value, however, in reality the value changes due to the dynamic change in vertical load. It is found, from the experimental result and from the definition of C_f in [32], that the ratio of the vertical load is around 0.63 between the inner and outer wheels.

On the other hand, from the experiment condition, and the vehicle geometry and parameters, for a given lateral acceleration, the vertical load of the front wheels can be roughly calculated as:

$$N_{zFL} = \frac{mgl_r}{L} + \frac{2mhl_r}{dL}a_y \tag{2.25}$$

$$N_{zFR} = \frac{mgl_r}{L} - \frac{2mhl_r}{dL}a_y \tag{2.26}$$

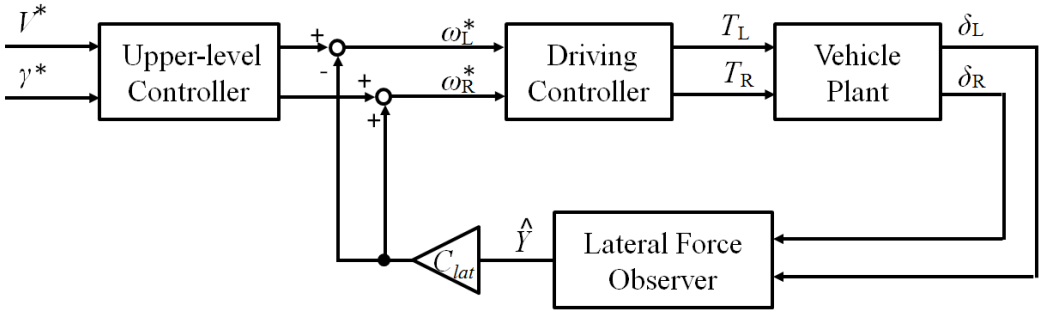

Figure 2.13: Understeer gradient controller.

where, a_y of this experiment was $1.87m/s^2$, thus the ratio N_{zFL}/N_{zFR} should be around 0.69, which is fairly close to the value from the experiment result. This observation implies that, by using the lateral force observer, the dynamic load transfer of a running vehicle can be calculated without attaching any special sensors such as a potentiometer. More investigation needs to be done for better accuracy.

Understeer Gradient Control

Furthermore, it is also possible at a high vehicle speed to change the understeer characteristics by using the lateral force feedback control. In this paper, this will be referred as the understeer gradient control. The understeer gradient K_{us} is one of the major vehicle dynamic characteristics during cornering.

CIMEV inherently is a severely under steered vehicle due to the free rotation of the casters, however, by using this control it becomes close to a neutral steered one. The understeer gradient controller makes α_f smaller by giving the positive feedback of the estimated lateral force $\hat{Y}$ to the direct yaw moment M_z, and thus it virtually makes the cornering stiffness C_f larger: refer to [32]. Consequently K_{us} can be controlled to approach zero. The control scheme is shown in Fig. 2.13, and the experimental results are shown in Fig. 2.14 and 2.15. The vehicle ran on a circle and was accelerated from 0 to 4 m/s.

Usually a passenger vehicle is understeered, and has a peak in yaw rate gain at a certain vehicle speed called the characteristic speed V_{char}, like the red dotted case in Fig. 2.14 and 2.15, so the radius of cornering gets bigger as the vehicle accelerates. On the other hand, the neutral steered vehicle can run on a circle of a constant radius regardless of its speed, which gives the driver a natural (linear) feeling during cornering. Using the understeer gradient control, the cornering characteristics of CIMEV can be tuned to the driver's favor, i.e. the value can be controlled by changing the gain C_{lat} as shown in Fig. 2.14.

Bank Angle Estimation

Another advantage of using the lateral force observer is the estimation of the road bank angle on which the vehicle is running. It is based on a simple kinematic relation between the gravitational force and the lateral force of the front wheels as shown in Fig. 2.16 without using any

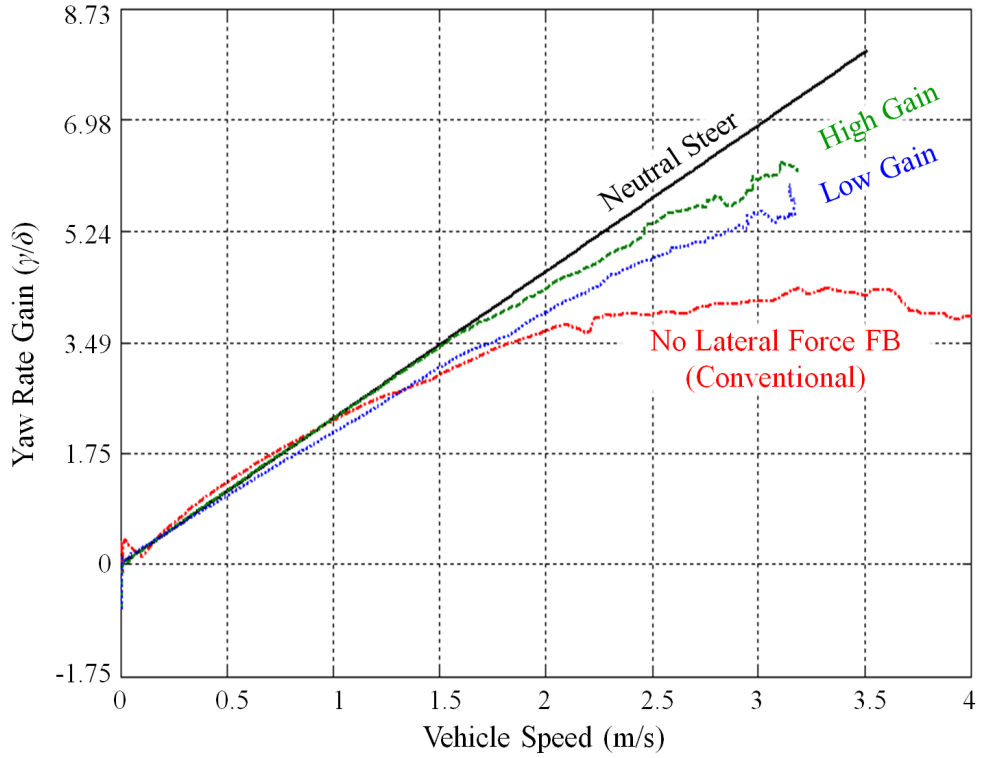

Figure 2.14: Understeer gradient control: Change in slope (understeer gradient K_{us}).

special sensors. When a vehicle is running straight on a road which has a bank angle of φ, from the kinematic relation it is expressed as:

$$\hat{Y} = \frac{l_r}{L} mg \sin\varphi \tag{2.27}$$

thus φ can be estimated as:

$$\hat{\varphi} = \sin^{-1} \frac{\hat{Y}L}{l_r mg} \simeq \frac{\hat{Y}L}{l_r mg} \tag{2.28}$$

It can be seen in Fig. 2.18 that the two lateral acceleration signals agree well, and the estimated and measured values are acceptable. The bank angle of the road is 10.5 degrees, which assigns 1.79 m/s^2 of lateral acceleration due to gravity. The vehicle was released at $t = 2$ by hand, and the vehicle speed increases up to 2 m/s. As the vehicle starts to run, the lateral force observer works properly.

It is a simple and cost effective method, however in order to apply this method to a passenger vehicle, decoupling the effects of the bank angle and the lateral acceleration during cornering needs to be investigated. Ryu et al. have worked on this issue, using the Global Positioning System (GPS) and the Internal Navigation System (INS) [38]. GPS and INS nowadays are good enough for vehicle state estimation, however, the use of external information, especially

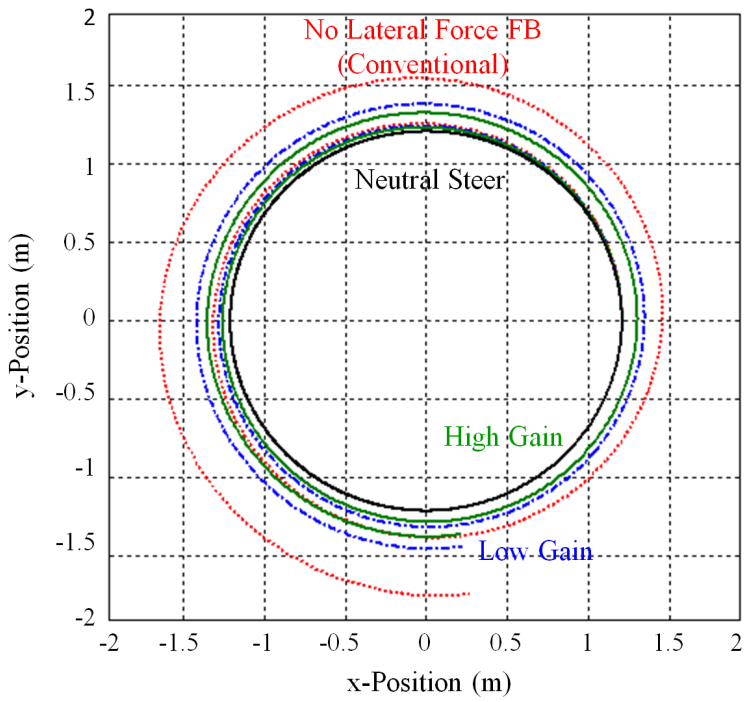

Figure 2.15: Understeer gradient control: Vehicle trajectory during an accelerating circle run.

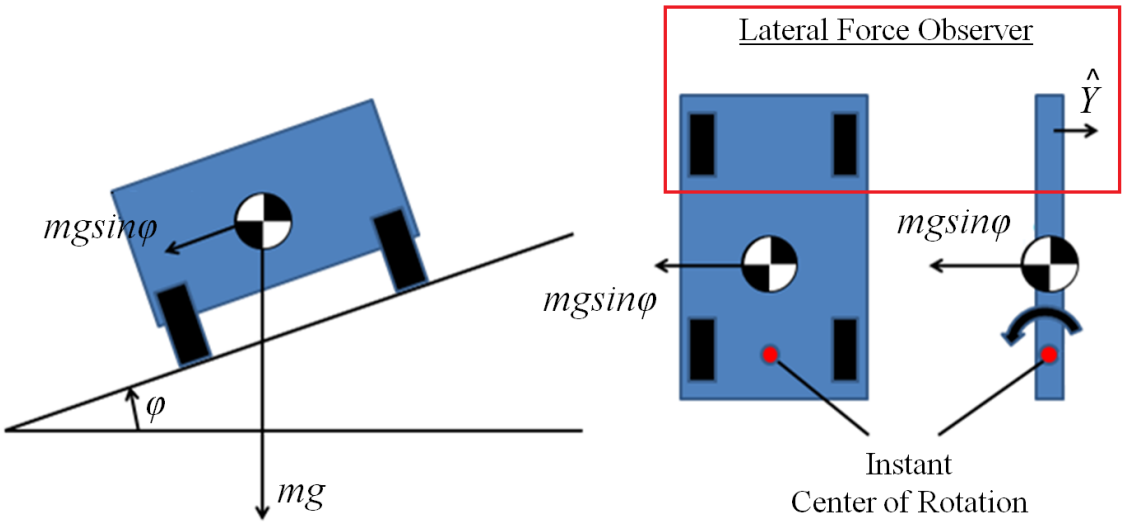

Figure 2.16: Kinematic Relations of Bank Angle Estimation.

GPS, can be a potential risk factor. The proposed mechanism of this work is applicable to eliminate the risk of using external information, by providing the exact measurement internally using kinematics.

Figure 2.17: Bank where the experiment was carried out. The bank angle is 10.5 degrees.

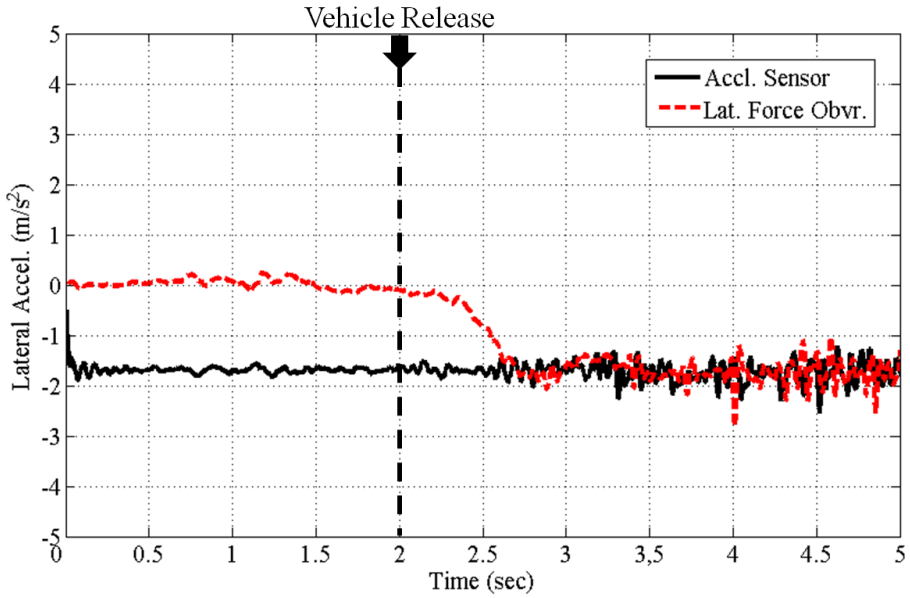

Figure 2.18: Lateral acceleration signal from the acceleration sensor and the lateral force observer. Vehicle is released at $t = 2$, and the vehicle speed increases up to $2m/s$.

2.5 Human-Friendliness of CIMEV

From the discussions and observations above, we can conclude that CIMEV is a suitable form of mobile robots working in human environments. By introducing compliant mechanical elements — caster wheels — in the system, the robot's safety, reliability, and adaptability are improved. The human-friendliness of the global system is evaluated as an example in Chapter 5, to show that CIMEV has higher lumped compliance — which is elaborated in detail in Chapter 5 — than the opponent. In addition to that, the agility in motion and sensitivity to the changes in environment, that the mechanical configuration gives, are the properties required

for human-friendly mobile robots of the future. Note that the general improvements in performance of the proposed system underpin the argument that the human-friendly control should accompany innovations in mechanical design. Table 2.3 shows the summarized comparison between the proposed system and the conventional mobility platform.

Table 2.3: Comparison between CIMEV and the conventional mobility platform.

Criteria	CIMEV	Conventional Platform
Lumped Compliance	High	Low
Safety Velocity	High	Low
Agility	High (zero radius turning)	Low
Maneuverability	Linear and natural	Understeered
Sensitivity to environment	High with observers	None unless sensors are attached

2.6 Summary

In this chapter, a future mobility platform, CIMEV, is configured and introduced based on a thorough study of the required properties for future mobile robot platforms. By adopting compliant mechanical elements – caster wheels here – in the system, the lumped compliance (the human-friendliness) of the whole robot is significantly improved. In addition, the compliant control algorithms exploited in the system help the robot to perceive and adapt itself to the changes of the surrounding environments. Mobile robots working in human environments are required to have high agility, maneuverability, and controllability, which are realized by exploiting the dynamic properties of caster wheels in CIMEV. In sum, the system's safety, reliability, and adaptability are remarkably improved thanks to the compliant control accompanying the mechanical innovations for compliance.

Chapter 3

JUMPBiE and Biologically Inspired Manipulators

In this chapter, biologically inspired manipulators, including JUMPBiE, are introduced. The systems' high compliance, that animal-like musculo-skeletal structure provides, enables safe and human- and environment-friendly motion in robot manipulation. The homogeneity in stiffness distribution and output force characteristics of the bi-articular actuation helps to improve the performance of the robots in human environments. Also, the use of compliant mechanical elements helps to enhance the human-friendliness of robot manipulators.

3.1 Introduction

In many aging societies, demands for robots for welfare and humanitarian purposes are rising. To satisfy these demands and to bring robots closer to the real life, problems regarding safety, performance, and cost must be resolved. Biomimicry is one of many approaches to clear these problems. Mimicry of different organisms, from micro-creatures to primates, can be seen at different levels such as structural, physiological, functional, and behavioral. Many biologically inspired robots have been introduced in recent years, to be successful in achieving given tasks effectively and energy-efficiently [39][40].

As a particular field of bio-mimetic robotics, there are a few research groups, including ours, who are focused on the animal musculo-skeletal structure, especially on bi-articular muscles. The bi-articular actuation is one of the most promising fields of bio-mimetic robotics, due to that bi-articular muscles enable mechanical energy transfer from proximal to distal joints [41][42], impedance modulation in accordance with disturbances [43][44], and thus stabilization and accuracy of motion [45]. In addition, bi-articular muscles help to provide homogeneous output force in respect to working direction, with having transverse force component, from the proximal joint to the tip of the end-effector, which coincides with the direction of the motion [46].

These advantages of bi-articular muscles are particularly appropriate and essential for robots working in human environments. High compliance which bi-articular muscles provide enables safe and, human- and environment-friendly motion of robots. Homogeneity in output force characteristics of bi-articular muscles helps to improve the performance of the robots in human

environments. Last but not least, use of bi-articular muscles effectively can reduce the cost, decreasing the number of actuators required, and thus make robots more affordable and accessible to more latent users. The novelty of the mechanical configuration which enables reduction of the number of actuators and thus in the complexity of control while keeping the advantages of bi-articular actuation, is one of the most important contributions of this work.

3.2 Bi-articularly Actuated Manipulators

A bi-articular muscle refers to a muscle that exerts the same amount of torque to the two adjacent joints simultaneously. The effectiveness of bi-articular muscles in animal motions was extensively studied by Kumamoto et al. [47], showing that the existence of bi-articular muscles enables not only force and energy transmission in animal limbs, but also the precise position control during movement. With bi-articular muscles, it is generally known that animals can move smoothly, rapidly, and precisely without using positional feedback signal of the end-effector; remain stable in their posture regardless of external disturbances; control the stiffness of the extremities by using the antagonistic muscle pair; and easily exert forces in the straight forward direction.

Hogan in [43] proposed a 3-pair 6-muscle two-link manipulator model as shown in Fig. 3.1. as the fundamental structure of an animal limb, including human arms. e_1 and f_1 in the figure are the mono-articular extensor and flexor muscles for the upper joint, e_2 and f_2 are the mono-articular extensor and flexor muscles for the lower joint, and e_3 and f_3 are the bi-articular

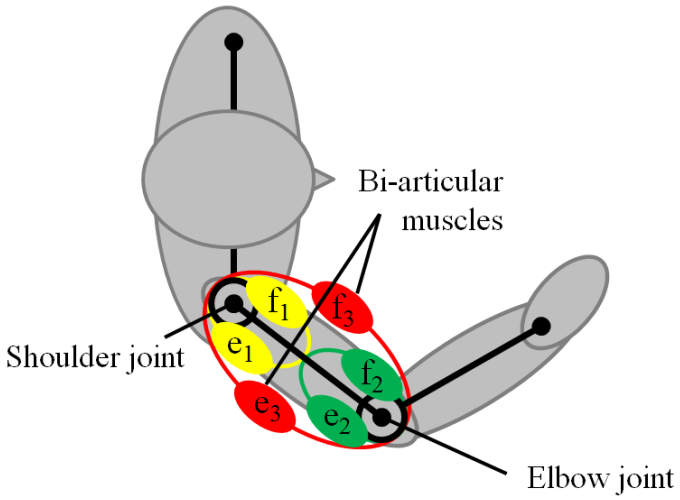

Figure 3.1: The schematic model of a human arm. e_1 and f_1 are the mono-articular extensor and flexor muscles for the shoulder joint, e_2 and f_2 are the mono-articular extensor and flexor muscles for the elbow joint, and e_3 and f_3 are the bi-articular extensor and flexor muscles for the two adjacent joints.

extensor and flexor muscles for the two adjacent joints.

Bi-articularly Actuated Manipulators

The model has been widely accepted and used by many researchers, and its validity has been verified by a number of research works. Especially, researchers from our group — Oh [48], Yoshida [49], Salvucci [50], and Kimura [51] — made great contributions to the field by verifying the model via simulations and experiments. The output force profile and the stiffness ellipse introduced in those works provided in-depth insights into animal motion, and opened possibilities to adopt bi-articular actuation in robot manipulators. Their robots are shown in Fig. 3.2, 3.3, and 3.4.

Figure 3.2: A bi-articularly actuated two-link manipulator using 3 motors and timing belts [49].

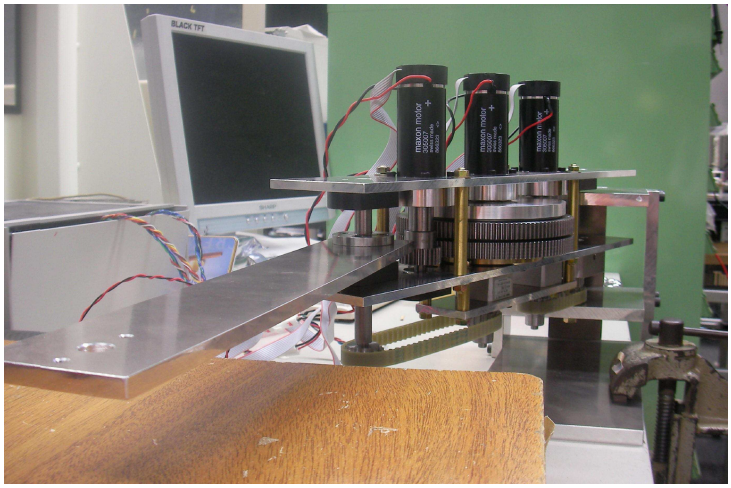

Figure 3.3: A bi-articularly actuated two-link manipulator using 3 motors and planetary gears [51].

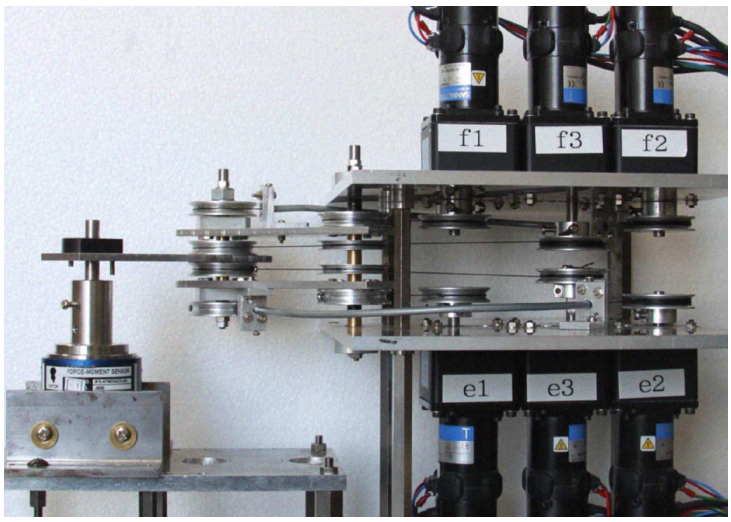

Figure 3.4: BiWi: A bi-articularly actuated two-link manipulator using 6 motors and wire-pulley transmission [50].

Yoshida et al. [49] showed that manipulators of this kind can easily be controlled in a feed-forward way, with a robot arm that has three motors connected to timing belts to transmit the torque they produce (Fig. 3.2), where each motor represents each pair of e_1–f_1, e_2–f_2, and e_3–f_3. Kimura et al. [51] experimentally showed that planetary gears can simulate the torque distribution of the muscles, with a robot arm that has three motors connected to planetary gears (Fig. 3.3), where each motor also represents each pair of e_1–f_1, e_2–f_2, and e_3–f_3. Savucci et al. [50] built a robot arm that has six motors connected to wire to transmit the torque they produce (Fig. 3.4), where each motor also represents each antagonistic muscle of e_1, f_1, e_2, f_2, e_3, and f_3. In sum, these robots provided ways to the implementation of the bi-articular actuation, by proposing various mechanical configurations.

However, there is an important engineering problem remaining in this topic: the redundancy problem. In realizing the 3-pair 6-muscle model in two dimensional space, Yoshida and Kimura respectively used three electric motors, while Salvucci used six electric motors to realize the 3-pair 6-muscles, i.e. these systems are redundant. In animals' case, redundancy provides additional degrees of freedom in motion, which can help to avoid postural singularities, and to back up when partially disabled. However, on the other hand, it is rather too much for robotic systems. High cost and system complexity, brought about by redundancy, estrange robots from the potential users. Moreover, redundancy sometimes imposes difficult control problems in dealing with manipulator statics and dynamics [52].

Mono-Bi Configuration

The main motivation for the proposal of the mono-bi configuration is to reduce redundancy, system complexity and thus cost. Among many researchers, Oh et al. in [53] first attempted to resolve the redundancy problem by elimination, and proposed a way to eliminate it by using combinations of two actuators among three for the two dimensional motion. The results showed that the combination of the mono-articular muscle of the upper joint and the bi-articular muscle

can possibly eliminate the redundancy without losing the output force characteristics. This combination was then named the mono-bi configured system. Based on this, recently Sonokawa et al. introduced a novel leg space coordinate system and velocity control method for two link robotic arm equipped with mono-bi-actuators [54].

Spring-Loaded Mono-Bi Configuration (SLMB)

Furthermore, considering the fact that bi-articular muscles function as an energy transmitter in animals' jumping motion as reported in [41] and [42], a spring can replace an active bi-articular actuator for applications like jumping robots. The system consisting of a mono-articular electric motor and a bi-articular spring is hereafter called the spring-loaded mono-bi (SLMB) configured system. The SLMB can vary in forms according to the output requirements, for example, as shown in Fig. 3.5. JUMPBiE adopts the first variation of the SLMB configurations, based on the consideration that it has to have capability to jump forward and backward.

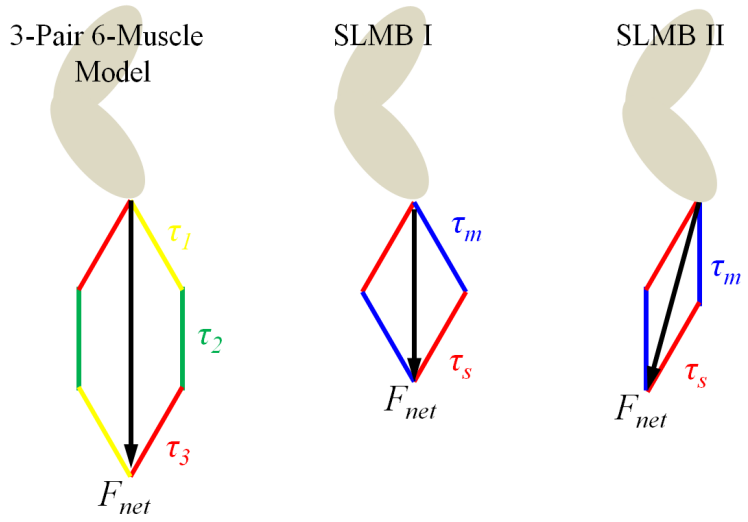

Figure 3.5: 3-pair 6-muscle model and the variations of SLMB configuration. SLMB I has isotropic output force characteristics, while that of SLMB II is slated. The directionality can be counseled with the design requirements of each specific application.

3.3 JUMPBiE

An mono-pedal robotic leg, JUMPBiE (Jumping Leg using Passive Bi-articular Elements; shown in Fig. 3.6) is designed and fabricated to experimentally verify the feasibility and the effectiveness of the SLMB configuration.

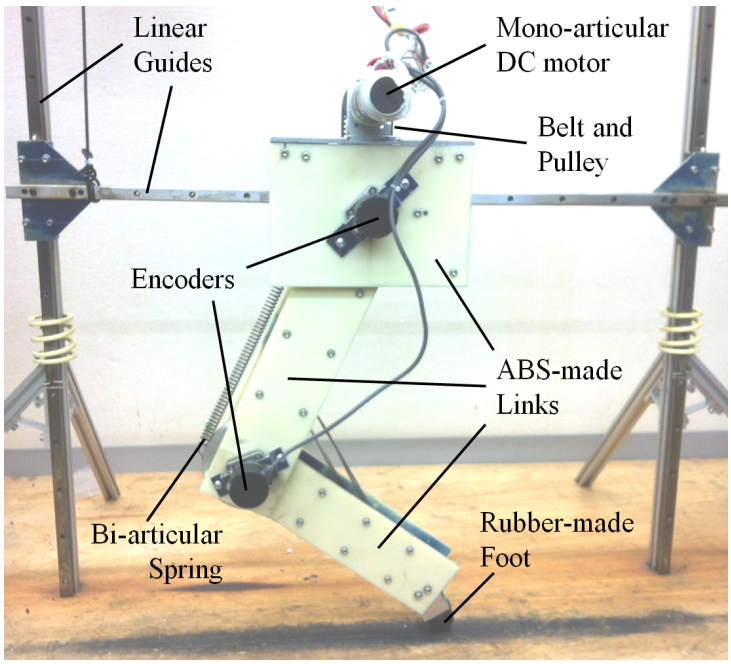

Figure 3.6: A mono-pedal robotic leg with a bi-articular spring and a mono-articular electric motor, JUMPBiE.

Robot Design

Its design background and basic control strategy are introduced in [55] and [56]. JUMPBiE has one electric motor attached to the upper joint, and a passive bi-articular spring which applies torque to the upper and the lower joint simultaneously. The theoretical background of the system is elaborated in detail in [48], [50], and [51].

The construct of the robot leg and body is made of ABS, which is the toughest engineering plastic with over 300 J/m of Izod impact strength, the half of aluminum. At the same time the specific weight of ABS is 1.05, which is much lighter than aluminum which has 2.69, and still strong enough to endure the impact of jumping. For the mono-articular actuator, a 150W DC motor with 1/43-reduction ratio was chosen, together with a tensional spring whose stiffness is 1.88N/mm, which is equivalent to 4.70 Nm/rad. Two links are fixed and free to rotate at the hip and knee joints, while the robot body is fixed to a 2-DOF linear guide, which allows two dimensional translational motion but prevents rotation. Two encoders of 3600 ppr are attached to each joint to measure the angular displacements, and the Compact RIO of National Instruments Corp. is used as the controller. The control period is set at 1 kHz.

From the mechanical design of the robot, the necessary torque and power for jumping can be calculated using Jacobian. Due to the kinematics of the bi-articular linkage, the motor only need to compensate the horizontal force exerted from the bi-articular spring. By using the kinematics, we can calculate the necessary torques given that the weight of the robot is known. For example, assuming that the resting position of the robot is at $\theta_1 = -30$ degrees and $\theta_2 = 60$ degrees, the necessary net force which should be exerted by both the motor and spring is equal to the weight of the robot, i.e. say 80 N including the weight of the linear guide. Thus the spring should exert 100 N, and regarding the range of the leg rotation, the spring constant should be

around 2 N/mm and its initial length should be less than 10 cm. To compensate the horizontal force exerted by the spring, which is around 50 N at the resting position.

The mechanical parameters of JUMPBiE are indicated in Table 3.1. The values are measured, and/or computed based on the measured ones.

Table 3.1: Physical Parameters

Parameters	Meanings	Values
M	total mass	6.55 kg
M_c	counter mass	3.65 kg
M_e	effective mass	2.90 kg
m_1	mass of l_1	0.371 kg
m_2	mass of l_1	0.308 kg
I_1	Inertia moment of l_1 at the hip joint	0.0808 kgm^2
I_2	Inertia moment of l_2 at the knee joint	0.0019 kgm^2
l	Length of each link	0.300 m
K_s	bi-articular spring coefficient	4.70 Nm/rad
g	gravitational acceleration	9.81 m/s^2

Kinematics of the System

Oh et al. showed the effectiveness of the mono-bi configuration in the two-link manipulator [53]. When considering economy and performance, it is shown that using the mono-articular actuator in the upper joint and the bi-articular one between the upper and the lower joints is effective.

The system schematic is shown in Fig. 3.7. Assuming that the length of each link is identical without losing generality [53], i.e.:

$$l_1 = l_2 = l \tag{3.1}$$

the kinematics of the system can be described as:

$$\begin{aligned} \begin{bmatrix} \tau_m \\ \tau_s \end{bmatrix} &= J_m^T \begin{bmatrix} f_x \\ f_y \end{bmatrix} \\ &= l \begin{bmatrix} -s_1 & c_1 \\ -s_{12} & c_{12} \end{bmatrix} \begin{bmatrix} f_x \\ f_y \end{bmatrix} \end{aligned} \tag{3.2}$$

$$\begin{bmatrix} f_x \\ f_y \end{bmatrix} = \frac{1}{l s_2} \begin{bmatrix} c_{12} & -c_1 \\ s_{12} & -s_1 \end{bmatrix} \begin{bmatrix} \tau_m \\ \tau_s \end{bmatrix} \tag{3.3}$$

where $s_i = \sin\theta_i$, $c_i = \cos\theta_i$, $s_{ij} = \sin(\theta_i + \theta_j)$, and $c_{ij} = \cos(\theta_i + \theta_j)$. τ_m is the output torque of the mono-articular motor, and τ_s is the bi-articular spring torque. The modified Jacobian matrix J_m^T has its inverse unless $\theta_2 = \pi/2 + n\pi$, which cannot be reached due to that lower link is mechanically constrained to the range of $\pi/12 \leq \theta_2 \leq \pi/3$.

And the bi-articular spring torque τ_s is represented as follows from its construct:

$$\tau_s = -K_s \Delta(\theta_1 + \theta_2) \tag{3.4}$$

where, K_s represents the torsional stiffness of the bi-articular spring in [Nm/rad].

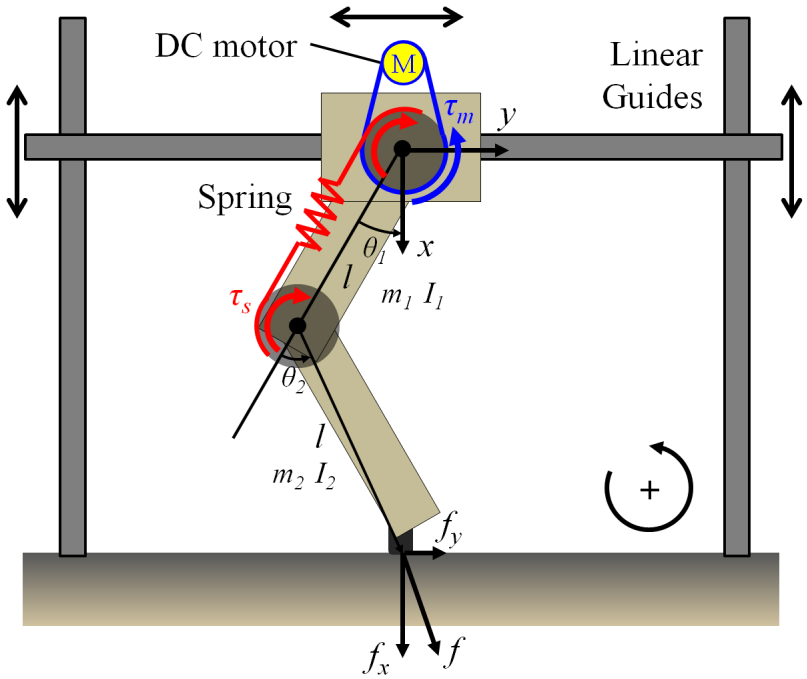

Figure 3.7: The system construct and the frame of reference.

Dynamics of the System

The dynamics of the system is written as follows. Coulomb friction is neglected.

$$M(\Theta)\ddot{\Theta} + C(\Theta, \dot{\Theta}) + V\dot{\Theta} + G(\Theta) = T \tag{3.5}$$

where,

$$\Theta = [\theta_1 \ \theta_2]^T \tag{3.6}$$

$$T = [\tau_m + \tau_s \ \tau_s]^T \tag{3.7}$$

$$M(\Theta) = \begin{bmatrix} M_{11} & M_{12} \\ M_{21} & M_{22} \end{bmatrix} \tag{3.8}$$

$$C(\Theta, \dot{\Theta}) = \begin{bmatrix} -2R\dot{\theta}_1\dot{\theta}_2 s_2 - R\dot{\theta}_2{}^2 s_2 \\ R\dot{\theta}_1{}^2 s_2 \end{bmatrix} \tag{3.9}$$

$$V = \begin{bmatrix} V_1 & 0 \\ 0 & V_2 \end{bmatrix} \tag{3.10}$$

$$G(\Theta) = \begin{bmatrix} G_1 \\ G_2 \end{bmatrix} \tag{3.11}$$

and

$$M_{11} = I_1 + I_2 + \frac{1}{4}m_1 l^2 + \frac{5}{4}m_2 l^2 + m_2 l^2 c_2 \tag{3.12}$$

$$M_{12} = M_{21} = I_2 + \frac{1}{4}m_2 l^2 + \frac{1}{2}m_2 l^2 c_2 \tag{3.13}$$

$$M_{22} = I_2 + \frac{1}{4}m_2 l^2 \tag{3.14}$$

$$R = \frac{1}{2}m_2 l^2 \tag{3.15}$$

$$G_1 = gl\left(\frac{1}{2}m_1 s_1 + \frac{1}{2}m_2 s_{12} + m_2 s_1\right) \tag{3.16}$$

$$G_2 = \frac{1}{2}g m_2 l s_{12} \tag{3.17}$$

where, the viscous friction coefficients V_1 and V_2 are empirical values. The parameters shown in the Table 3.1 are used for the others.

The output force of the manipulator, described in (3.3), results in the ground reaction force f_{GRF} when the tip of the end-effector touches the ground. Then, the jumping motion of the robot leg can be simply modeled as that of a rigid body using f_{GRF} as the propulsion force, as shown in Fig. 3.8.

The simplified model is described as follows.

$$(M + M_c)\ddot{x} + V_x\dot{x} = f^x_{GRF} - (M - M_c)g \tag{3.18}$$

$$M\ddot{y} + V_y\dot{y} = f^y_{GRF} \tag{3.19}$$

where, the coefficients V_x and V_y have empirical values resulting from the viscous friction of the linear guides. And the momentum is written as:

$$(M + M_c)\dot{x}_0 = \int_0^\tau (f^x_{GRF} - (M - M_c)g - V_x\dot{x})dt \tag{3.20}$$

$$M\dot{y}_0 = \int_0^\tau (f^y_{GRF} - V_y\dot{y})dt \tag{3.21}$$

where, $\dot{x}_0$ and $\dot{y}_0$ are the velocities of the rigid body in x- and y- direction at the very moment of each take-off. These are the entities that be controlled during jumping motion, due to the fact that the momentum of the rigid body relies on the impulse transmitted from the ground. τ is the duration of ground contact.

Bouncing Direction Control

By using the mono-bi configuration, the output stiffness seen at the end-effector can be modeled as Fig.3.9. Since the bi-articular torque is given by passive elements, the stiffness of the springs K_{Spring} is fixed.

By arranging the magnitude of the motor stiffness K_{Motor}, the net stiffness seen at the end-effector can be controlled in the vicinity of the resting position.

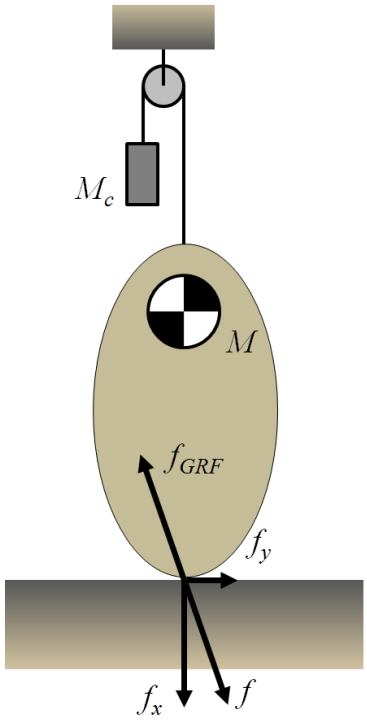

Figure 3.8: Jumping motion of a rigid body is assumed. The ground reaction force f_{GRF} works as the propulsion force of the rigid body M. A counter mass M_c is used to lighten the effective mass.

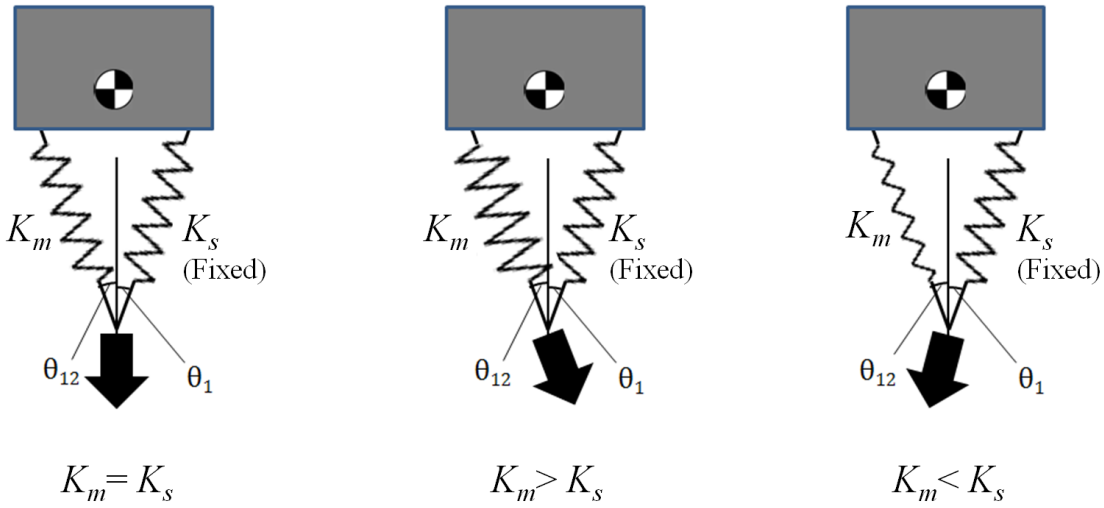

Figure 3.9: Equivalent spring model of the mono-bi configuration. Note that $\theta_{12} = \theta_1 + \theta_2$.

The direction of the net stiffness at the end-effector can be controlled by changing the motor stiffness of the upper joint J_1. For the propulsion control of JUMPBiE, the net stiffness model shown in Fig.3.9– the equivalent spring model is used. Note that the magnitude of the net

stiffness also changes along with the direction.

For the implementation of the concept, a simple feedback control loop (Fig. 3.10) is designed. The initial resting position is given, and the control loop tries to regulate the position at the initial. Then the feedback gain K_{Motor} is seen as the stiffness of the motor, as the motor applies torque to the upper joint J_1 with a magnitude which is proportional to the angular displacement of J_1.

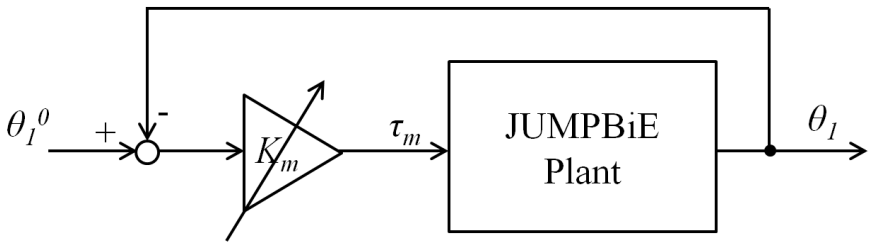

Figure 3.10: Feedback control loop.

Considering the mechanical design and the control logic of the robotic leg:

$$\tau_{motor} = -K_M \Delta\theta_1 \tag{3.22}$$
$$\tau_{spring} = -K_S \Delta(\theta_1 + \theta_2 + R) \tag{3.23}$$

where R means the residual displacement of the spring, its mathematical model, equation (3.3) can be rewritten as:

$$\begin{bmatrix} F_{X_l} \\ F_{Y_l} \end{bmatrix} = \begin{bmatrix} \frac{1+c_2}{s_2 l_m}\big((K_S - K_M)\Delta\theta_1 + K_S\Delta\theta_2 + K_S R\big) \\ -\frac{1}{l_m}\big((K_S + K_M)\Delta\theta_1 + K_S\Delta\theta_2 + K_S R\big) \end{bmatrix} \tag{3.24}$$

Around the vicinity of the initial position where θ_1 and θ_2 are given, the net stiffness seen at the end-effector changes in its magnitude and direction as shown in Fig. 3.11. Then the robotic leg acts like a basketball, bouncing on the ground with a controlled ground reaction force.

Experimental Results

With the control concept shown in the previous section, simple experiments are done. While changing the motor stiffness K_{Motor}, JUMPBiE was dropped from a certain height to see the direction and the magnitude of the reaction force at the ground. Fig.3.12.3.13. and 3.14. show the stroboscope pictures taken at every 10ms from release. Time flows from left to right, and from top to bottom.

By setting K_{Motor} equals to K_{Spring}, JUMPBiE jumps in place without moving its center of mass laterally (See Fig.3.12). The lowest point comes at t=90ms, in the 10th frame.

By setting K_{Motor} smaller than K_{Spring}, JUMPBiE jumps forward, to the right in the picture (See Fig.3.13). The lowest point comes at t=140ms, in the 15th frame.

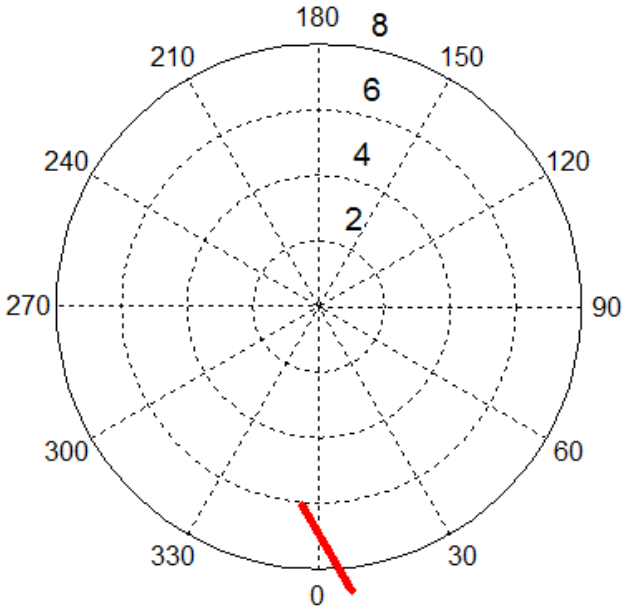

Figure 3.11: The net stiffness K_{equiv} with changing K_M. The magnitude is in N/mm, given that $\theta_1 = -\frac{\pi}{6}$ and $\theta_2 = \frac{\pi}{3}$. (Calculated)

By setting K_{Motor} larger than K_{Spring}, JUMPBiE jumps backward, to the left in the picture (See Fig.3.14). The lowest point comes at t=70ms, in the 8th frame.

It is shown that the mono-bi-configuration with passive bi-articular elements can be an effective solution for the propulsion for a robotic leg only using a simple feedback control. However, the magnitude of the net stiffness changes along with the direction, which causes the change in jumping frequency. As it can be observed in the experimental results, when the net stiffness is large (jumping backwards) the frequency is high, while the frequency is low if the net stiffness is small (jumping forward).

State Feedback and Impulse Shaping

Based on the model developed in the previous section, the state feedback controller is designed. And the actual parameters are used for the study.

State Space Representation

Equations introduced in the previous section are transformed into state space representation. By substituting all parameters, the model is rewritten into the form below.

$$\ddot{\theta_1} = 0.103(\dot{\theta_2}^2 + 2\dot{\theta_1}\dot{\theta_2}) + 0.152\dot{\theta_1}^2 + 17.2$$
$$+19.3(\theta_1 + \theta_2) - 0.0855\dot{\theta_1} + 0.0632\dot{\theta_2} + 8.55\tau_m \quad (3.25)$$
$$\ddot{\theta_2} = -1.34\dot{\theta_1}^2 - 0.152(\dot{\theta_2}^2 + 2\dot{\theta_1}\dot{\theta_2}) - 245$$
$$-467(\theta_1 + \theta_2) + 0.127\dot{\theta_1} - 0.561\dot{\theta_2} - 12.7\tau_m \quad (3.26)$$

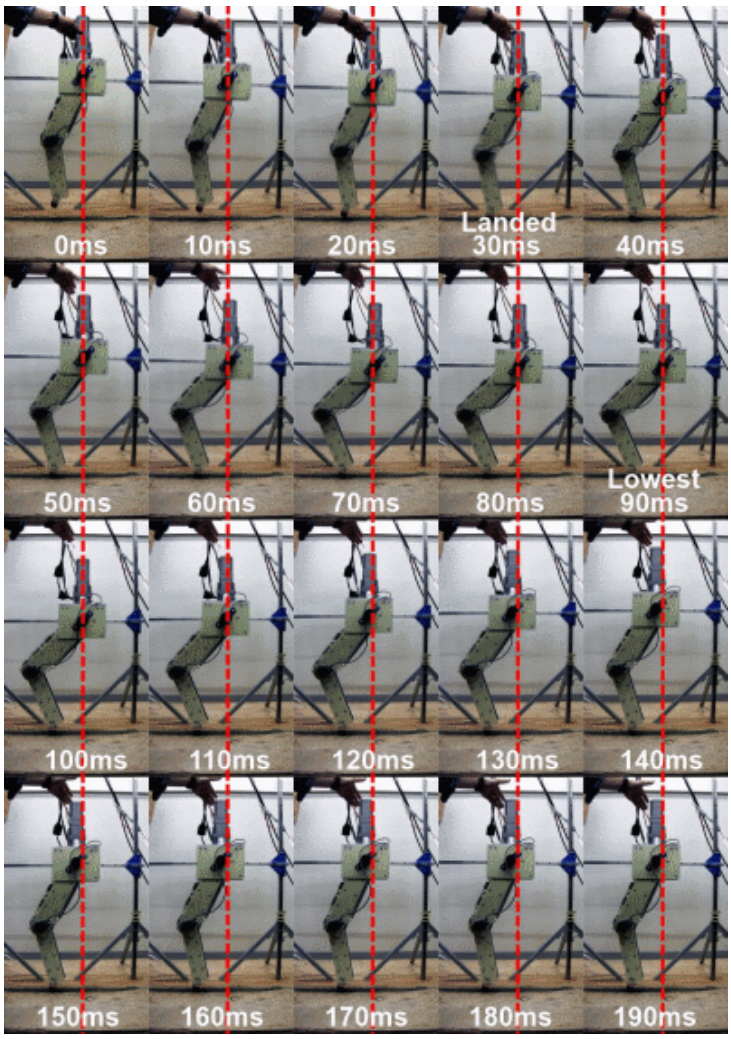

Figure 3.12: Jumping in place. K_{Motor} equals to K_{Spring}. Taken at every 10ms from release. The lowest point comes at t=90ms.

Then the equations are linearized around the vicinity of the operating position, which is the given initial position of $\theta_{10} = -pi/6$ and $\theta_{20} = pi/3$, and transformed into the state space system representation. Constant terms are canceled out at the initial position due to the fact that motor torque balances the residual spring torque to stand still. Then, the system is written as follows.

$$\dot{X} = AX + B\tau_m \tag{3.27}$$

$$Y = CX + D\tau_m \tag{3.28}$$

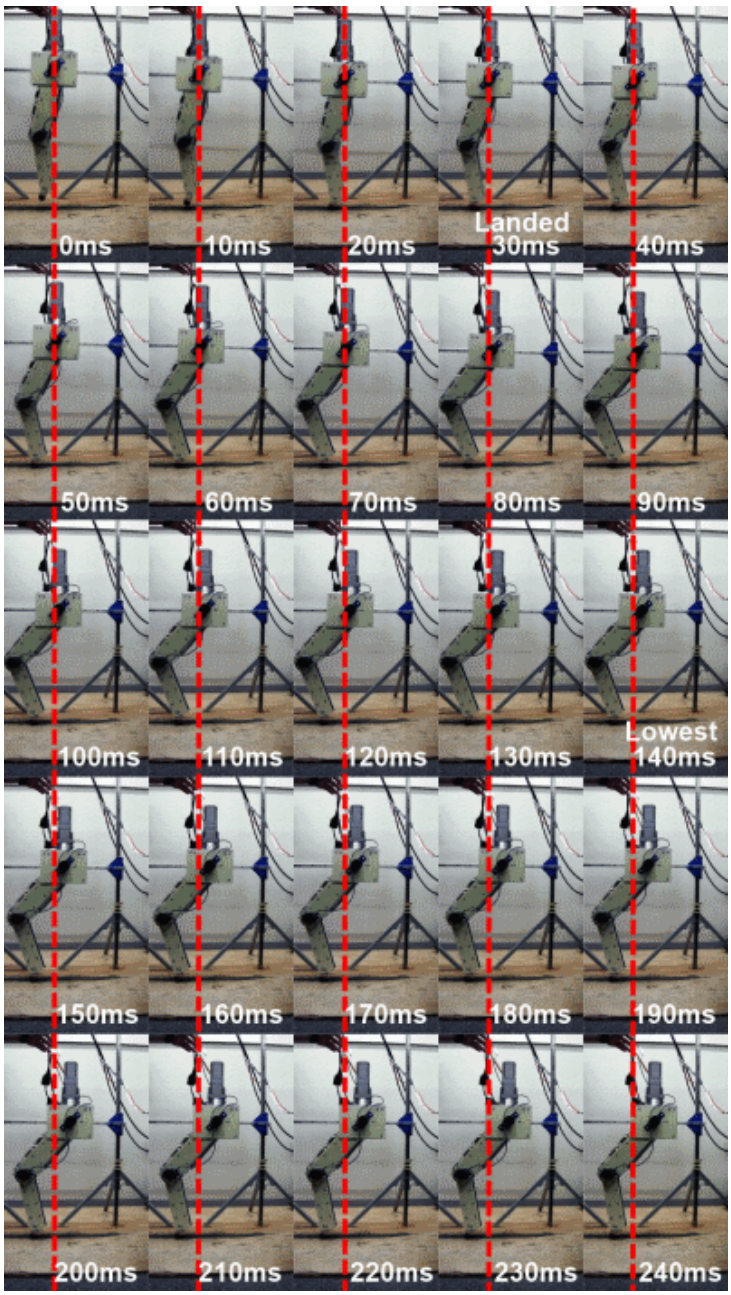

Figure 3.13: Jumping forward. K_{Motor} is smaller than K_{Spring}. Taken at every 10ms from release. The lowest point comes at t=140ms.

where,

$$X = \begin{bmatrix} \theta_1 \\ \theta_2 \\ \dot{\theta}_1 \\ \dot{\theta}_2 \end{bmatrix} \tag{3.29}$$

$$Y = \begin{bmatrix} f_x \\ f_y \end{bmatrix} \tag{3.30}$$

$$r = \begin{bmatrix} f_x^{ref} \\ f_y^{ref} \end{bmatrix} \tag{3.31}$$

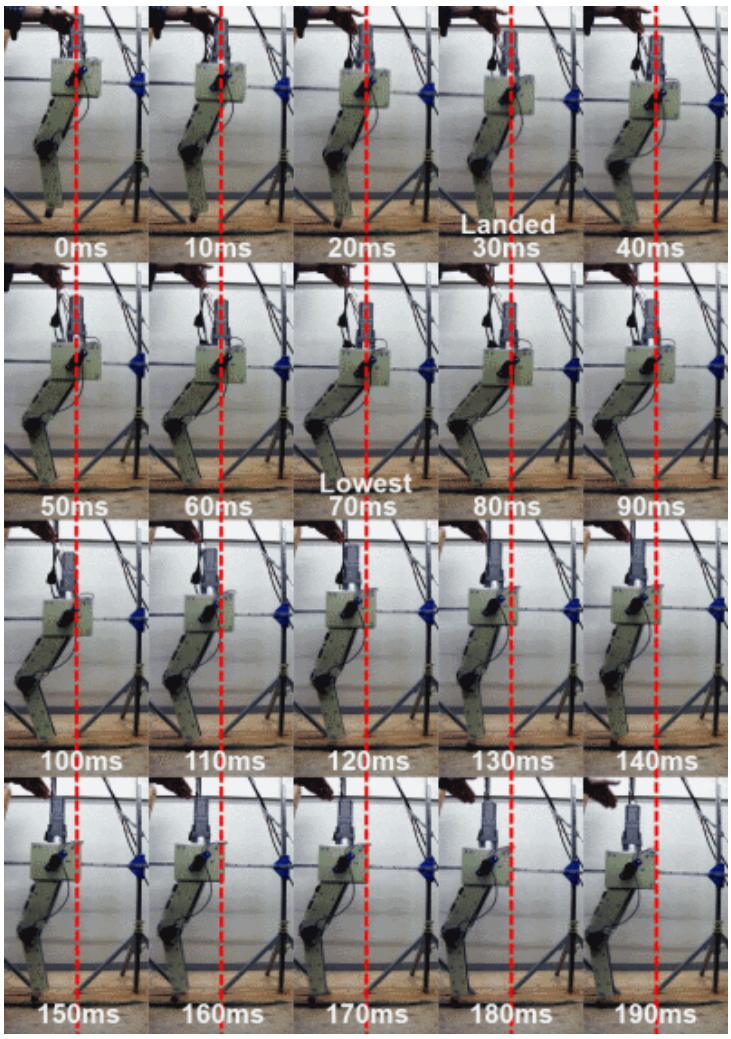

Figure 3.14: Jumping backward. K_{Motor} is larger than K_{Spring}. Taken at every 10ms from release. The lowest point comes at t=70ms.

The system matrices are written as:

$$A = \begin{bmatrix} 0 & 0 & 1 & 0 \\ 0 & 0 & 0 & 1 \\ 19.3 & 19.3 & -0.0855 & 0.0632 \\ -467 & -467 & 0.127 & -0.561 \end{bmatrix} \tag{3.32}$$

$$B = \begin{bmatrix} 0 \\ 0 \\ 8.55 \\ -12.7 \end{bmatrix} \tag{3.33}$$

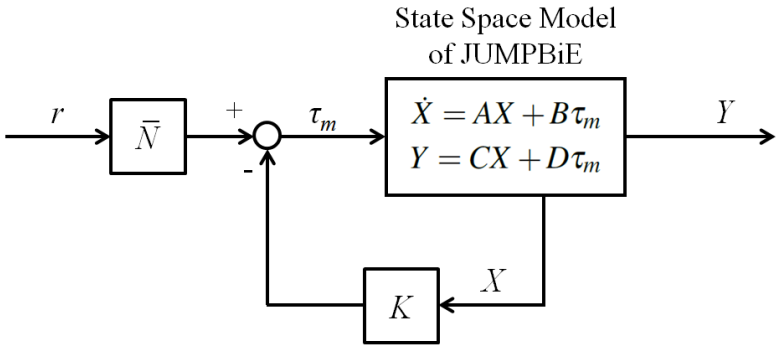

Figure 3.15: State Feedback Control Schematic of JUMPBiE.

and from the kinematics in (3.3),

$$C = \begin{bmatrix} 15.7 & 15.7 & 0 & 0 \\ -9.05 & -9.05 & 0 & 0 \end{bmatrix} \tag{3.34}$$

$$D = \begin{bmatrix} 3.33 \\ 1.92 \end{bmatrix} \tag{3.35}$$

Using this system, a state feedback loop is designed as shown in Fig. 3.15. The feedback gain matrix K is designed via pole placement to assign multiple poles at -10 rad/sec, as below.

$$K = \begin{bmatrix} -34.4 & -37.1 & -6.15 & -7.24 \end{bmatrix} \tag{3.36}$$

Then the closed loop system can be rewritten as follows.

$$\begin{aligned} A_{cl} &= A - BK \\ &= \begin{bmatrix} 0 & 0 & 1 & 0 \\ 0 & 0 & 0 & 1 \\ 313 & 337 & 52.5 & 62.0 \\ -904 & -938 & -78.0 & -92.5 \end{bmatrix} \end{aligned} \tag{3.37}$$

$$\begin{aligned} B_{cl} &= B \\ &= \begin{bmatrix} 0 \\ 0 \\ 8.55 \\ -12.7 \end{bmatrix} \end{aligned} \tag{3.38}$$

$$\begin{aligned} C_{cl} &= C - DK \\ &= \begin{bmatrix} 130 & 139 & 20.5 & 24.1 \\ 57.0 & 62.2 & 11.8 & 14.0 \end{bmatrix} \end{aligned} \tag{3.39}$$

$$\begin{aligned} D_{cl} &= D \\ &= \begin{bmatrix} 3.33 \\ 1.92 \end{bmatrix} \end{aligned} \tag{3.40}$$

Now, the input gain $\bar{N}$ which shapes the force output of the end-effector is designed. $\bar{N}$ is designed by scaling the force gains as follows.

$$\bar{N} = \begin{bmatrix} 2.52 & 5.04 \end{bmatrix} \tag{3.41}$$

Then the force reference r can be designed as follows.

$$\begin{bmatrix} f_x^{ref} \\ f_y^{ref} \end{bmatrix} = \begin{bmatrix} P \\ V_y \left(0.52\dot{\theta}_1 + 0.26\dot{\theta}_2\right) \end{bmatrix} \tag{3.42}$$

where, P is the derivative of an arbitrary impulse, which provides the robot with necessary jumping momentum, and V_y is empirically set.

Simulation Results

A simulation study was done with the given initial position of $\theta_{10} = -pi/6$ and $\theta_{20} = pi/3$, using the physical parameters shown in Table I. P in (3.42) was given as a square wave at every two second for 100 ms, with the magnitude equivalent to 10 Nm at Joint 1.

The resultant output force is shown in Fig. 3.16 without state feedback or impulse shaping. It is oscillatory because of the existence of the bi-articular spring. The result with state feedback and impulse shaping is shown in Fig. 3.17; in can be confirmed that the system is stabilized. The shape of the force in each direction is similar to each other, while there exists the difference in magnitude. It is assumed that when the robot is off the ground, the manipulator output forces do not act on the ground, i.e. the ground does not react. They act and react only when the robot leg is touching the ground.

Fig. 3.18 shows the impulse resulting from the robot-ground action and reaction considering these different jumping phases. The sharp rises in impulse during the first 100 ms enable the robot to take off, however at the same time, to a certain degree the robot moves in horizontal direction according to the magnitude of the horizontal impulse. This is due to the fact that the output forces in x- and y- direction are strongly coupled because of the SLMB construct.

Fig. 3.19 shows the simulated trajectory of the center of gravity of JUMPBiE, when the impulse introduced above is given. The trajectory seems rather erratic, because the oscillation cycle of the equivalent stiffness of the whole robot does not coincide with the period of the impulse given. The SLIP (Spring-Loaded Inverted Pendulum) model in [58] and [59], which packages the robotic leg as a mass-spring model, gives hints for solving this problem.

The SLMB construct improves the cost performance of the system, however at the same time it generally imposes instability to the system such as the oscillatory behavior. As the simulation study result implies, by using state feedback and impulse shaping technique, the robot can be stabilized and made to jump.

3.4 Human-Friendliness of JUMPBiE

In general, the result is comparable to that of [57], where four linear actuators are used in realizing jumping motion. One linear actuator is used for bi-articular muscle, another for mono-articular muscle for the upper joint, and the other two for mono-articular muscles for the lower joint. Since both JUMPBiE and the opponent are using bi-articular actuation in their mechanical configuration, they show equivalence in the lumped compliance, safety velocity, and output

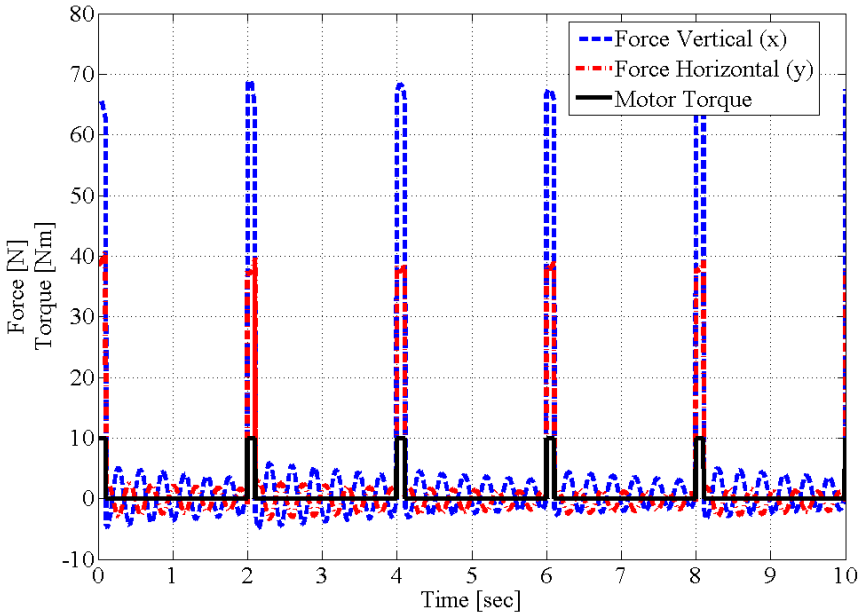

Figure 3.16: End-effector output force without state feedback or impulse shaping. The bi-articular spring makes the system oscillatory.

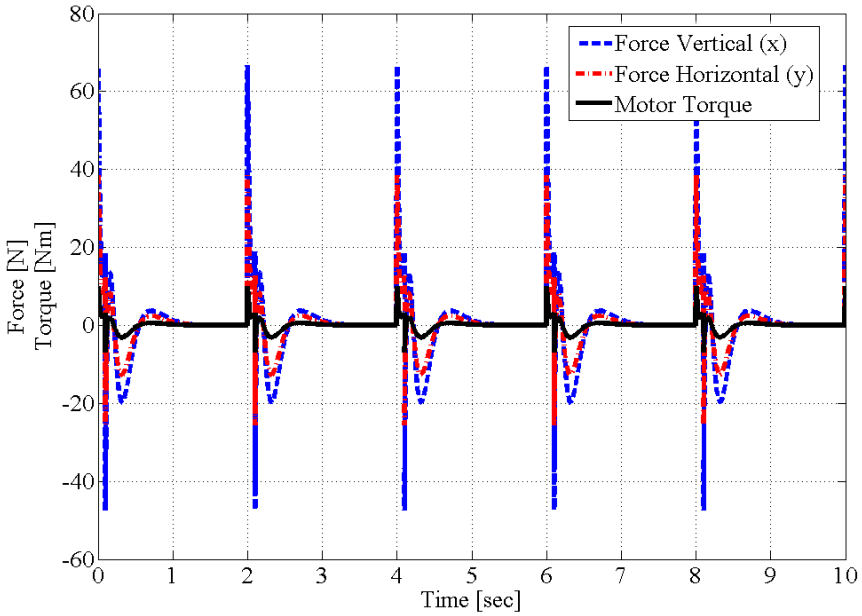

Figure 3.17: End-effector output force when using state feedback and impulse shaping.

isotropy. However, for the same motion, JUMPBiE uses the SLMB configuration which makes the system much simpler and more affordable. Thus, in a broad sense, it can be said that JUMP-BiE has more human-friendly characteristics than the opponent. Table 3.2 shows a comparison

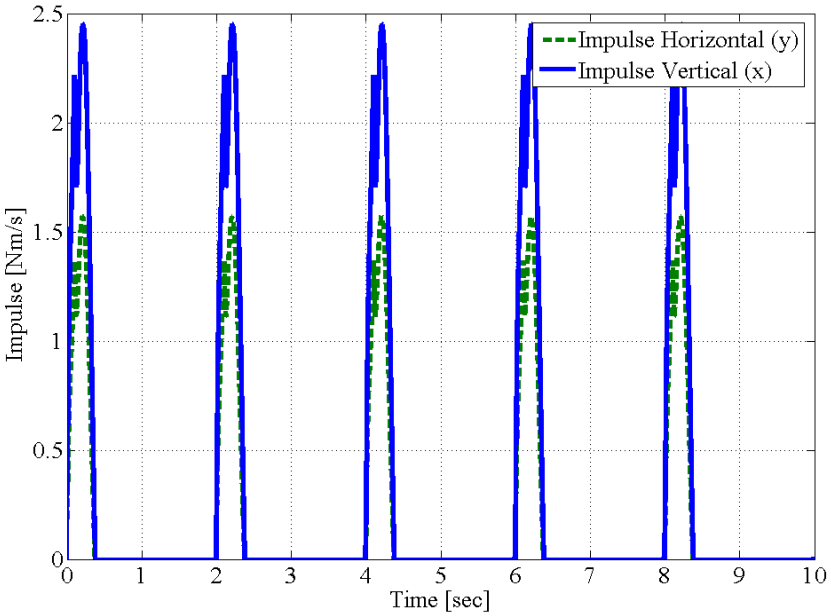

Figure 3.18: Impulse resulting from the end-effector output and its ground reaction force.

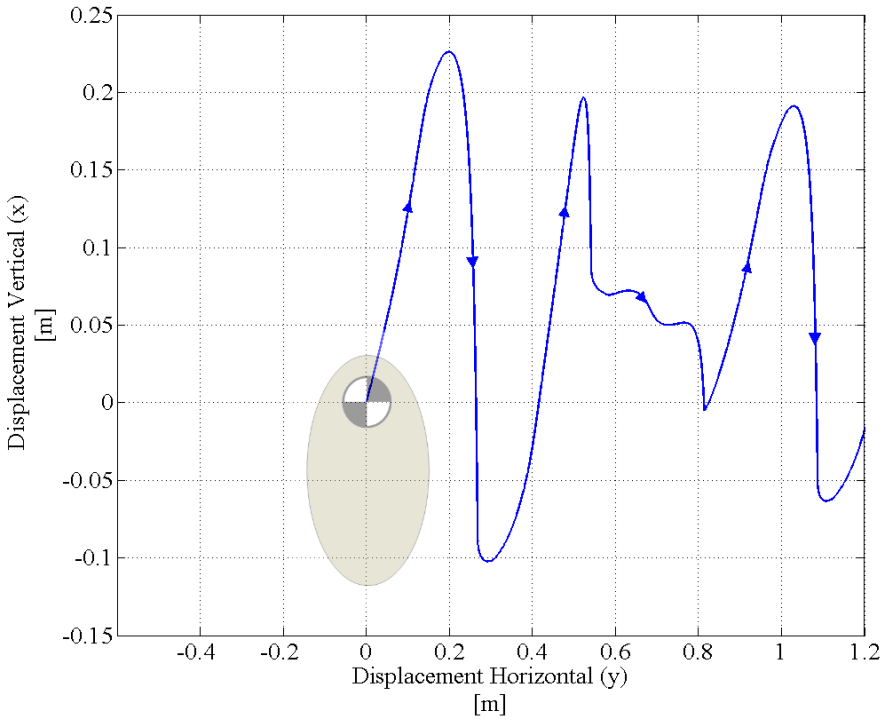

Figure 3.19: Simulated trajectory of the center of mass of JUMPBiE when the impulse is given in a feed-forward fashion.

between JUMPBiE and its opponent in terms of the human-friendliness.

The human-friendliness of JUMPBiE comes from its use of bi-articular actuation along with springs, which are inherently compliant. JUMPBiE's mechanical construct, the SLMB, enables reduction of the number of actuators, and thus reduction in the complexity of control, and at the same time retains the advantages of bi-articular actuation: energy efficiency, high compliance, and homogeneity in force output. And as shown in the simulation study, by using state feedback and the impulse shaping technique, the robot jumps in a stable way, resolving the inherent instability due to the existence of the bi-articular spring. The SLMB configuration is the solution for robot actuation in human environment, optimizing cost and guaranteeing compliance.

Table 3.2: Comparison between JUMPBiE and its opponent.

Criteria	JUMPBiE	Opponent [57]
Lumped Compliance	High	High (Linear motor)
Safety Velocity	High	High
Number of Actuators	1	4
Output Isotropy	Good	Good
Sensitivity to environment	High	Medium

3.5 Summary

In this chapter, biologically inspired manipulators, including JUMPBiE, are introduced. The systems' high compliance, that animal's musculo-skeletal structures provide, enables safe and human- and environment-friendly motion in robot manipulation. The homogeneity in stiffness distribution and output force characteristics of the bi-articular actuation helps to improve the performance of the robots in human environments. It is also shown that the use of compliant mechanical elements also helps to enhance the human-friendliness of robot manipulators.

Chapter 4

H-FEX: An Exoskeleton for Rehabilitation

In this chapter, a human-friendly exoskeleton for rehabilitation, H-FEX, is introduced after a thorough consideration on the human bio-mechanical characteristics. Based on a study on human body kinematics and muscle activation, an algorithm to estimate the muscle group activation rates during gait is formulated. Then, the estimation result leads us to the implementation of an advanced design and control for exoskeletons for rehabilitation, by specifying the deteriorated muscle groups, where to assist. Moreover, the viscoelastic characteristics of human muscles opens a way to the extensive use of springs and dampers, which eventually enhance the human-friendliness of the devices.

4.1 Introduction

With continually increasing life expectancies and decreasing birth rates, many issues regarding aging are rising in importance in many societies around the world. Concerns regarding incidences of age-related pathologies are a part of the issues. In treating those patients, rehabilitating them, and helping them return to their daily lives and enjoy them, robot technologies and applications have contributed enormously, and their missions are expected to grow in importance. In an attempt to deal with these issues, there are robots that are attached to physically disabled patients on their disabled parts of body. Especially, walking assist devices help them at a very fundamental level, considering the importance of walking ability in human life. Due to the fact that walking ability is essential for quality of life and participation in social and economic activities, gait disorders eventually disturb the patients' life itself. As the world population becomes older, the demand for such devices is increasing and expected to grow more. Moreover, not only the patients suffering from age-related pathologies involving gait disorders, such as Parkinson's Disease and the stroke, but also the young patients who have gait disorders caused by congenital and acquired diseases are the beneficiaries.

Many walking assist devices have been introduced and commercialized to rehabilitate the patients, and help them to return to their daily life activities. For example, the AlterG Bionic Leg of AlterG Inc. is well know for its performance improving the mobility of stroke patients. ReWalk is also a well known personal exoskeletal rehabilitation system, which allows the user to sit, stand, turn, and climb and descend stairs. Some other works of the field show the increasing interests in the interaction between the patient and the robotic system utilizing

combined sensors and actuators as in [62] and [63]. They measure the force and torque of the user's body, and decide whether and how to augment them — in most cases simply amplifying them — which is inherently an indirect way, compared to the ones based on the segmental characteristics of the human body beforehand.

However, studies on the intrinsic characteristics the human limbs and relating them to the assist devices, are relatively few in the literature considering the substantial importance. Meanwhile, there are a number reported research works that tried identifying the parameters using external measurements, Hatze [64] first showed in 1981 that the external information of constraint forces and moments along with the human body dynamics could make the system of equations overdetermined, which enabled Vaughan et al. [65] to estimate the segmental parameters of the human body. More recently, many other researchers, including Li et al. [66] and [67], have worked on model-based estimation of segmental muscle forces during movements, yet the complexity of the estimation scheme costs much.

This work presents a simple and fast method to improve accuracy and repeatability in estimating the segmental muscle forces of the human leg during walking using the inverse dynamics embodying Hill's muscle model, with only the external measurements: the angular displacements of the hip, knee, ankle joints along with time; and the ground reaction forces. This analysis enables the simple diagnosis of each patient about his/her muscle deterioration, and the deviation from the normal muscle group activation during the gait. Consequently, the results can be used for the gait rehabilitation, and the advanced walking assist device control.

4.2 Human Body Joint-Link Model

In this section, muscles in scope are defined, and the human body is modeled by adopting Hill's three-element muscle model, which has been widely used in the field of biomechanics as a standard model.

Muscles in Scope and Groups

In order to make the problem simple and clear, the walking motion is assumed limited in the sagittal plane, consisting of the vertical downward (x-) and the horizontal forward (y- direction), leaving 23 muscles in scope, which are gluteus maximus (GM), iliacus (IA), pectineus (PC), psoas major (PM), tensor fasciae latae (TFL), rectus femoris (RF), biceps femoris (BF), gracilis (GR), semimembranosus (SM), semitendinosus (ST), sartorius (SA), vastus intermedius (VI), vastus lateralis (VL), vastus medialis (VM), popliteus (PP), gastrocnemius (GN), extensor digitorum longus (EDL), flexor digitorum longus (FDL), flexor hallucis longus (FHL), soleus (SO), tibialis posterior (TP), extensor hallucis longus (EHL), and tibialis anterior (TA). This assumption is base on the idea that the forces and the moments related to lateral motion are symmetric over the sagittal plane. 23 muscles that have force components in the sagittal plane are shown and categorized in Table 4.1. Then they are modeled into a multi-link mechanical structure, where each muscle has joints and moment arm to act on. The parameters are collected from [68], which are based on anatomical measurements and normalization.

Fig. 4.1 shows the schematic view of the assumed multi-link structure. The 23 muscles are sorted into 10 categories according to their acting joints and working direction, based on the

Table 4.1: Human Lower Limb Muscle Parameters in Scope [68]

Muscles	Group	PCSA [cm^2]	θ_m [deg]	d [cm]	F_{Cmax} [N]	l_0 [cm]
GM	e1	30.4	21.9	6.5	1852.6	15.7
IA	f1	10.2	14.3	5	621.9	10.7
PC	f1	1.8	0.0	5	177.0	13.3
PM	f1	7.9	10.7	5	479.7	11.7
TFL	f1	1.8	3.0	5	155.0	9.5
RF	e12	13.9	5.0	5, 4	848.8	7.6
BF	f12	16.8	12.0	6.5, 4	1021.0	11.0
GR	f12	2.3	8.2	6.5, 4	137.3	22.8
SM	f12	19.1	15.1	6.5, 4	1162.7	6.9
ST	f12	4.9	12.9	6.5, 4	301.9	19.3
SA	x12	1.9	1.3	5, 4	113.5	40.3
VI	e2	16.8	4.5	4	1024.2	9.9
VL	e2	37.0	18.4	4	2255.4	9.9
VM	e2	23.7	29.6	4	1443.7	9.7
PP	f2	2.0	0.0	4	176.4	3.1
GN	f23	31.3	11.0	4, 5	1814.4	5.5
EDL	e3	5.7	10.8	5	345.4	6.9
FDL	e3	4.5	13.6	5	274.4	4.5
FHL	e3	7.2	16.9	5	436.8	5.3
SO	e3	58.0	28.3	5	3585.9	4.4
TP	e3	14.8	13.7	5	905.6	3.8
EHL	f3	2.7	9.4	5	436.8	5.3
TA	f3	11.0	9.6	4	673.7	6.8

fact that the lumped force output characteristics of the muscles vastly depend on the direction of the attachment and the number of the joint-link they involve [46][47], which are: e_1 and f_1, the extensors and flexors at the hip joint (J1); e_2 and f_2, the extensors and flexors at the knee joint (J2); e_3 and f_3, the extensors and flexors at the ankle joint (J3); e_{12}, the bi-articular muscles that bend the hip and at the same time extend the knee; f_{12}, the bi-articular muscles that extend the hip and at the same time bend the knee; x_{12}, the bi-articular muscles that bend the hip and at the same time bend the knee; and f_{23}, the bi-articular muscles that bend the knee and at the same time extend the ankle outwards. Specific names and the categories of the 23 muscles are indicated in Table 4.1.

Hill's Muscle Model

Hill's three-element muscle model has been widely adopted for describing muscle behavior, and has become a standard in the field of biomechanics. For the estimation in this work, Hill's is used to model the muscles in scope. The model describes the muscle-tendon unit (MTU) force with three different elements, which are the contractile element (CE), the parallel element

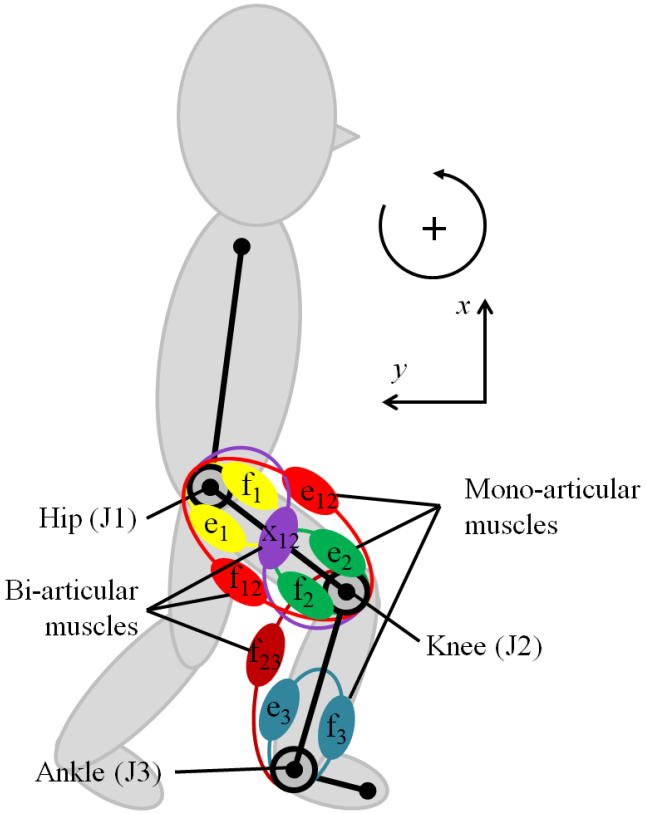

Figure 4.1: 10 categories of a human leg muscles. e_1 and f_1 are the mono-articular extensor and flexor muscles for the hip joint, e_2 and f_2 are the mono-articular extensor and flexor muscles for the knee joint, and e_3 and f_3 are the mono-articular extensor and flexor muscles for the ankle joint. e_{12}, f_{12}, f_{23}, and x_{12} are the bi-articular muscles that exert the same amount of torque to their adjacent joints.

(PE), and the series element (SE). The force that an MTU produce is written as follows.

$$F_{MTU} = F_{CE} + F_{PE} \tag{4.1}$$
$$F_{SE} = F_{CE} \tag{4.2}$$

where, the transient characteristics of F_{SE} are usually neglected assuming that the stiffness of a tendon is high enough. Then, an MTU can be modeled with only F_{CE} and F_{PE}, which are written as follows.

$$F_{CE} = f_{Cv} \cdot f_{Cl} \cdot F_{Cmax} \cdot \cos\theta_m \cdot a_m \tag{4.3}$$
$$F_{PE} = f_{Pl} \cdot F_{Pmax} \cdot \cos\theta_m + f_{Pv} \tag{4.4}$$

where, a_m is the activation level of the contractile element of the MTU which has a value between 0 and 1, θ_m is the pennation angle of the muscle fiber, and F_{Cmax} and F_{Pmax} are the

maximal contractile force and the maximal isometric force, respectively, which are all constants. f_{Cv}, f_{Cl}, f_{Pl}, and f_{Pv} are the nonlinear functions of the muscle velocity (v) and the muscle length (l), which are defined as below.

$$f_{Cv} = \frac{0.143}{0.107 + \exp\left(-1.41 \sinh\left(\frac{3.20v}{v_{max}} + 1.60\right)\right)} \tag{4.5}$$

$$f_{Cl} = \exp\left(-0.5\left(\frac{l/l_0 - 1.05}{0.19}\right)^2\right) \tag{4.6}$$

$$f_{Pl} = \frac{\exp\left(10\left(l/l_0 - 1\right)\right)}{148.41} \tag{4.7}$$

$$f_{Pv} = -Bv^2 \tag{4.8}$$

where, v_{max} is the maximal contractile velocity of a muscle which is known to be around 0.50 m/s [69], l_0 is the resting length of the muscle fiber, and every coefficient in the equations is empirically given by [70] and [71].

In addition, each muscle has different maximal force output, and consequent torque according to the place of attachment, the physiological cross-section area (PCSA), and the length of moment arm d. These parameters vary from person to person and even according to the posture. However in this work, a subject, who is 177cm tall with 70kg body mass and the average body proportion, is assumed for simplicity, and the postural variation is neglected regarding that it is relatively small. Then these parameters can be assumed constant, as given in Table 4.1.

Equations of Motion

Then, the muscle model introduced in the previous section is embedded into the joint-link model of the human body, to formulate the estimation algorithm. In this work, a human body is modeled to consist of 4 links with correspondent masses, which are connected via 3 joints as schematically shown in Fig. 4.1.

Assuming that there exists no external force nor moment other than the ground reaction force (F_{GRF}) applied to the subject, the equation of motion of a leg in scope during normal walking is written as follows, regardless of the number of supporting legs: single or double support phases, i.e. during double support phase, two equations for each leg are superpositioned with the smooth transition assumption [72]. The frame of reference is assumed attached at the hip joint for the description.

$$M\ddot{\Theta} + C + G + RF_{MTUs} + J^T F_{GRF} = 0 \tag{4.9}$$

for one leg in scope, where, Θ is the angular displacement vector of the three joints of the two legs, $M(\Theta)$ is the mass and inertia matrix, $C(\Theta, \dot{\Theta})$ is the Coriolis terms, $G(\Theta)$ is the gravitational terms, $R(\Theta)$ is the muscle embedding transformation, F_{MTUs} is the force output vector of the muscle-tendon units, $J(\Theta)$ is the Jacobian, and lastly F_{GRF} is the ground reaction force vector. To be specific, these terms are written as follows.

$$\Theta = [\theta_1\ \theta_2\ \theta_3]^T \tag{4.10}$$

$$M(\Theta) = \begin{bmatrix} M_{11} & M_{12} & M_{13} \\ M_{21} & M_{22} & M_{23} \\ M_{31} & M_{32} & M_{33} \end{bmatrix} \tag{4.11}$$

$$C(\Theta, \dot{\Theta}) = [C_1\ C_2\ C_3]^T \tag{4.12}$$

$$G(\Theta) = [G_1\ G_2\ G_3]^T \tag{4.13}$$

$$R(\Theta) = \begin{bmatrix} R_{11} & R_{12} & \dots & R_{123} \\ R_{21} & R_{22} & \dots & R_{223} \\ R_{31} & R_{32} & \dots & R_{323} \end{bmatrix} \tag{4.14}$$

$$F_{MTUs}(\Theta, \dot{\Theta}) = [F_{MTU1}\ F_{MTU2}\ \dots\ F_{MTU23}]^T \tag{4.15}$$

$$J(\Theta) = \begin{bmatrix} J_{11} & J_{12} & J_{13} \\ J_{21} & J_{22} & J_{23} \end{bmatrix} \tag{4.16}$$

$$F_{GRF} = \begin{bmatrix} f_x \\ f_y \end{bmatrix} \tag{4.17}$$

where,

$$M_{11} = \frac{m_2 l_1^2}{4} + I_2 + (m_3 + m_4) l_1^2 \tag{4.18}$$

$$M_{12} = M_{21} = \left(\frac{m_3 l_1 l_2}{2} + m_4 l_1 l_2\right) \cos(\theta_2 - \theta_1) \tag{4.19}$$

$$M_{13} = M_{31} = \left(\frac{m_4 l_1 l_3}{2}\right) \cos(\theta_3 - \theta_1) \tag{4.20}$$

$$M_{22} = \frac{m_3 l_2^2}{4} + I_3 + m_4 l_2^2 \tag{4.21}$$

$$M_{23} = M_{32} = \left(\frac{m_4 l_2 l_3}{2}\right) \cos(\theta_3 - \theta_2) \tag{4.22}$$

$$M_{33} = \frac{m_4 l_3^2}{4} + I_4 \tag{4.23}$$

$$C_1 = -\left(\frac{m_3 l_1 l_2}{2} + m_4 l_1 l_2\right)\dot{\theta}_2^2 \sin(\theta_2 - \theta_1) - \left(\frac{m_4 l_1 l_3}{2}\right)\dot{\theta}_3^2 \sin(\theta_3 - \theta_1) \tag{4.24}$$

$$C_2 = \left(\frac{m_3 l_1 l_2}{2} + m_4 l_1 l_2\right)\dot{\theta}_1^2 \sin(\theta_2 - \theta_1) - \left(\frac{m_4 l_2 l_3}{2}\right)\dot{\theta}_3^2 \sin(\theta_3 - \theta_2) \tag{4.25}$$

$$C_3 = \left(\frac{m_4 l_1 l_3}{2}\right)\dot{\theta}_1^2 \sin(\theta_3 - \theta_1) + \left(\frac{m_4 l_2 l_3}{2}\right)\dot{\theta}_2^2 \sin(\theta_3 - \theta_2) \tag{4.26}$$

$$G_1 = -gc_1\,(m_1 h) \tag{4.27}$$

$$G_2 = -gc_2\left(m_1 l_1 + \frac{m_2 l_1}{2}\right) \tag{4.28}$$

$$G_3 = -gc_3\left(m_1 l_2 + m_2 l_2 + \frac{m_3 l_2}{2}\right) \tag{4.29}$$

$$R_{ij} = \pm \epsilon d_i \tag{4.30}$$

where, $\epsilon = 1$ if muscle j works on the joint i, otherwise $\epsilon = 0$. Sign of R_{ij} depends on the direction of the torque the muscle j exert on the joint i.

$$J_{11} = -l_1 s_1 - l_2 s_{12} - l_3 s_{123} \tag{4.31}$$

$$J_{12} = -l_2 s_{12} - l_3 s_{123} \tag{4.32}$$

$$J_{13} = -l_3 s_{123} \tag{4.33}$$

$$J_{21} = l_1 c_1 + l_2 c_{12} + l_3 c_{123} \tag{4.34}$$

$$J_{22} = l_2 c_{12} + l_3 c_{123} \tag{4.35}$$

$$J_{23} = l_3 c_{123} \tag{4.36}$$

where, $s_i = \sin\theta_i$, $c_j = \cos\theta_j$, $s_{ij} = \sin(\theta_i + \theta_j)$, and $c_{ijk} = \cos(\theta_i + \theta_j + \theta_k)$, respectively, and the corresponding parameters used in the estimation algorithm are shown in Table 4.2. Where, the foot link length l_3 is assumed to be proportional to the step cycle to have 0 at hill-strike and l_3 at toe-off in the model.

Estimation Algorithm Embodying Hill's Muscle Model

As briefly shown above, one of the keys for the estimation is the use of nonlinear muscle model in the human body dynamics. The equations introduced above are transformed into the estimation algorithm, which is recursive least squares in this work. The formulation is as follows. Splitting F_{MTUs} into F_{CEs} and F_{PEs}, then equation (4.9) becomes

$$M\ddot{\Theta} + C + G + RF_{CEs} + RF_{PEs} + J^T F_{GRF} = 0 \tag{4.37}$$

Table 4.2: Parameters of Human Body Joint-Link Model

Symbol	Meaning	Value [Unit]
I_1	Upper Body Inertia Mnt	2.87 [kgm^2]
I_2	Upper Leg Inertia Mnt	0.112 [kgm^2]
I_3	Lower Leg Inertia Mnt	0.051 [kgm^2]
I_4	Foot Inertia Mnt	0.006 [kgm^2]
m_1	Upper Body Mass	47.46 [kg]
m_2	Upper Leg Mass	7.00 [kg]
m_3	Lower Leg Mass	3.26 [kg]
m_4	Foot Mass	1.02 [kg]
l_1	Upper Leg Link Length	0.421 [m]
l_2	Lower Leg Link Length	0.423 [m]
l_3	Foot Link Length	0.261 [m]
g	Gravitational Aceel.	9.81 [m/s^2]

then, substituting equation (4.3), it becomes

$$R\left[f_{Cvi}f_{Cli}F_{Cmaxi}\right]A_m = -\left[M\ddot{\Theta} + C + G + RF_{PEs} + J^T F_{GRF}\right] \tag{4.38}$$

where, $[f_{Cvi}f_{Cli}F_{Cmaxi}]$ is the muscle grouping matrix (23×10), and A_m is the muscle group activation rate vector (10×1) which is estimated. Further formulation for the estimation algorithm follows in the next section.

4.3 Muscle Group Activation Estimation

In this section, using the model elaborated in the previous section, the individual muscle group activation rates are estimated. The schematic flow and estimation algorithm verification via a simulation study are explained and given.

Schematic Flow

As shown in Fig. 4.2, when people walk, the outputs, which are easily measurable, are the joint angles and the ground reaction forces, using encoders and force sensors. The point of this work is to estimate the inputs from 23 actuators in 10 groups–muscles in human plant, by only using those external measurements. The schematic flow of this work consists of the data reconstruction, and the estimation of the individual muscle group activation rates using the least squares algorithm. Then the estimation results are compared with evidences from EMG signal measurements and verified in the following sections.

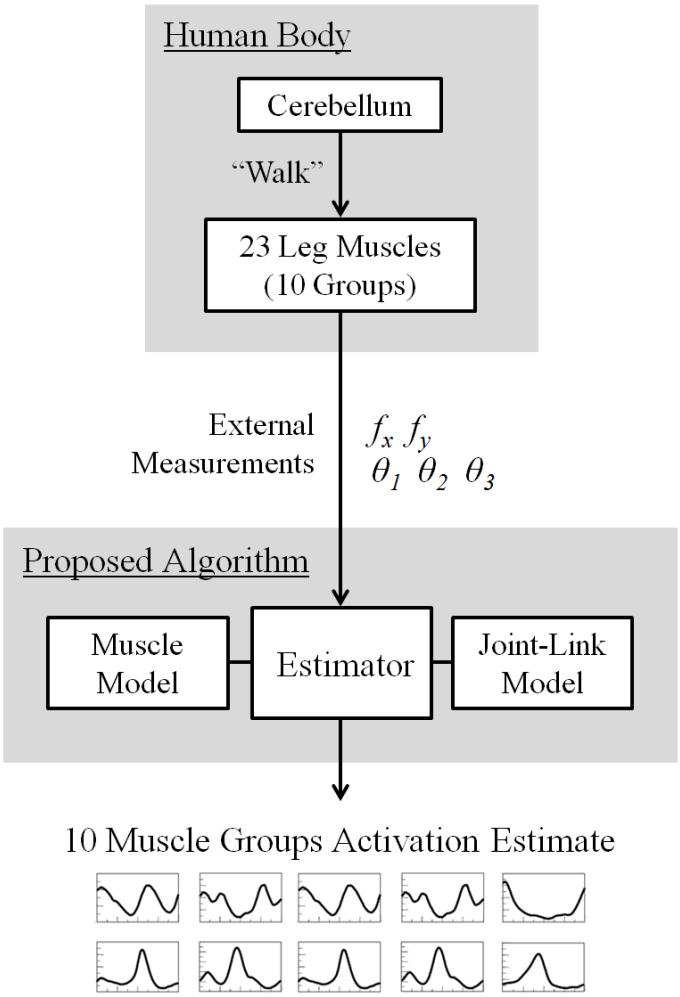

Figure 4.2: Schematic flow of the proposed method.

Simulation for Algorithm Verification

Measurement Data Reconstruction

The external measurement signals used in this work, are reconstructed ones based on findings of the literature. The angular displacement profiles of the hip, knee, and ankle joints, and the ground reaction force profiles are stacked with time, and fed into the estimation algorithm.

The angular displacements of the human lower limb joints are reconstructed based on the measurement data from [74], and the ground reaction force profiles are reconstructed using the measured data in [75]. Standard deviation originating from multiple subjects and trials of the measurements is reflected in the reconstructed signals, which are stacked and synchronized along with time, and normalized to meet the average subject assumption. The reconstructed joint angle displacements are shown in Fig. 4.11 for the average normal subject and 4.12 for the average patient, and the reconstructed ground reaction forces are shown in Fig. 4.13 for the average normal subject and 4.6 for the average patient with knee disease. Throughout the estimation scheme, a normal walking, which is characterized by approximately 1.2 m/s and

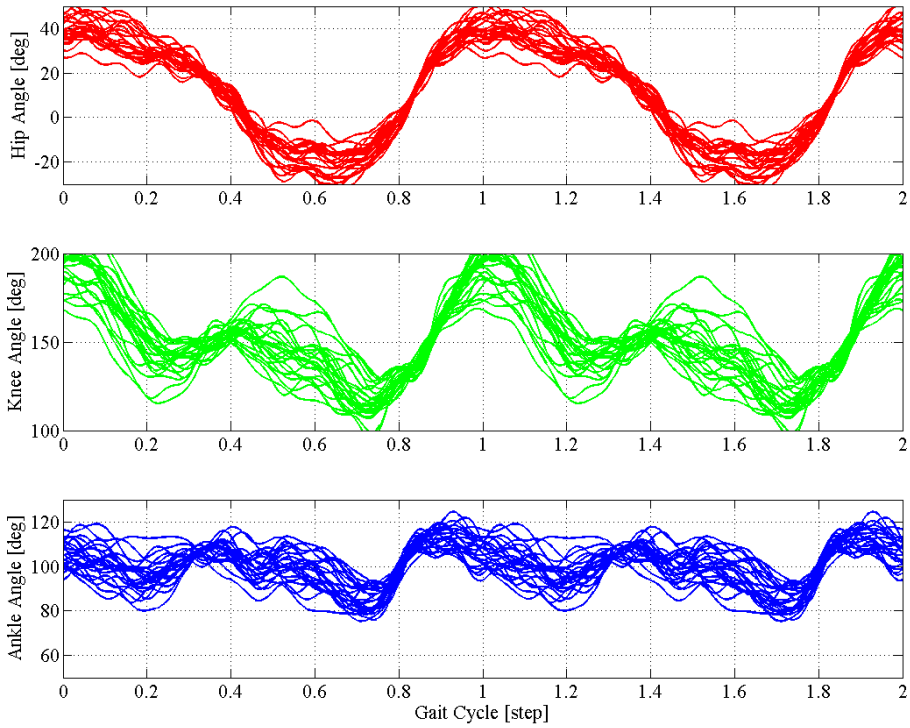

Figure 4.3: Reconstructed joint angle displacements of the average normal subject during walking. Hip angle (upper), knee angle (middle), and ankle angle (lower) are shown with respect to the gait cycle.

105 steps per minute, is assumed. Parameters used in the algorithm comply with those in Table 4.1 and 4.2.

Algorithm: the Recursive Least Squares

For the estimation, the recursive least squares algorithm is used. Using the external measurements from the sets of experimental data and equation (4.38), the muscle group activation vector A_m 10×1 is estimated. Where,

$$A_m = \begin{bmatrix} a_{m1} & a_{m2} & \dots & a_{m10} \end{bmatrix} \tag{4.39}$$

and $0 \leq a_{mi} \leq 1$. The estimate vector A_m is calculated at every 1 ms with the moving window of 50 samples. Using this activation vector, and putting

$$\Phi = R\left[f_{Cv_i} f_{Cl_i} F_{Cmax_i} \cos\theta_{m_i}\right] \tag{4.40}$$

$$Y = -\left[M\ddot{\Theta} + C + G + RF_{PEs} + J^T F_{GRF}\right] \tag{4.41}$$

we can rewrite (4.38) as:

$$\Phi A_m = Y \tag{4.42}$$

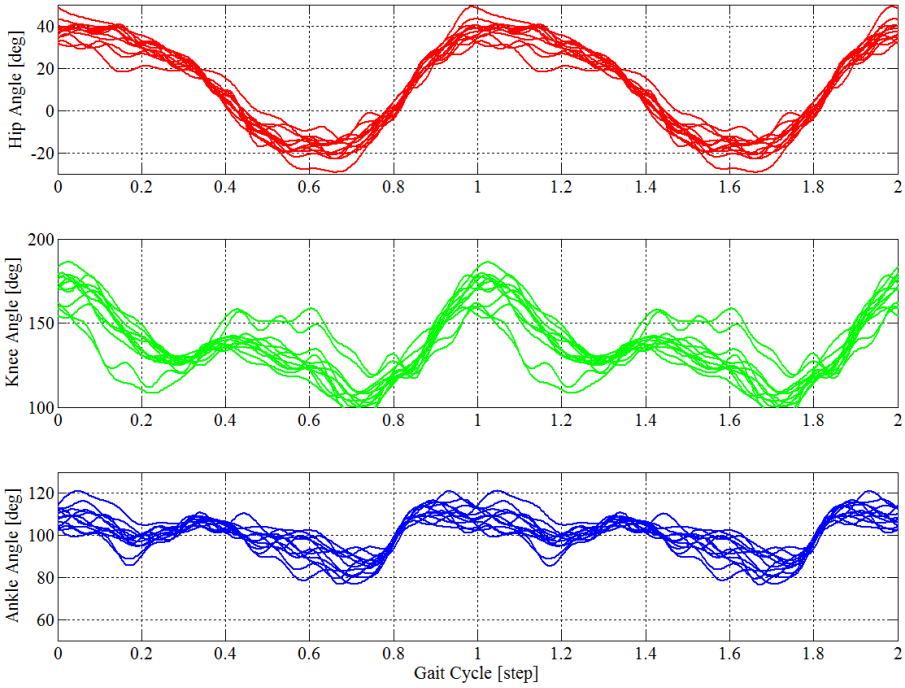

Figure 4.4: Reconstructed joint angle displacements of the average patient with knee disease during walking.

and

$$\hat{A}_m = \left(\Phi^T \Phi\right)^{-1} \Phi^T Y \tag{4.43}$$

for the RLS. Where, the rank of $\Phi^T\Phi$ is always full 50, the matrix is always positive definite, and the limits of the matrix components exist at all times: the system is persistently excited (PE).

The estimation results from the proposed algorithm are compared to the measurement data using EMG (electromyographic) signal. The patterns from [76] are used for the main reference of the comparison.

As shown in Fig. 4.7, the estimation result of the average normal subject is fairly comparable to the EMG measurement results, which supports the validity of the estimation. And in Fig. 4.8, it is shown that the patient's muscle activation atrophied with low activation levels for all muscle groups. However, the accuracy of the estimation should be enhanced via refinement.

4.4 Experimental Results and Discussion

A series of experiments were performed to acquire external measurements synchronized with one another for estimating the leg muscle activation rates during gait. Four sets of data during normal walking, and two sets during manipulated walking were recorded.

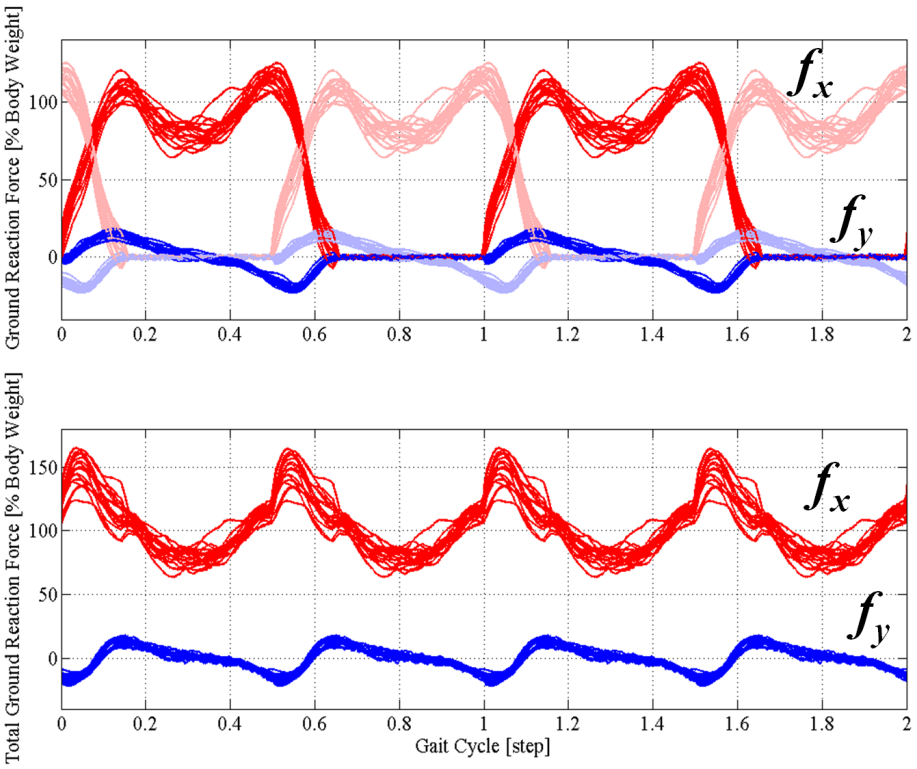

Figure 4.5: Reconstructed ground reaction forces (GRF) of the average normal subject during walking. Vertical component of GRF in red has larger in amplitude than horizontal component in blue. GRFs of both legs are shown in the upper graph, and the sum of the two is shown in the lower with respect to the gait cycle.

Experimental Setup

The external signals used in this work, are actually measured by using an experimental exoskeleton – the H-FEX (Human-Friendly Exoskeleton) – shown in Fig. 4.9. Then the angular displacement profiles of the hip, knee, and ankle joints, and the ground reaction force profiles are stacked with time, and fed into the estimation algorithm.

The H-FEX consists of a linear encoder for measuring the angular displacement of the hip joint, two rotary encoders for the knee and ankle joints, four pressure sensors in soles to measure the ground reaction forces, a DSP (NI-cRIO), and two DC power sources which supply 5V-DC and 24V-DC to the system. The entire system is powered by 100V-AC via a power cable. The physical properties of the H-FEX is shown in Table 4.3.

Throughout the estimation scheme, a normal walking, which is characterized by approximately 1.43 steps per second, is assumed. Parameters used in the algorithm comply with those indicated in Table 4.1, 4.2, and 4.3.

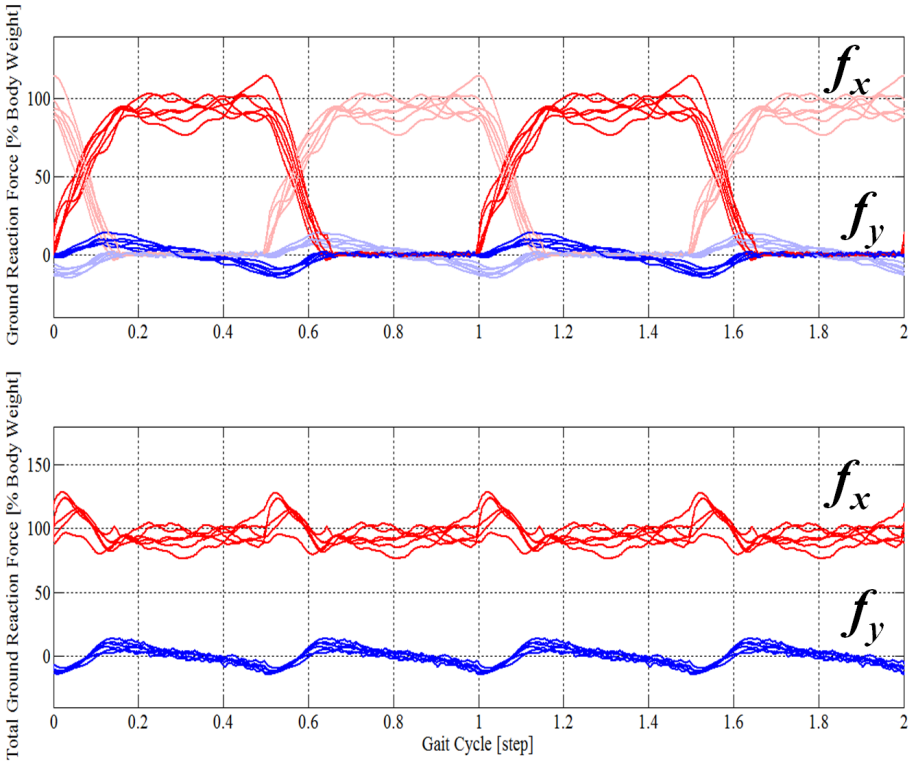

Figure 4.6: Reconstructed ground reaction forces (GRF) of the average patient with knee disease during normal walking.

Table 4.3: Physical Properties of the H-FEX

Parameters	Value [Unit]
Backpack Mass	7.60 [kg]
Orthosis Mass	1.98 [kg]
Link Lengths	As in Table 4.2
Sampling Period	1 [ms]

Method

The normal walking was done by a male subject of the parameters shown in Table 4.2 wearing the H-FEX of the parameters shown in Table 4.3 while the external measurements were recorded. On the other hand, yet by the same subject, the manipulated walking was done with a torsional spring attached to the knee joint, which exerts counter torque to the joint proportional to the angular displacement at the rate of 12 Nm/rad. The spring can be mechanically activated or deactivated as shown in Fig. 4.10.

The joint angle displacements are shown in Fig. 4.11 for normal gait, and Fig. 4.12 for manipulated gait, and the ground reaction forces from both conditions are shown in Fig. 4.13. These are, then, fed into the algorithm to estimate the activation rates of the muscle groups.

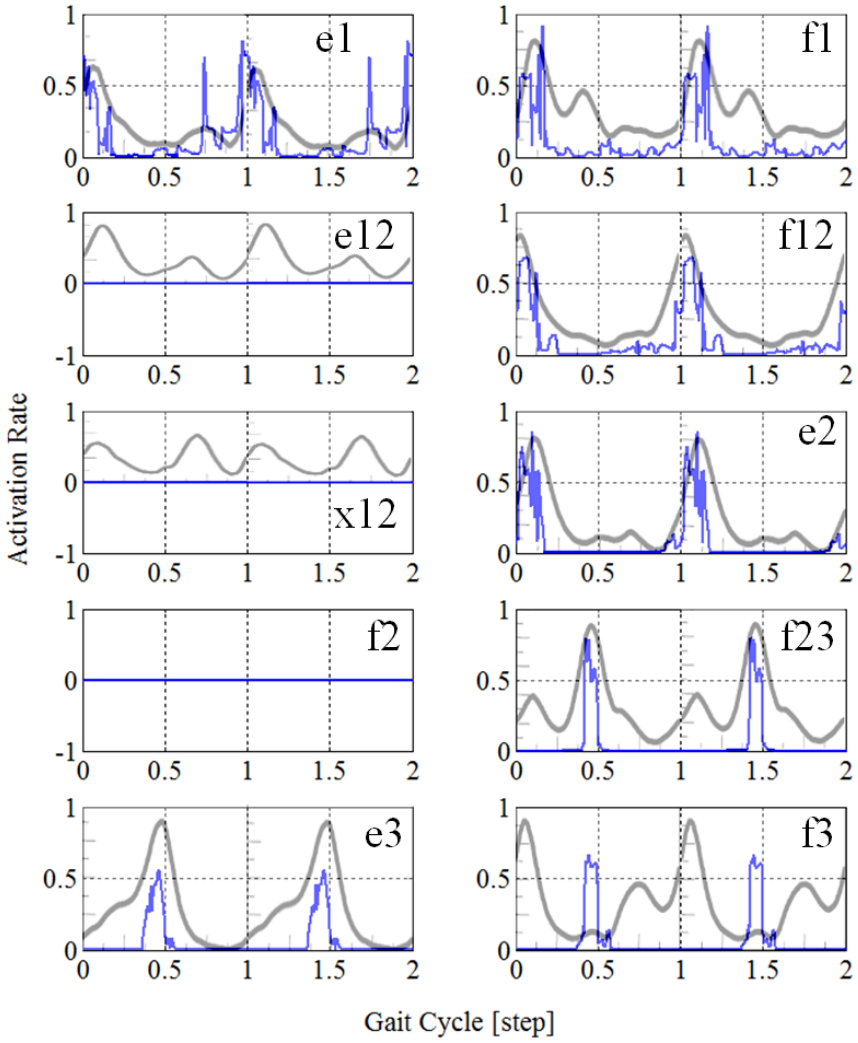

Figure 4.7: Estimated results of the human leg muscle group activation rate of the average normal subject. From the top left to the right and then to the bottom, the activation rates of 10 muscle groups labeled in Table 4.1 are shown. The transparent gray lines indicate the EMG measurements [76] of the representative muscles of the corresponding groups.

Estimation Results and Discussion

The corresponding estimation results are shown in Fig. 4.14 and 4.15, which are summarized in Fig. 4.16. Compared with those of the normal walking, the estimates of the manipulated walking show: increased activation rates in f_1, e_2, e_3, and f_3; decreased activation rates in e_1, f_2, and f_{12}; and significantly little activation in f_{23}.

The results can be explained by introducing the following hypotheses:

- The increase in e_2 and the decrease in f_2 are expected since the spring attached to the knee joint works as such. This can further verified by doing experiments with changing

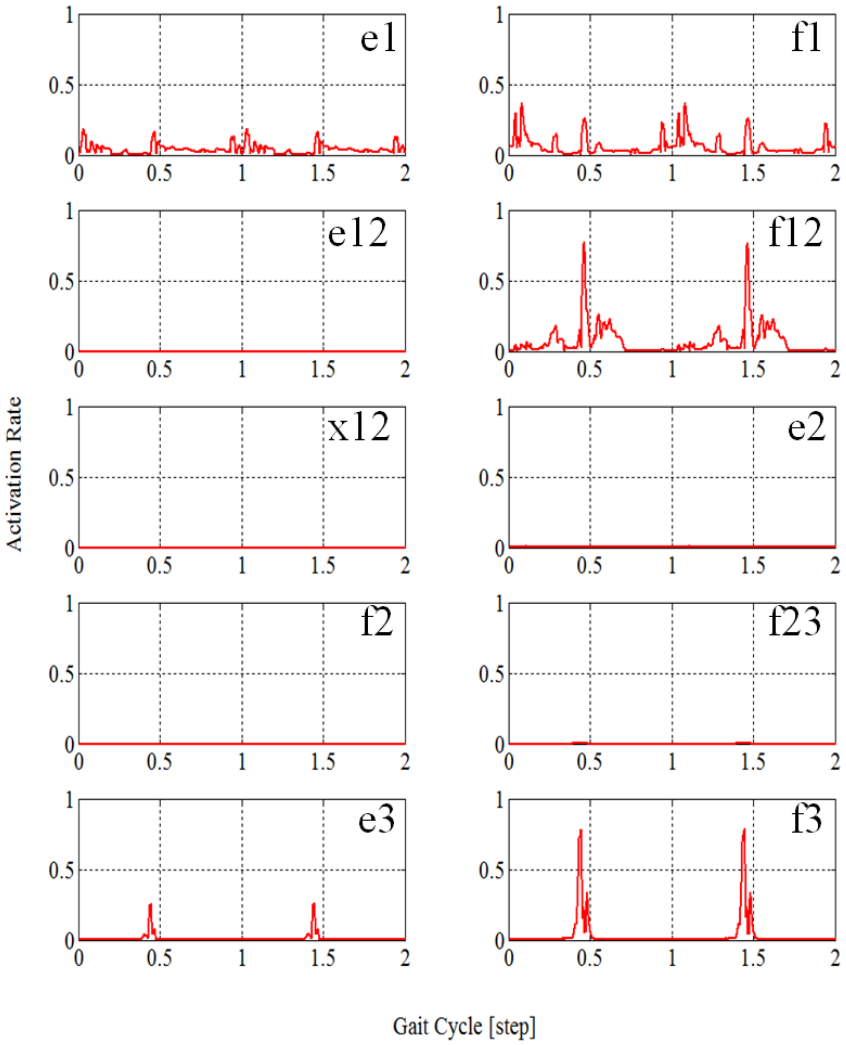

Figure 4.8: Estimated results of the human leg muscle group activation rate of the average patient. From the top left to the right and then to the bottom, the activation rates of 10 muscle groups labeled in Table 4.1 are shown.

spring coefficient, and by changing the joints and links where the spring is attached.

- Based on the result that e_{12} and f_{12} are activated at almost the same level as normal walking even though f_{12} decreased a little, it can be assumed that l_t, l_1, and l_2 form a linkage such the one shown in Fig. 4.17 (a). Then, in order to maintain the gait pattern, it is reasonable to think that e_1 is decreased and f_1 is increased to compensate the changes in e_2 and f_2.

- Due to the fact that the spring attached to J_2 not only reinforces e_2, but also restricts J_2 from bending, which results in decreased f_{12} and f_{23} deactivation, the torques to maintain the gait pattern need to be generated at J_3, since the torques do not come from

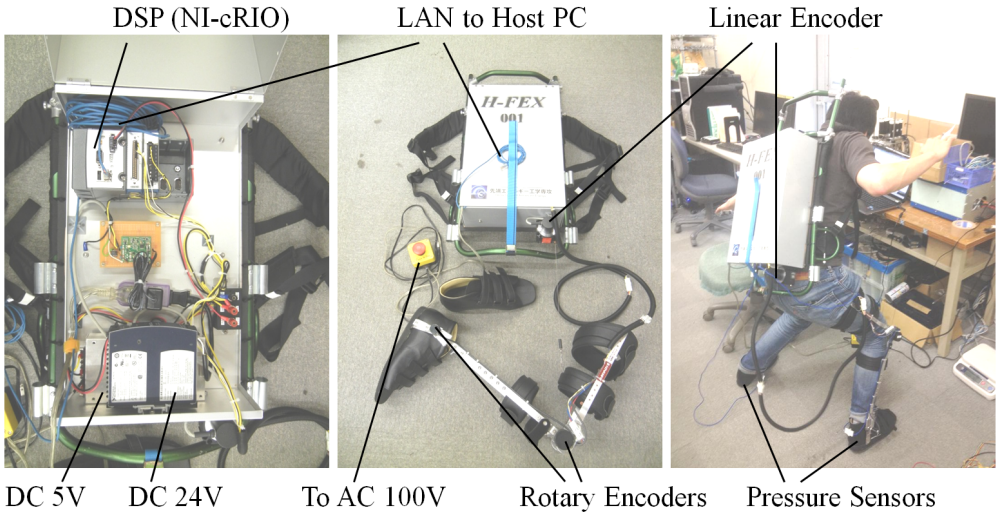

Figure 4.9: The H-FEX is used for the measurement of the angular displacements and the ground reaction forces. The system consists of a linear encoder for hip joint, two rotary encoders for knee and ankle, four pressure sensors in soles, a DSP, and two DC power sources.

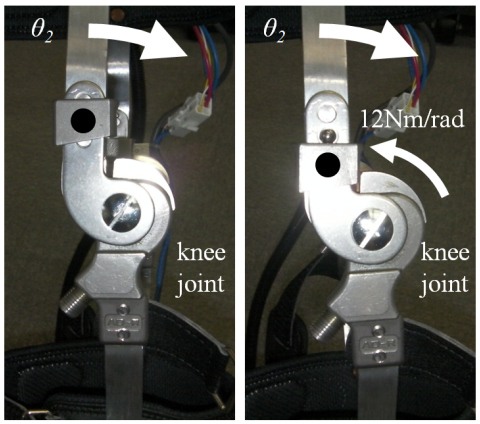

Figure 4.10: Torsional spring attached to the knee joint, which has the spring coefficient of 12 Nm/rad.

the proximal joints via bi-articular muscles. One can easily confirm this by locking one's knees straight and walking for a while, to feel the muscle pain (fatigue) in ankles.

Overall, the experimental results are reasonable and seem to have internal consistency, if the hypotheses are true: it needs to be further verified with corroborative investigation which is to follow.

However, the experimental estimate patterns do not match well with the EMG (electromyography) patterns, for example the ones in [76]. The reason for this could be that EMG is of one muscle while the estimate is of a muscle group, and that the muscle model and/or the joint-link model used in the estimation algorithm cannot be perfect having model inaccuracies. Nevertheless this is not a substantial problem, if and only if the proposed algorithm secures its own

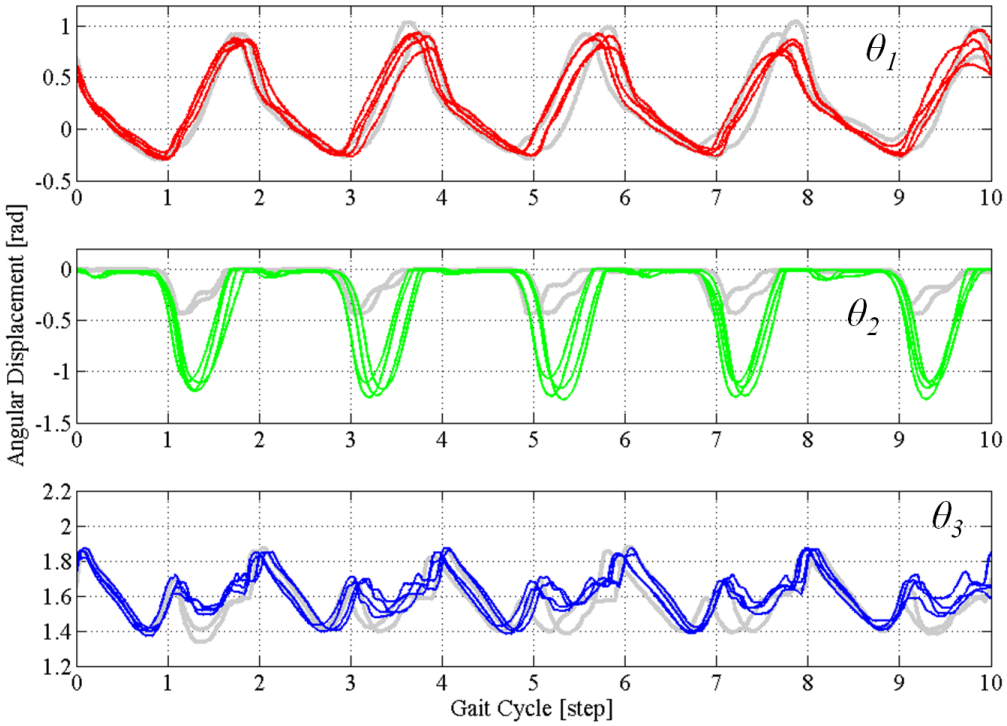

Figure 4.11: Joint angle displacements of normal walking (4 trials). Hip angle (upper), knee angle (middle), and ankle angle (lower) are shown with respect to the gait cycle. Grey lines are of manipulated walking.

internal consistency.

4.5 Human-Friendliness of H-FEX

The human-friendliness of H-FEX comes from its adaptability to the changes of the user by diagnosing the muscle activation state throughout the time of usage. Moreover, since it is based on the musculo-skeletal structure of human body, using only passive mechanical elements, or minimal number of actuators, the H-FEX provides the user with high compliance, better output isotropy, and consequently better performance in assisting the patients.

Table 4.4: Comparison between H-FEX and its opponent.

Criteria	H-FEX	Opponent [77]
Lumped Compliance	High	Low
Safety Velocity	High	Low
Number of Actuators	0	1
Output Isotropy	Good	Bad
Sensitivity to environment	High	Low

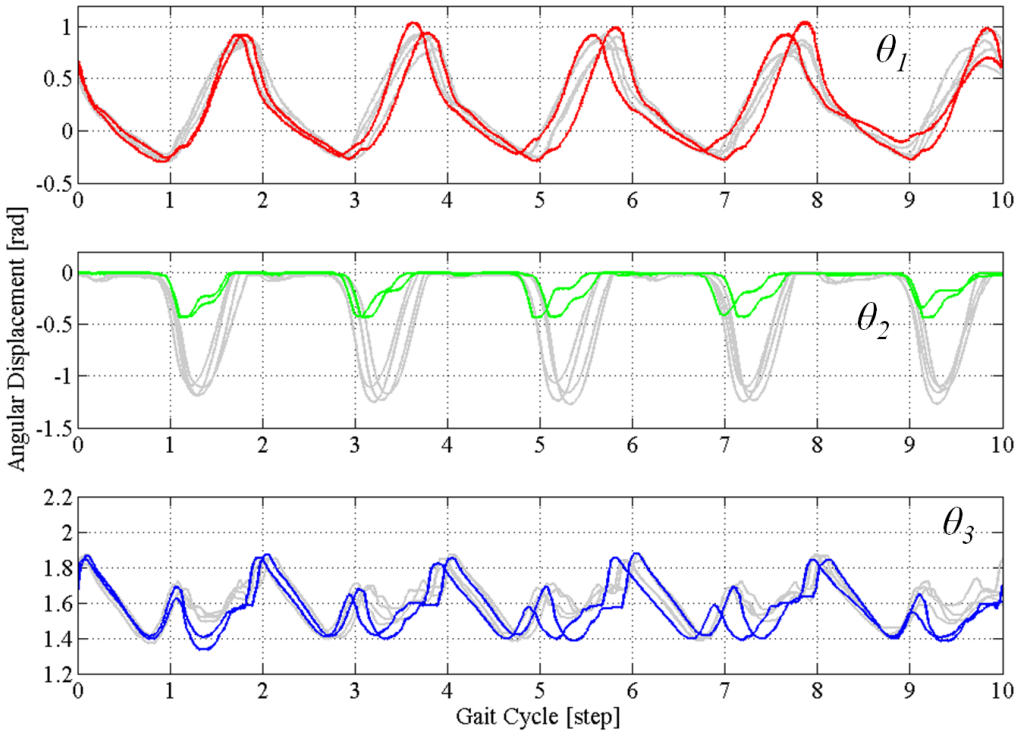

Figure 4.12: Joint angle displacements of manipulated walking (2 trials). A torsional spring is attached to J_2 which reinforces e_2 and attenuates f_2. Hip angle (upper), knee angle (middle), and ankle angle (lower) are shown with respect to the gait cycle. Grey lines are of normal walking.

The H-FEX is comparable to the assistive robot using the compact RSEA in [77], which has a motor with high gear ratio at its knee joint coupled with a compact rotary series elastic actuator (cRSEA) in it. A comparison between the H-FEX and its opponent is made, using the proposed criterion — equation (5.2) and (5.11). Fig. 4.18 and 4.19 show the comparisons of the lumped stiffness and corresponding safety velocity between the H-FEX and its opponent. Since the mechanism of the opponent uses a pair of worm and worm gear to acquire enough output torque, the back-driveability of the mechanism solely depends on the SEA performance, where the torsional stiffness of SEA has a typical value of 0.5 Nm/rad. Based on their mechanical configuration, the lumped stiffness for the both exoskeletons from the knee joint and below is calculated and shown in Fig. 4.18. Then, the corresponding safety velocity for safe pHRI is calculated and compared in Fig. 4.19. During the human normal walking, the maximum speed that the human leg could possibly reach [78] is also plotted in the figure, and it shows, RSEA has lower safety velocity than required. In sum, table 4.4 shows a comparison between H-FEX and a typical conventional power assist exoskeleton for rehabilitation, which presumably has a rotary motor at its knee joint, such as the one shown in [77].

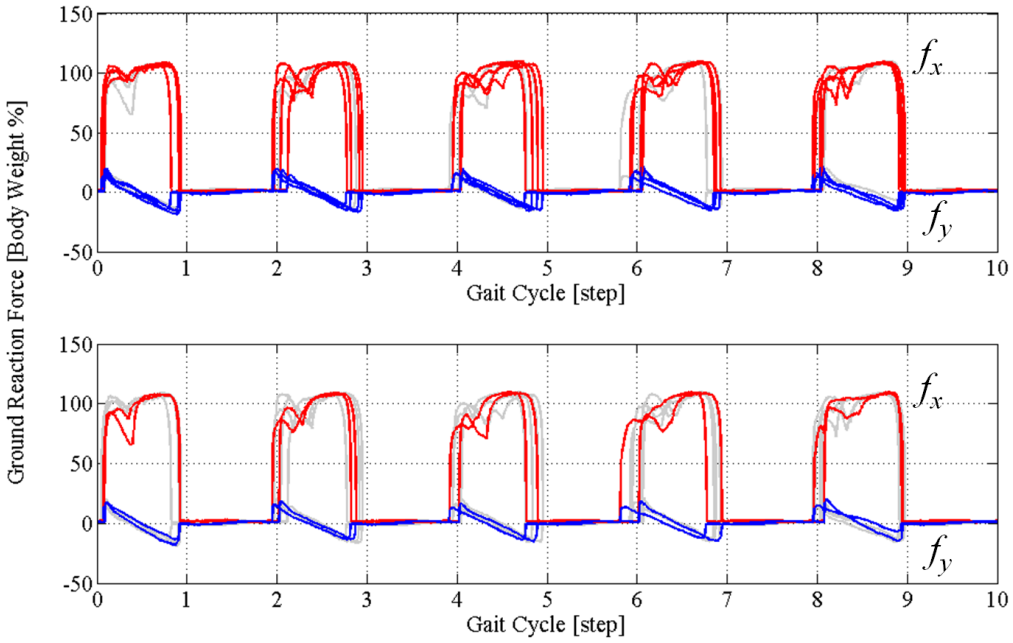

Figure 4.13: Measured ground reaction forces (GRF) of normal walking (upper) and, those of manipulated walking (lower). Vertical component of GRF in red has larger in amplitude than horizontal component in blue. Gray lines show the opponent for reference.

4.6 Summary

A simple, fast, and less invasive estimation method for extracting the activation rates of human leg muscle groups, using the H-FEX and the recursive least squares algorithm embodying Hill's muscle model is proposed. It is experimentally shown that the activation rate of each leg muscle group is simply estimated from a set of external measurement data.

The proposed method seems to be feasible and internally consistent in determining how much each muscle group is used. This method enables quick diagnosis of the patients' muscle activation and deterioration state, which is essential for setting the orientation of the medical treatment and rehabilitation. Considering the importance of the information it provides, the proposed method is expected to greatly contribute to the progress in helping people with gait disorders.

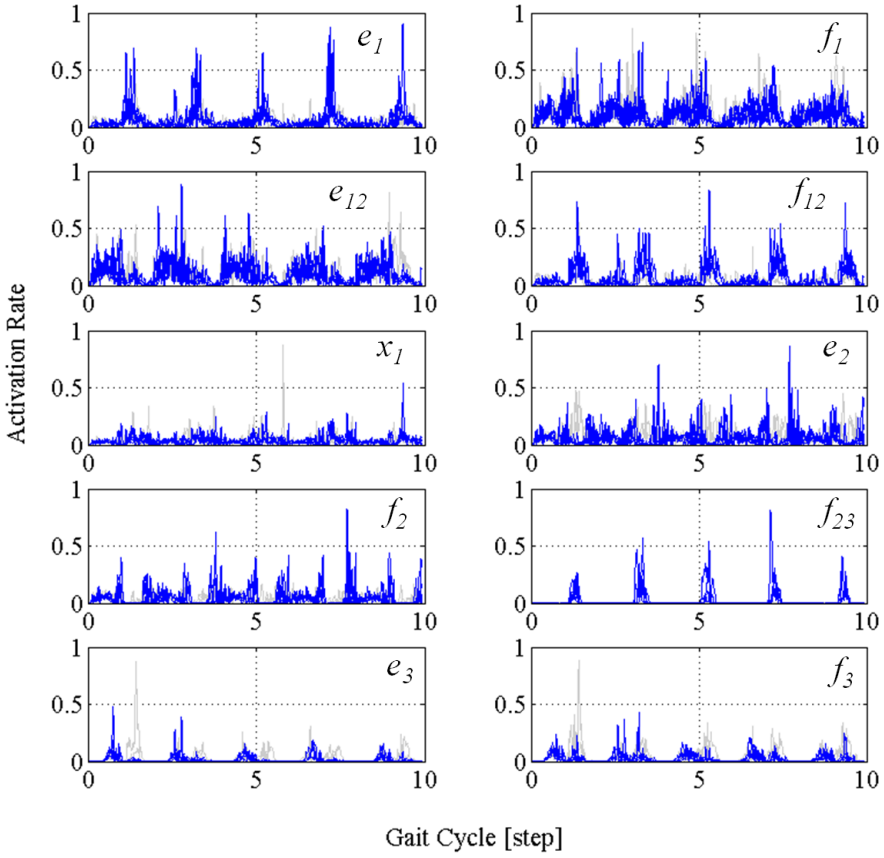

Figure 4.14: Estimation results of the human leg muscle group activation rate during 10 steps of normal walking. From the top left to the right and then to the bottom, the activation rates of 10 muscle groups labelled in Table 4.1 are shown. The grey lines indicate the measurements from the manipulated walking.

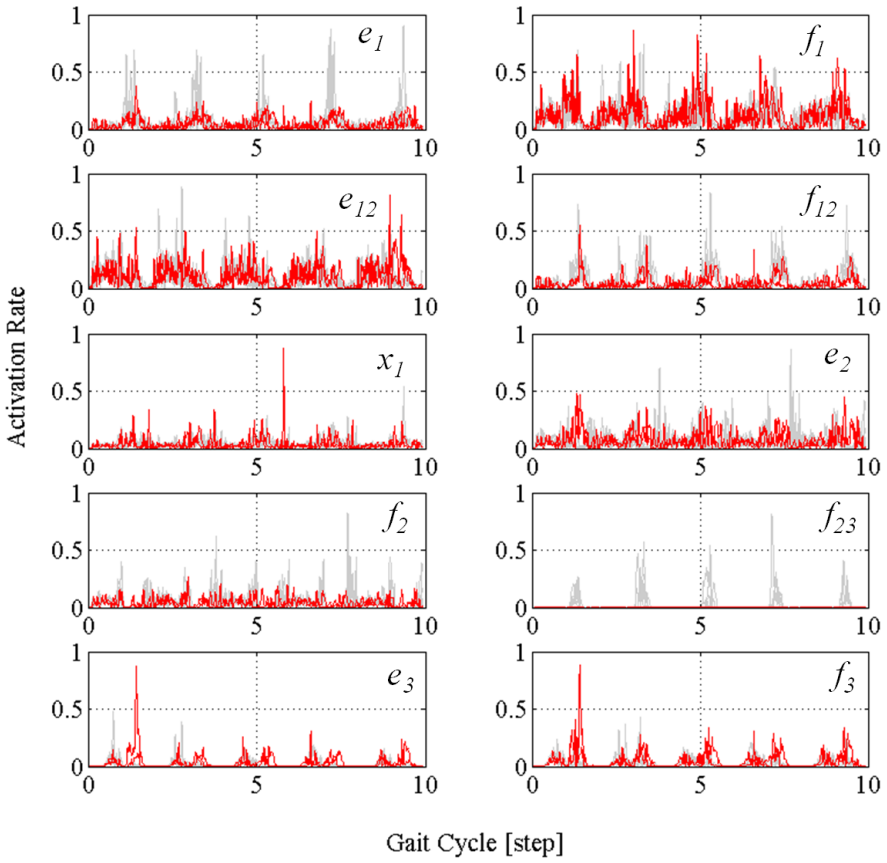

Figure 4.15: Estimation results of the human leg muscle group activation rate during 10 steps of manipulated walking. From the top left to the right and then to the bottom, the activation rates of 10 muscle groups labelled in Table 4.1 are shown. The grey lines indicate the measurements from the normal walking.

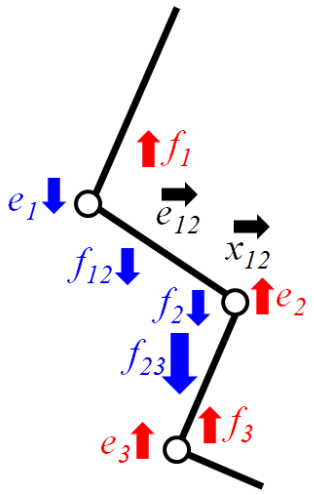

Figure 4.16: Overall results of the estimation: the changes in estimates of each muscle group when a spring is attached to J_2, compared to the results of normal walking.

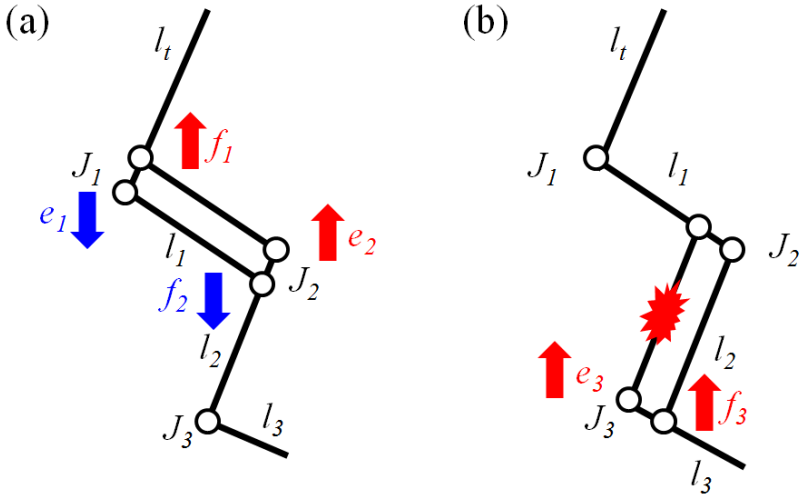

Figure 4.17: (a) e_{12} and f_{12}, when normally activated, form a linkage like this. It seems such that e_1 decreases when e_2 increases and, f_1 increases when f_2 decreases in order to maintain the gait pattern. (b) When f_{23} is disabled, both e_3 and f_3 are more active to compensate the torques in need during walking.

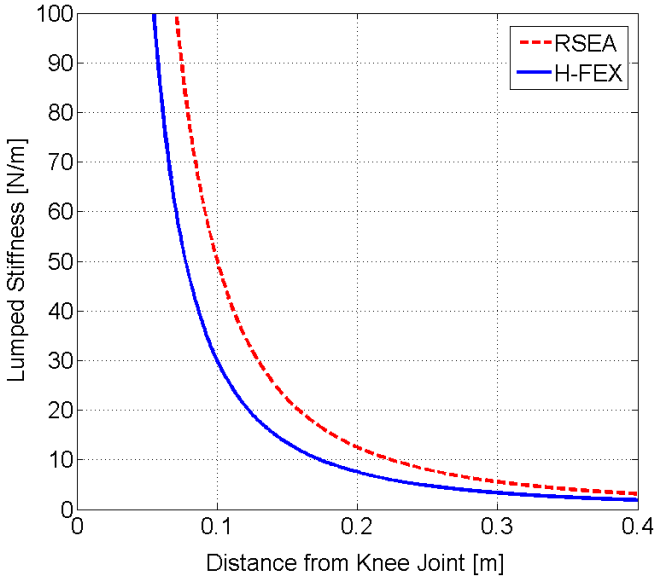

Figure 4.18: Lumped stiffness of the H-FEX and its opponent [77]. Solid blue line indicates the lumped stiffness of the H-FEX seen at a point with a certain distance downward from the knee joint. Dotted red shows that of the opponent.

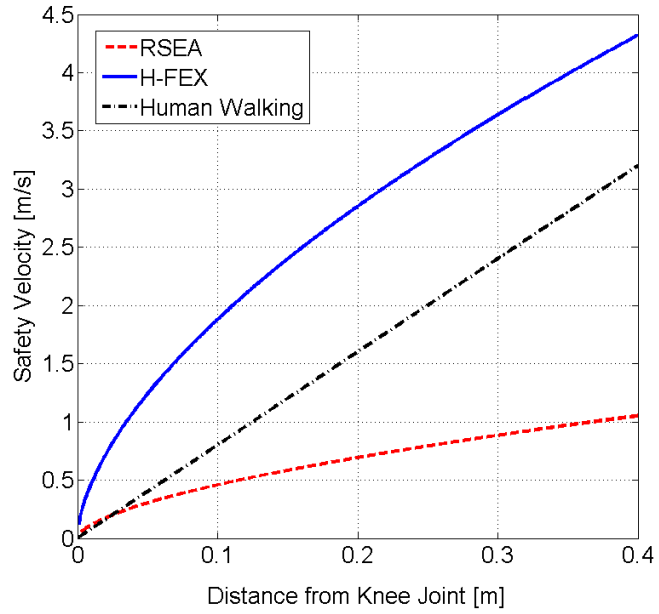

Figure 4.19: Safety velocity of the H-FEX and its opponent [77]. Solid blue line indicates the safety velocity of the H-FEX seen at a point with a certain distance downward from the knee joint. Dotted red shows that of the opponent. Chain black line is the required maximum during the normal walking.

Chapter 5

On Human-Friendliness of Robots

The term 'human-friendly' has become widely used in the field of robotics to express sensitivity of the sensors, tenderness of the actuators, intuitiveness of the interface, and so on. However, it has not reached a consensus yet despite its importance, mainly due to that each work postulates different concepts and applications. As pointed out in Chapter 1, now it is time to set the standard about how robots should be designed, controlled and evaluated. In this chapter, a brief survey on the 'human-friendliness' issues is given, and a novel standard of the human-friendliness is set based on the observations and contemplation made in the previous chapters using the laboratory-made three robots.

5.1 Efforts for Human-Friendly Robots

The issues regarding the human-friendliness of robots in human environments can be boiled down to safety and dependability in physical human-robot interactions (pHRI) [79]. In dealing with them, a wide spectrum of issues involving many different fields of study has to be addressed. For instance, Fig. 5.1 shows the issues to be cleared and their lying domains for successful introduction of robots to human environments [80].

For further development of the discourse, the domains can be divided into two parts according to the nature of each: design, control, and biomimetics account for the robot body; sensors, software, and planning account for the robot mind. This dissertation is dedicated to the body part of the issues, which consists of design, control, and biomimetics. As for the robot body, according to De Santis [80], the basic principle is simple: robots should be designed to have light weight and high compliance; robots should be controlled to secure safety and performance; and robots should consider human-robot interfaces and human metrics in them. Yet, when it comes to implementation, we have an infinite number of solutions. Firstly in this chapter, we might be able to deepen our insight on the issue by taking a look into what have been done so far in each domain.

Design

To cut a long story short, the robot design for light weight and high compliance can be paraphrased as the actuator design with high power and compliance, which simply led to the de-

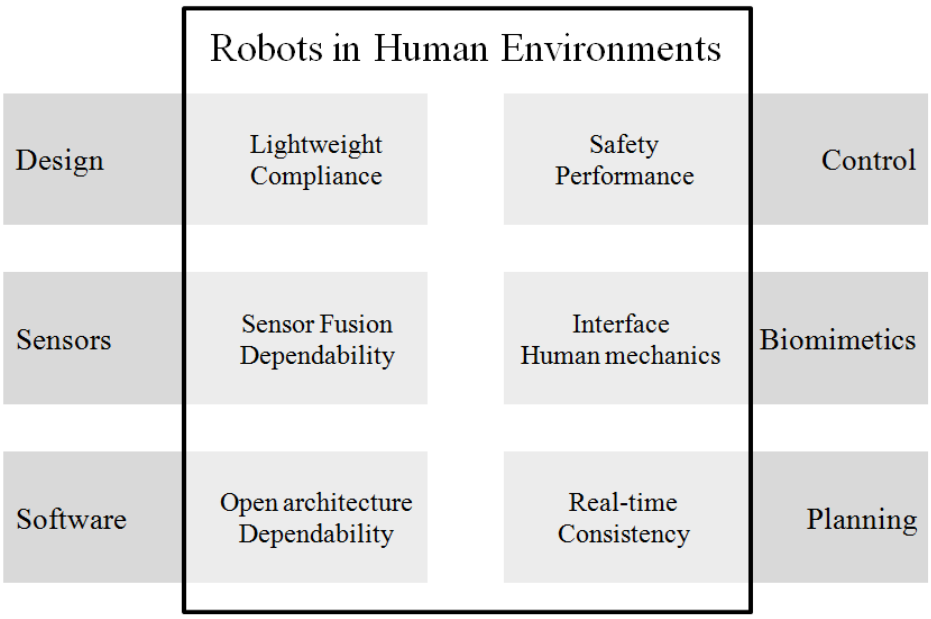

Figure 5.1: The map of robotics in human environments: main issues for pHRI [80].

velopment of compliant actuators of various kinds. And these actuators can be categorized according to their degree of activeness (or passiveness) as shown in Table 5.1. Activeness (or passiveness), in this sense, means the degree of intervention of software control for their implementation.

Table 5.1: Actuators for enhanced compliance.

Category	Actuators
Active Compliance	Hydraulic actuator, Pneumatic actuator, Electromagnetic actuator, Distributed macro-micro actuator (DM^2), Joint-torque-controlled actuator
Semi Active Compliance	Shape memory alloy, Piezoelectric actuator, Electro-fluidic actuator,
Passive Compliance	Spring, Damper, Mechanical impedance adjuster, Series elastic actuator (SEA), Variable stiffness actuator (VSA)

These actuators for enhanced compliance have been adopted particularly for robot arms, and more in general, the use of compliant transmissions has introduced link and joint elasticity. Many research works including [81], [82], and [83] have been devoted to solving the trade-off problems between compliance and bandwidth in controlling them. The design efforts, in this context, are limited to local, in the sense that the compliance of an actuator or an element does not necessarily mean the compliance of the entire robot.

Control

In order to secure safety and performance, the control for robots working in human environments is migrating from position-based ones to force-based ones [84], which is an obvious consequence considering that pHRI consists of force exchanges between humans and robots. And this gives birth to the actuators such as SEA and VSA that enable force control by converting positional displacements into force dimension. However, introducing compliant transmissions in the robot system, in general, negatively affects the performance, and thus the issues regarding the human-friendly robot control also fall on the trade-off problems between compliance and bandwidth.

In addition, one can also find efforts like [85], which tried to enhance the compliance of robots without changing their mechanical structures. By using virtual compliance, which can be realized by introducing the disturbance observer (DOB), the force-sensor-less control, or the variable impedance control (Fig. 5.2), robots with the conventional configuration are controlled in a more human-friendly way. However, in the sense that robot's compliance is determined to a certain degree by its own mechanical configurations, it can be generally said that human-friendly control has to accompany design efforts to improve compliance.

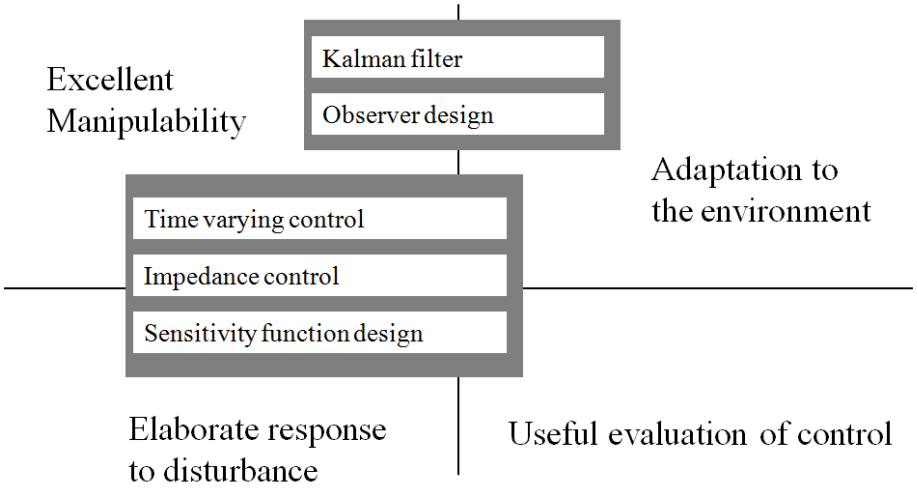

Figure 5.2: Control algorithms for the human-friendliness of robots [85].

Biomimetics

Robots based on considerations of human-robot interfaces and human metrics can be realized by introducing bio-inspired mechanisms, which are inherently human-friendly because humans have them. One of the key motivations for the biologically inspired robots is the apparent simplicity, with which biological organisms manage to survive in a ceaselessly changing environment. It has been argued that no existing algorithm running on today's fastest supercomputers could enable a robot to fly around a room, avoid obstacles, land upside down on the ceiling, feed, reproduce, and perform many of the other tasks that an insect learns to perform without training or supervision [86]. Consequently, it is inferred and widely acknowledged

that the mechanisms adopted by biological systems allow animals perform such tasks without needing sophisticated control algorithms. For instance, many models including [87] showed that biologically inspired mechanisms could perform smooth, rapid, and precise movements with only a simple command without use of feedback control, which eventually lead to the human-friendliness of robots.

5.2 Existing Guidelines for Robot Safety

Many efforts have been made to improve compliance (the human-friendliness) of robots so far. However, as it can be inferred, it seems that we have an infinite number of solutions without reaching a consensus yet. In this context, there rises a necessity that we need to set a set of constraints to shape the human-friendliness itself. In this section, a brief survey on the existing safety evaluation criteria and guidelines that might help in designing robots working in human environments.

ISO and KS Standards

The first ISO standard administering the robot safety is ISO 10218, which was first published in 1992 [88]. Then the standard had been continuously amended to keep pace with the new and emerging technologies, to be updated to new safety standards for industrial robots: ISO 10218-1 and 10218-2, in 2011 [89][90]. In the new standards, for the fulfillment of safety requirements in pHRI during robotic collaborative tasks, they specify the conditions as follows, and guide that at least one of the three conditions always has to be satisfied.

- Tool center point velocity must be less than or equal to 0.25m/s.
- Maximum dynamic power should not exceed more than 80W.
- Maximum static force should never be more than 150N.

However, those ISO 10218s are definitely not enough, and still need reinforcement for assuring safe pHRI in robots collaborating with humans on industrial sites, considering that 0.25m/s seems very restrictive for new industrial robots, and on the other hand 150N is considerably high assuming robots' high stiffness, not to mention that those are not applicable to the robots working in human environments.

Recently, a new ISO standard on service robots, ISO 13482, has just been published in February 2014 [11]. This new standard defines the perimeter of the administration, and the requirements for enhanced pHRI safety for robots used in human environments. The core part of the standard, which is essentially different from the former ones, is that it suggests robots be designed to be inherently safe, for example,

- The robot's joints (e.g. those in the manipulator) shall be designed in a way that parts of the human body cannot be crushed when the joint is moved as intended by the manufacturer. This can be done by choosing the robot geometry as well as by restricting the joint limits inherently.

- In all application tasks involving physical human-robot interaction, a personal care robot shall be designed to reduce, as far as is reasonably practicable, any levels of skin-robot friction, shear stresses, dynamic torques, arcs of center of gravity, weight-bearing transfers and supports of the human body.

and so on. According to the standard, the robots working in human environments should be inherently safe. However, as read from the above, the guidelines are not clear, and rather vague. Of course, based on this standard, more specified standards, which administer the test methods and requirements (for wheeled mobile robots, first of all), are being formulated and will be published soon [91]. Considering that the ISO standards are based on the existing related local standards of the member countries, by having a look at the existing one of the national standards we might be able to imagine what ISO would be like. For example, KS B 6939 and 6940 of the Republic of Korea [92][93] define the test methods and the requirements for the wheeled mobile robots. To our great disappointment, however, their only concern is tip-overs. It is definite that we need to set a standard which administers the force exchanges between humans and robots.

Collision Safety Criteria

Another guideline we can refer to is the collision safety criteria. Collision safety in pHRI itself is also a broad topic of research and has its own long history and tradition. The severity of human injuries caused by collision with machines is well studied, with particular regard to such domains as car accidents. Based on the studies, nowadays, the new car assessment programs (NCAP), which administer the safety test methods and requirements of automobiles, are mandatory for all new cars for the most markets of the world.

Among the car-accident-related safety criteria, more general and, at the same time, robot-applicable indexes include the Gadd Severity Index (GSI) [94] and the Head Injury Criterion (HIC) [95]. To tell the long story short, the HIC is the mathematically refined version of the GSI. The HIC criterion, then, has been widely adopted and used for the safety assessment in pHRI of machines including robots. The proposed criterion also adopts the HIC, which is defined as follows, in calculation.

$$HIC = T \left[\frac{1}{T} \int_0^T a(\tau) d\tau \right]^{2.5} \tag{5.1}$$

where T is the final time of impact. As the choice of this time is often difficult, it is recommended to consider the worst-case HIC at varying T, which corresponds to taking T equal to the time at which the head reaches its maximum velocity $v(T)$ (typically, $T \leq 15$ms). An HIC value of 1000 or greater is usually associated with extremely severe head injury. And on the other hand, an HIC of 100 can be considered suitable to normal operation in pHRI [96].

A generalization of the HIC to collisions with other parts of human body can be done by replacing the exponent 2.5 by other empirically determined values [96]. By integration using parameters from [96], we get the generalized formula as follows.

$$HIC = 2\left(\frac{2}{\pi}\right)^{\frac{3}{2}}\left(\frac{K_{col}}{M_{human}}\right)^{\frac{3}{4}}\left(\frac{M_{col}}{M_{col}+M_{human}}\right)^{\frac{7}{4}} v^{\frac{5}{2}} \tag{5.2}$$

where K_{col} is the stiffness of the colliding object, M are the masses of the colliding object and the human, and v is the velocity of impact. Equation (5.2) is important here, since it is a simple but empirical function of K_{col} and v of which we are able to find the values by setting the maximum HIC number we want.

5.3 Thesis: Human-Friendliness of Robots

The main idea of this dissertation is given in this section. The requirements for human-friendly robots, a novel evaluation criterion, and hardware-wise/software-wise suggestions are formulated and proposed.

Requirements

Robots that will work in human environments must have the following aspects. The design and control suggestions shown in the latter part are based on these requirements.

- Safety: absence of injury or possibility of injury of the user and the environment. Introducing physical and virtual compliance in robot system design, and preparing fail-safe algorithms in their control will assure safety in pHRI.
- Reliability: continuity of accomplishing given tasks with a satisfactory performance. Reducing complexity of the system, and designing the system in an optimal way to balance compliance and performance, robots will be reliable and dependable at all times.
- Adaptability: ability to undergo maintenance and modifications over time according to the changes of the user and the environment. By reducing complexity and cost of the system, maintenance and modifications become easier and more affordable. Also, system design and control which enable self-adjustment will help to adapt robots to the continuously changing user and environment.

As inferred from the above, the key aspect of the human-friendliness is compliance of the system. Compliance in this context means both mechanical and virtual ones. By using compliant actuators and passive compliant elements such as the ones in Table 5.1, and by using control algorithms that provide robots with sensitivity, the human-friendliness — safety, reliability, and adaptability — of robots will be improved.

Local to Global

Mechanisms that provide compliance are basically one-dimensional, although the coordinate of the displacement varies according to each configuration. Many systems adopting compliance, consequently, are focused on improving compliance in a restricted manner. It is good as long

as the user interface with robots is restricted to the dimension, and many systems are designed in this way. However, considering the cases of autonomous service robots that we cannot limit the space and dimensions of the interface, compliance in a global sense is needed. It can simply be realized by combining the compliant mechanisms to the global kinematics of the system, through careful design and/or control laws that enable global linkage. The applications introduced in the previous chapters are exemplary in such sense. Similarly, the evaluation of the human-friendliness of robots should also be in a global manner.

Evaluation Criterion

The basic idea of the proposed criterion is that, from (5.2), we first set the maximum HIC value to assure safe pHRI, then we can control $K_{col} = K_{lump}$, $M_{col} = M_{robot}$, and v to meet the HIC requirements. The secondary problem is how to calculate the lumped stiffness of the robot K_{lump}, which is elaborated in the following subsection.

The Cartesian Stiffness Matrix

The proposed criterion is based on the calculation of the lumped stiffness of robots and the generalized HIC for human body. For doing the calculation we first derive the Cartesian stiffness matrix K, which is defined as

$$W = K\Delta S \tag{5.3}$$

where

$$W = \begin{bmatrix} F_x & F_y & F_z & \tau_\alpha & \tau_\beta & \tau_\gamma \end{bmatrix}^T \tag{5.4}$$

$$\Delta S = \begin{bmatrix} \delta_x & \delta_y & \delta_z & \delta_\alpha & \delta_\beta & \delta_\gamma \end{bmatrix}^T \tag{5.5}$$

for a given system. Then K becomes a 6 by 6 matrix, which is in general posture-dependent, non-symmetric, frame-variant.

Indexes for Stiffness Performance Evaluation

Once we get the matrix K, there are many indexes that evaluate the global stiffness of the system. For example, we can compute a global index as

$$GI_d = min|det(K)| \tag{5.6}$$

where we can find the singularities of the system, as it means the system has at least one singularity if GI_d equals to zero.

If the design requirement is to have an isotropic behavior in terms of stiffness, it is useful to compute as

$$GI_{cn} = \frac{\int \kappa(K) dV}{L^3} \tag{5.7}$$

where κ is a function that removes dimension inconsistency between the systems in scope [97], which is defined as follows.

$$\kappa(K) = \frac{max(\lambda_K)}{min(\lambda_K)} \tag{5.8}$$

Besides the indexes introduced above, there are many other global stiffness indexes for various purposes.

Stiffness Barrier and Safety Velocity

In order to have in-depth insights about the lumped stiffness of mobile robots, a graphical representation is desirable. Thus, here, a simple norm – the Euclidean norm – of the matrix K, as defined below, is used with regard to the changing external force and the kinematics of the given system on a 2-dimensional plane.

$$||K|| = max\left(\lambda_K\right) \tag{5.9}$$

Then we have the lumped stiffness of the given system with regard to the direction of the force applied. If we use this as

$$K_{lump} = ||K|| \tag{5.10}$$

in equation (5.2), we get the impact velocity, which is here the safety velocity as follows, since we set the maximum HIC value for safe pHRI in advance.

$$v_{safe} = \left(\frac{HIC_{max}}{HIC}\right)^{\frac{2}{5}} \tag{5.11}$$

for every direction in which the external force is applied.

The proposed criterion is universally applicable for most robotic systems by applying test forces and calculating (or measuring) the consequent deformations. And it is applied to each robot introduced in the latter part to evaluate their human-friendliness.

An Example: Application to a Mobile Robot

Here, as an example, a simulation study was done using the proposed criterion formulated in the previous section using a novel type mobile robot, CIMEV [98], in comparison with a conventional type one. The parameters in Table 5.2 are used for both types in the simulation.

The simulation is limited to the motion in 2-dimensional space, thus K are 3 by 3 matrices, which mediate the following vectors.

$$W = \begin{bmatrix} F_x & F_y & \tau_\gamma \end{bmatrix}^T \tag{5.12}$$

$$\Delta S = \begin{bmatrix} \delta_x & \delta_y & \delta_\gamma \end{bmatrix}^T \tag{5.13}$$

Table 5.2: Measured Parameters

Parameters	Meanings	Values
m	Robot mass	18.5 kg
h	C.G. Height	0.185 m
N_f	Normal force on each front wheel	39.2 N
N_r	Normal force on each rear wheel	51.5 N
I_z	Moment of inertia (vehicle)	0.409 kgm^2
I_w	Moment of inertia (caster wheel)	0.009 kgm^2
e	Caster arm length	0.040 m
l_f	Distance, from C.G. to front axle	0.247 m
l_r	Distance, from C.G. to rear axle	0.188 m
L	Wheel base	0.435 m
d	Tire track	0.355 m

for both systems.

The displacement vector ΔS for both systems are simply calculated from the kinematics as follows.

$$\Delta S = \begin{bmatrix} \frac{2h^2F_x}{(lf+lr)^2k_s)} \\ \frac{2h^2F_y}{d^2k_s} + \frac{l_reF_y}{2(l_r+l_f)k_c} \\ \tan^{-1}\left(\frac{eF_y}{2k_c(lf+lr)}\right) \end{bmatrix} \tag{5.14}$$

for CIMEV, and

$$\Delta S = \begin{bmatrix} \frac{2h^2F_x}{(lf+lr)^2k_s)} \\ \frac{2h^2F_y}{d^2k_s} + \frac{l_reF_y}{2(l_r+l_f)k_n} \\ \tan^{-1}\left(\frac{eF_y}{2k_n(lf+lr)}\right) \end{bmatrix} \tag{5.15}$$

for the counterpart. k_s, k_c, and k_n are the mechanical stiffness of the suspension system, caster wheel, and the conventional steering system (rack and pinion, or whatever system with high reduction ratio), for which typical values are given in the calculation as: k_s=10000N/mm for both systems, k_c=10Nm/rad for soft caster and 100Nm/rad for hard caster, and k_n=5000Nm/rad for normal steering. Then with the parameters given, $||K||$ and v_{safe} for both systems are calculated in accordance with the changing external force.

Fig. 5.3∼5.5 are showing the results of the calculation. Fig. 5.3 indicates the lumped stiffness of the systems in scope in accordance with the direction, and Fig. 5.4 and 5.5 show the safety velocity for those systems. From the figures, the compliance performance of the robots can be visually and intuitively perceived. The proposed criterion, therefore, is useful for evaluating the robots working in human environments, and eventually obtaining in-depth insights when designing robots in the immediate future.

The proposed criterion consists of the Cartesian stiffness matrix and the generalized concept of the Head Injury Criterion combined, to graphically show the lumped stiffness – eventually

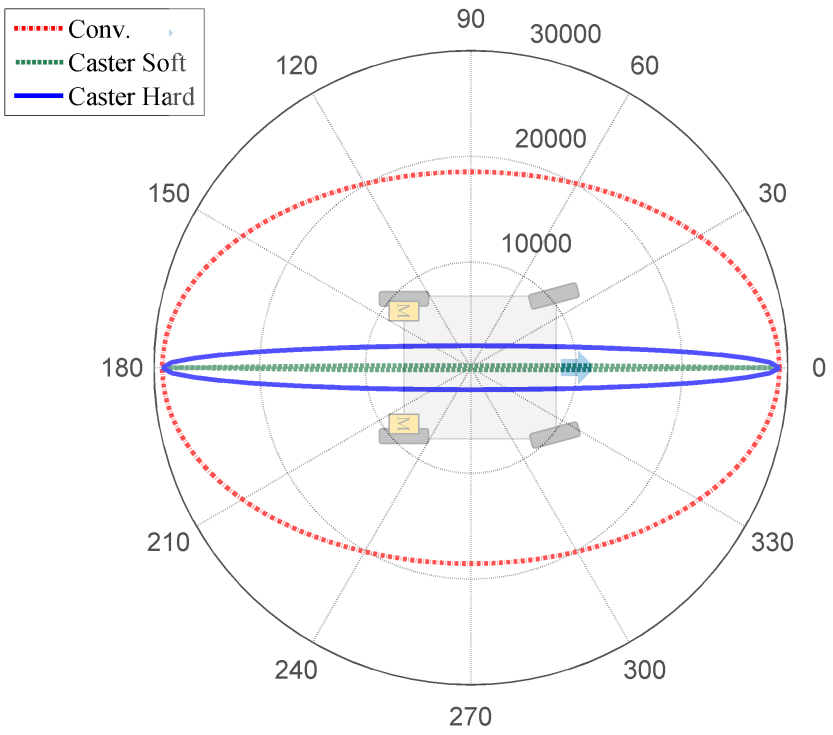

Figure 5.3: Calculated lumped stiffness $||K||$ of the mobile robots in scope. [N/mm]

the lumped compliance – of a mobile robot in its plane of motion, and the safety velocity of the robot for the safe human-robot coexistence and interaction. The criterion is applied to a novel type mobile robot, CIMEV, in comparison with a conventional one. The result shows that CIMEV is significantly more compatible for human-robot coexistence than the counterpart.

The proposed criterion can possibly be applied to other robotic machines such as bio-inspired robotic manipulators, human-friendly exoskeletons, or even wheelchairs. It is used in evaluating the human-friendliness of the robots introduced in this work, and the results are shown with discussion at the end of each chapter.

5.4 Suggestions

According to the prespecified definition and the requirements The keys for the human-friendliness of robots are: introducing compliant mechanical elements and utilizing them to enhance the global (lumped) compliance; and using control algorithms which make robots virtually compliant in combination with exploiting mechanical compliance, and even when mechanical configuration alone is not sufficiently compliant.

For the human-friendliness of robots working in human environments, in the first place, the extensive use of compliant actuators and mechanical compliance along with systematic

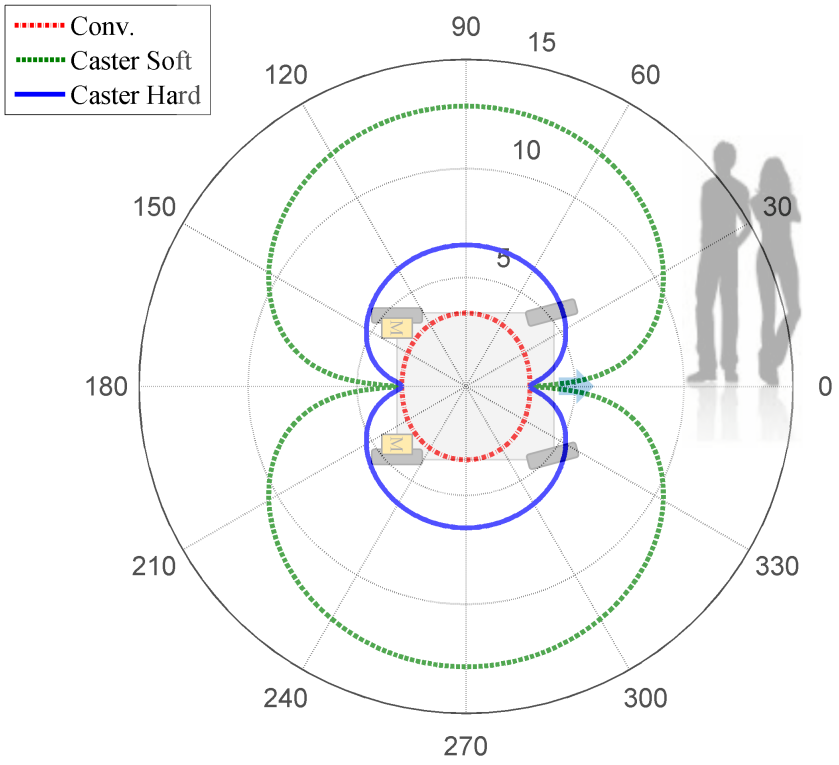

Figure 5.4: Safety velocity for the mobile robots in scope. Collision with 70kg human body assumed. [m/s]

connections to the global kinematics of the system is required. Not only the active, semi active, and passive compliance introduced in Table 5.1, but also linkage structures, which transmit the compliance to the whole system, such as the bi-articular actuation, and caster wheels, are necessary for robot designs.

In combination with the compliant robot design, the control portion will increasingly play important roles. Dealing with the negative effects of compliance in the system is the one that comes first. Moreover, adopting algorithms to make the system virtually compliant imposes many control problems on the system. As in Fig. 5.2, various control entities are applicable for the human-friendly robots, thus fusioning them with other mechanisms in different engineering layers is another important work to do.

5.5 Summary

In this chapter, the concept of the human-friendliness of robots is presented. First, a brief survey on the efforts for human-friendly robots and existing guidelines for physical human-robot interactions is given. Then, in order to provide answers to the problems that we find in Chapter 1,

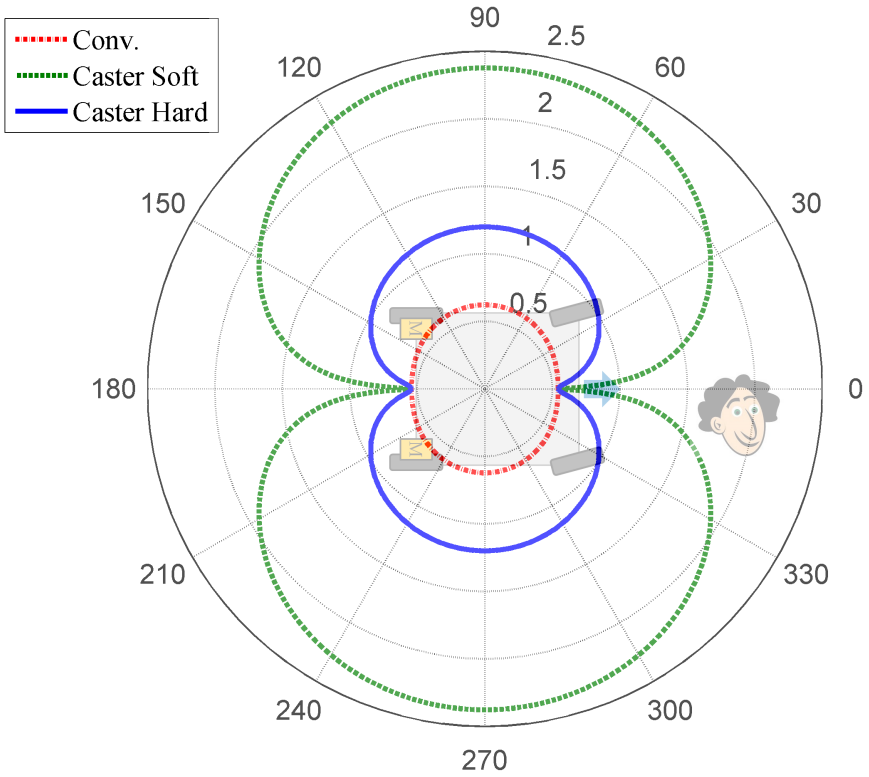

Figure 5.5: Safety velocity for the mobile robots in scope. Collision with 5kg human head assumed. [m/s]

a novel definition and a criterion is formulated to tell how human-friendly robots are. Based on the findings and contemplation made in the previous chapters using three robotic applications, a set of common requirements that robots of the near future should meet is provided, showing that the proposed definition and criterion comply with it. The new definition of human-friendliness adopts the concept of the lumped compliance, whose derivation and application methods are elaborated. Based on it, design and control suggestions for enhancing the human-friendliness are provided both hardware-wise and software-wise, which are implemented in designing and controlling the robots introduced in the previous chapters.

Chapter 6

Concluding Remarks

This research addresses the human-friendliness of robots working in human environments by suggesting the requirements, an evaluation method, and relevant applications throughout the thesis, which all can inspire the next. This chapter presents a summary and the conclusion with a short discussion on the open issues for future research recommendations.

6.1 Conclusions

The term 'human-friendliness' has been widely used in the fields of engineering, however, it has not reached any consensus so far, which was one of the major difficulties associated with designing and controlling robots of the new kind. By defining the requirements and formulating the evaluation criterion, this work provides quantitative and qualitative means to deal with the concept of human-friendliness and eventually helps to improve physical human-robot interactions in a way that humans are centered.

Hardware wise, compliant elements and mechanisms, such as caster wheels, springs, and structures embodying compliant elements, will enhance the inherent safety performance of robots by providing high global compliance. CIMEV, a novel mobile platform introduced in Chapter 2, shows better mobility performances, adaptation to the environment, and most importantly high compliance with humans in the range of its activity. By using a spring as its bi-articular actuator, JUMPBiE, a novel jumping robot introduced in Chapter 3, enables a much simpler control algorithms in performing jumping tasks while keeping the merits of using bi-articular actuators within the mechanism. As shown in Chapter 4, robots could be better designed if based on in-depth understanding about human musculoskeletal structure. H-FEX is enabled the real time diagnosis and augmentation control by using human musculoskeletal characteristics in estimating human efforts and applying the diagnosis to designing and controlling the actuation.

The enhanced human-friendliness of the applications introduced in this work, are evaluated unitarily by the criterion formulated and suggested in Chapter 5. The proposed criterion is useful when checking the global compliance of any kind of robot, which eventually forms the safety and human-friendliness of robots of any kind when humans encounter them within a close distance. Moreover, it is particularly strong in the sense that the global compliance is apparent one from the human side view point, i.e. it can involve the controlled properties such

as modulated impedance, disturbance assessment characteristics, and etc, and thus it can tell how safe the robot is after all.

Overall, main contributions of this work can be summarized as follows.

- The term 'human-friendliness' is newly defined, in a way that we can quantify and measure the property. Consequently we can tell whether and how much a robot is safe and human-friendly in the interactions between humans and robots.
- The requirements for human-friendliness of robots working in human environments are suggested in terms of selection of hardware configuration and control algorithm.
- Relevant robotic applications, which can inspire the next, are introduced and evaluated from mobility, manipulation, and rehabilitation perspectives. By designing robots in a way that the mechanisms meet the requirements proposed in Chapter 5, they show clear improvements in compliance performance while retaining the performance to accomplish the originally intended objectives.

6.2 Open Issues

Designing and controlling a robot is such a challenging problem that has infinite number of solutions. However, by adding an additional constraint in solving the problem, robots can show significantly improved performance in terms of 'human-friendliness' and safety in interacting with humans around. That is, the evaluation criteria and the requirements for robots must be set, and mechanisms have to be implemented according to the standards. Moreover, in-depth understanding of human physics and psychology is essential for designing and controlling robots that work in human environments. The requirements, criteria, and applications proposed in this work will surely do. Yet, further refinements and improvements, hopefully inspired by this work, will make perfection. In this context, the following issues are still open for new solutions.

- Refining, or redefining the 'human-friendliness' and its evaluation method.
- Inventing, or rediscovering mechanisms that can enhance the 'human-friendliness' of robots.
- Methodologies to implement such mechanisms and synthesize them with originally intended objectives.
- Designing and applying control algorithms that can inherently improve safety performance in human-robot interactions, putting humans at the center.
- Although understanding of human physics and psychology is essential for designing and controlling robotic devices for rehabilitation, there still remain many uncharted territories left in ourselves, such as human musculoskeletal structure. Trans-disciplinary studies between medical and engineering researchers can create synergies.

Last but not least, although one of the important backgrounds of this work is to cope with the problems concerning aging of the population, however, resolving the problems by introducing

more robots into our society to augment human labor is NOT a fundamental approach. It is definitely much more natural and desirable that we humans procreate so as to sustain a stable level of population. That said, it is particularly important to reform and improve our social systems and government policies in a way that they support childbirth, child-rearing, and parenthood.

References

[1] L. Nocks, 'The Robot: The Life Story of a Technology,' The Johns Hopkins University Press, Baltimore, 2008

[2] ABB Group, http://www.abb.com/

[3] Population Division of the Department of Economic and Social Affairs of the United Nations Secretariat, "World Population Prospects: The 2012 Revision," August 2013

[4] The International Federation of Robotics, "World Robotics 2013," September 2013

[5] Ministry of Economy, Trade, and Industry (METI) of Japan, "Trends in the Market for the Robot Industry 2012," July 2013

[6] Ministry of Health, Labor, and Welfare (MHLW) of Japan, Workplace Safety Database, http://anzeninfo.mhlw.go.jp/

[7] B. S. Dhillon, 'Robot Reliability and Safety,' Springer-Verlag, pp.49-68, New York, 1991

[8] J. Fryman, 'Robot Safety and You: Examples of Real-Life Accidents We Can Learn From,' Robotic Industries Association, Ann Arbor, February 2004

[9] I. Asimov, 'Runaround,' Street and Smith Publications, Inc., 1942

[10] BBC News, 'Robotic age poses ethical dilemma,' 7 March 2007, Retrieved from http://news.bbc.co.uk/

[11] ISO 13482:2014, Robots and robotic devices – Safety requirements for personal care robots

[12] Y. Hori, "Future Vehicle Driven by Electricity and Control – Research on Four-Wheel-Motored 'UOT Electric March II'," IEEE Transactions on Industrial Electronics, Vol. 51, No. 5, pp. 954-962, 2004

[13] K. Nam, H. Fujimoto, and Y. Hori, "Lateral Stability Control of In-Wheel-Motor-Driven Electric Vehicles Based on Sideslip Angle Estimation Using Lateral Tire Force Sensors," IEEE Transactions on Vehicular Technology, Vol. 61, No. 5, pp. 1972-1985, 2012

[14] N. Ando and H. Fujimoto, "Fundamental Study of Yaw-rate Control for Four Wheel Independent Drive Electric Vehicle with Driving/Braking Force Distribution of In-Wheel Motors," IEEJ Technical Meeting Record, pp. 13-18, 2009

[15] H. Sumiya and H. Fujimoto, “Electric Vehicle Range Extension Control System Based on Front- and Rear-wheel Sideslip Angle and Left- and Right-motor Torque Distribution,” IEEJ Transactions on Industry Applications, Vol. 132, No. 3, pp. 308-314, 2012 (in Japanese)

[16] K. Sawase, Y. Ushiroda, and T. Miura, “Left-Right Torque Vectoring Technology as the Core of Super All Wheel Control (S-AWC),” Mitsubishi Motors Technical Review, No. 18, pp. 16-23, 2006

[17] S. K. Mohan, “Torque vectoring systems: architecture, stability performance and efficiency considerations,” Proceedings of the Sixth All-Wheel Drive Congress, 2005

[18] R. A. Slay, “Motor-driven Wheeled Vehicles,” United States Patent No. 3,404,746, October 1968

[19] T. L. Lam, H. Qian, and Y. Xu, “Omnidirectional Steering Interface and Control for a Foul-Wheel Independent Steering Vehicle,” IEEE Transactions on Mechatronics, Vol. 15, No. 3, pp. 329-338, 2010

[20] T. Ebihara, K. Moriguchi, and K. Hayashi, “Electric Ride-on Mower,” International Patent Application No. WO2011/092908, August 2011

[21] M. B. Swisher, L. Boothe, and G. L. Boothe, “Powered Caster Wheel for Vehicles,” United States Patent No. 2,582,177, January 1952

[22] D. M. Brienza and C. E. Brubaker, “A steering linkage for short wheelbase vehicles: Design and evaluation in a wheelchair power base—A technical note,” Journal of Rehabilitation Research and Development, Vol. 36, No. 1, pp. 42-47, January 1999

[23] J. Borenstein and Y. Koren, “A Mobile Platform for Nursing Robots,” IEEE Transactions on Industrial Electronics, Vol. 32, No. 2, pp. 158-165, 1985

[24] J. C. Huston, B. J. Graves, and D. B. Johnson, “Three Wheel Vehicle Dynamics,” SAE Transaction, Vol. 91, No. 820139, 1982

[25] S. C. Peters and K. Iagnemma, “An Analysis of Rollover Stability Measurement for High-Speed Mobile Robots,” IEEE International Conference on Robotics and Automation Proceedings, 2006

[26] A. Hac, “Rollover stability index including effects of suspension design,” SAE Transaction, No. 2002-01-0965, 2002

[27] D. Odenthal, T. Bünte, and J. Ackerman, “Nonlinear steering and braking control for vehicle rollover avoidance,” European Control Conference Proceedings, 1999

[28] D. A. Messuri and C. A. Klein, “Automatic body regulation for maintaining stability of a legged vehicle during rough-terrain locomotion,” IEEE Journal Robotics and Automation, Vol. RA-1, pp. 132-141, 1985

[29] E. Papadopoulos and D. Rey, "A new measure of tip over stability margin for mobile base manipulators," IEEE International Conference on Robotics and Automation Proceedings, pp. 3111-3116, 1996

[30] R. Eising, "The Distance between a System and the Set of Uncontrollable Systems," Lecture Notes in Control and Information Sciences, Volume 58, pp. 303-314, 1984

[31] G. Somieski, "Shimmy Analysis of a Simple Aircraft Nose Landing Gear Model Using Different Mathematical Methods," Journal of Aerospace Science and Technology, No. 8, pp. 545-555, 1997

[32] M. Abe, "Automotive Vehicle Dynamics, Theory and Applications," TDU Press, pp. 69, 2008

[33] H. B. Pacejka, "Modeling of the pneumatic tire and its impact on vehicle dynamics behavior," Lecture Series DR 6.04, Carl-Cranz-Gesellschaft e.V., Oberpfaffenhofen, 1992

[34] E. Bakker, L. Nyborg, and H. B. Pacejka, "Tyre modeling for use in vehicle dynamics studies," SAE Paper, No. 870421, 1987

[35] D. de Falco, G. di Massa, and S. Pagano, "On the Castor Dynamic Behavior," Journal of the Franklin Institute, Vol. 347, pp. 116-129, 2010

[36] S. Komada, M. Ishida, K. Ohnichi, and T. Hori, "Disturbance Observer-based Motion Control of Direct Drive Motors," IEEE Transactions on Energy Conversion, Vol. 6, No. 3, 1991

[37] P. Yih, J. Ryu, and J. C. Gerdes, "Vehicle State Estimation Using Steering Torque," Proceedings of American Control Conference 2004, Vol. 3, 2004

[38] J. Ryu and J. C. Gerdes, "Estimation of Vehicle Roll and Road Bank Angle," Proceedings of American Control Conference 2004, Vol. 3, 2004

[39] C. Chang and P. Gaudiano, "Bio-mimetic Robotics Editorial," Robotics and Autonomous Systems, Vol.30, 2000

[40] D. W. Hong, "Biologically Inspired Locomotion Strategies: Novel Ground Mobile Robots at RoMeLa," Proc. the 3rd International Conference on Ubiquitous Robots and Ambient Intelligence, 2006

[41] R. Jacobs, M. F. Bobbert, and G. J. van Ingen Schenau, "Mechanical output from from individual muscles during explosive leg extensions: The role of bi-articular muscles," Journal of Biomechanics, Vol.29, No.4, pp.513-523, April 1996

[42] B. I. Prilutsky and V. M. Zatsiorsky, "Tendon action of two-joint muscles: Transfer of mechanical energy between joints during jumping, landing, and running," Journal of Biomechanics, Vol.27, No.1, pp.25-34, January 1994

[43] N. Hogan, "The mechanics of multi-joint posture and movement control," Biological Cybernetics, Vol.52, No.5, pp.315-331, 1985

[44] T. Horita, P. V. Komi, C. Nicol, and H. Kyröläinen, "Interaction between pre-landing activities and stiffness regulation of the knee joint musculoskeletal system in the drop jump: implications to performance," European Journal of Applied Physiology, Vol.88, No.1-2, pp.76-84, November 2002

[45] M. A. Daley, J. R. Usherwood, G. Felix, and A. A. Biewener, "Running over rough terrain: guinea fowl maintain dynamic stability despite a large unexpected change in substrate height," Journal of Experimental Biology, Vol.209, No.1, pp.171-187, January 2006

[46] T. Fujikawa, T. Oshima, M. Kumamoto, and N. Yokoi, "Output force at the endpoint in human upper extremities and coordinating activities of each antagonistic pairs of muscles," Trans. Japan Society of Mechanical Engineers, C, Vol.65, No.632, pp.1557-1564, 1999

[47] M. Kumamoto, T. Oshima, and T. Yamamoto, "Control properties induced by the existence of antagonistic pairs of bi-articular muscles – Mechanical engineering model analyses," Human Movement Science, Vol.13, No.5, pp.611-634, 1994

[48] S. Oh and Y. Hori, "Development of two-degree-of-freedom control for robot manipulator with bi-articular muscle torque," Proc. American Control Conference 2009

[49] K. Yoshida, S. Oh, and Y. Hori, "Muscular Viscoelasticity Design and Evaluation in Feedforward Position Control of Robot Arm based on Animal Musculoskeletal Model," Proc. the 11th IEEE International Workshop on Advanced Motion Control, pp.502-507, 2010

[50] V. Salvucci, Y. Kimura, S. Oh, and Y. Hori, "BiWi: Bi-articularly actuated and wire driven robot arm," Proc. International Conference on Mechatronics 2011, pp.827-833

[51] Y. Kimura, S. Oh, and Y. Hori, "Novel robot arm with bi-articular driving system using a planetary gear system and disturbance observer," Proc. IEEE International Workshop on Advanced Motion Control 2010, pp.815-820

[52] V. Salvucci, Y. Kimura, S. Oh, T. Koseki, and Y. Hori, "Comparing Approaches for Actuator Redundancy Resolution in Biarticularly-Actuated Robot Arms," IEEE/ASME Transactions on Mechatronics, 10.1109/TMECH.2012.2193670, 2013

[53] S. Oh, V. Salvucci, Y. Kimura, and Y. Hori, "Mathematical and Experimental Verification of Efficient Force Transmission by Bi-articular Muscle Actuator," Proc. World Congress of the International Federation of Automatic Control 2011, pp.13516-13521

[54] S. Sonokawa, Y. Kimura, S. Oh, and Y. Hori, "Center of Mass Velocity Control during Stance Phase by Endeffector Force Control in the Leg Coordinate for Bi-articularly-actuated Leg System," Proc. IEEJ Technical Meeting Record 2012, pp.117-122

[55] Y. Kim, S. Sonokawa, S. Oh, and Y. Hori, "JUMPBiE: Jumping Leg with Passive Bi-articular Elements, its Design and Propulsion Control using Equivalent Spring Model," Proc. IEEJ Industry Applications Society Conference 2012, Vol.II, pp.155-158

[56] Y. Kim, S. Sonokawa, Y. Kimura, V. Salvucci, S. Oh, and Y. Hori, "Design and Propulsion Control of a Robotic Leg with Passive Bi-articular Actuators," Proc. of the 30th Annual Conference of the Robotics Society of Japan 2012

[57] Y. Nakata, A. Ide, K. Hirata, and H. Ishiguro, "Hopping of a Monopedal Robot with a Bi-articular Muscle Driven by Electromagnetic Linear Actuators," Proc. of 2012 IEEE International Conference on Robotics and Automation, pp.3153-3160

[58] W. J. Schwind and D. E. Koditschek, "Characterization of Monoped Equilibrium Gaits," Proc. of the 1997 IEEE International Conference on Robotics and Automation, pp.1986-1992, April 1997

[59] R. J. Full and D. E. Koditschek, "Templates and Anchors: Neuromechanical Hypotheses of Legged Locomotion on Land," The Journal of Experimental Biology, Vol.202, pp.3322-3332, 1999

[60] AlterG Inc., http://www.alterg.com/, 2013

[61] Argo Medical Technologies Inc., http://rewalk.com/, 2013

[62] J. A. Blaya and H. Herr, "Adaptive control of a variable-impedance ankle-foot orthosis to assist drop-foot gait," IEEE Trans. on Neural System Rehabilitation Engineering, Vol.12, pp.24-31, 2004

[63] K. E. Gordon, G. S. Sawicki, and D. P. Ferris, "Mechanical performance of artificial pneumatic muscles to power an ankle-foot orthosis," Journal of Biomechanics, Vol.39, pp.1831-1841, 2006

[64] H. Hatze, "A comprehensive model for human motion simulation and its application to the take-off phase of the long jump," Journal of Biomechanics, Vol.14, pp.833-843, 1981

[65] C. L. Vaughan, J. G. Andrews, and J. G. Hay, "Selection of body segment parameters by optimization methods," Journal of Biomechanical Engineering, Vol.104, pp.38-44, 1982

[66] G. Li, K. R. Kaufman, E. Y. Chao, and H. E. Rubash, "Prediction of antagonistic muscle forces using inverse dynamic optimization during flexion/extension of the knee," Journal of Biomechanical Engineering, Vol.121, pp.316-322, 1999

[67] A. D. Kuo, "A least squares estimation approach to improving the precision of inverse dynamics computations," Journal of Biomechanics, Vol.120, No.1, pp.148-159, 1998

[68] E. M. Arnold, S. R. Ward, R. L. Lieber, and S. L. Delp, "A Model of the Lower Limb for Analysis of Human Movement," Annals of Biomedical Engineering, Vol.38, No.2, pp.269-279, 2010

[69] J. J. Widrick, J. G. Romatowski, M. Karhanek, and R. H. Fitts, "Contractile properties of rat, rhesus monkey, and human type I muscle fibers," Am. Journal of Physiology, Vol.272, pp.R34-R42, 1997

[70] J. Rosen, M. B. Fuchs, and M. Arcan, “Performances of Hill-Type and Neural Network Muscle Models – Toward a Myosignal-Based Exoskeleton,” Computers and Biomedical Research, Vol.32, pp.415-439, 1999

[71] L. Schutte, “Using musculoskeletal models to explore strategies for improving performance in electrical stimulation-included leg cycle ergometry,” Ph.D. dissertation, Stanford University, CA, USA, 1992

[72] L. Ren, R. K. Jones, and D. Howard, “Whole body inverse dynamics over a complete gait cycle based only on measured kinematics,” Journal of Biomechanics, Vol.41, pp.2750-2759, 2008

[73] I. P. Herman, “Physics of the Human Body (Biological and Medical Physics, Biomedical Engineering),” Springer, 2007

[74] A. Cappozzo, T. Leo, and A. Pedotti, “A General Computing Method for the Analysis of Human Locomotion,” Journal of Biomechanics, Vol.8, pp.307-320, 1974

[75] E. Schneider and E. Y. Chao, “Fourier analysis of ground reaction forces in normals and patients with knee joint disease,” Journal of Biomechanics, Vol.16, No.8, pp.591-601, 1983

[76] Y. P. Ivanenko, R. E. Poppele, and F. Lacquaniti, “Five basic muscle activation patterns account for muscle activity during human locomotion,” Journal of Physiology, Vol.556, No.1, pp.267-282, 2004

[77] K. Kong, J. Bae, and M. Tomizuka, “A Compact Rotary Series Elastic Actuator for Human Assistive Systems,” IEEE/ASME Trans. on Mechatronics, Vol.17, No.2, pp.288-297, 2012

[78] J. Bae, K. Kong, and M. Tomizuka, “Real-time Estimation of Lower Extremity Joint Torque in Normal Gait,” Proc. of the IFAC and SYROCO 2009, pp.577-582, 2009

[79] O. Khatib, K. Yokoi, O. Brock, K. Chang, and A. Casal, “Robots in human environments: basic autonomous capabilities,” International Journal of Robotics Research, Vol.18, No.7, pp.684-696, 1999

[80] A. De Santis, B. Siciliano, A. De Luca, and A. Bicchi, “An atlas of physical human-robot interaction,” Mechanisms and Machine Theory, Vol.43, pp.253-270, 2008

[81] M. Zinn, O. Khatib, B. Roth, and J. K. Salisbury, “A new actuation approach for human friendly robot design,” Experimental Robotics VIII, Springer Tracts in Advanced Robotics, Springer-Verlag, 2002

[82] K. Kong and D. Jeon, “Design and control of an exoskeleton for the elderly and patients,” IEEE/ASME Trans. on Mechatronics, Vol.11, No.4, p.428-432, 2006

[83] D. Shin, I. Sardellitti, Y. Park, O. Khatib, and M. Cutkosky “Design and Control of a Bio-Inspired Human-Friendly Robot,” The International Journal of Robotics Research, Vol.29, No.5, pp.571-584, 2010

[84] M. Zinn, O. Khatib, B. Roth, and J. K. Salisbury, “Playing it safe,” IEEE Robotics and Automation Magazine, 1070-9932, pp.12-21, 2004

[85] S. Oh, “Fundamental Research on Human-friendly Motion Control,” PhD Dissertation, Graduate School of Engineering, The University of Tokyo, 2006

[86] C. Chang and P. Gaudiano, “Bio-mimetic Robotics Editorial,” Robotics and Autonomous Systems, Vol.30, 2000

[87] M. Kumamoto, “Animal inspired motion control mechanism,” Proc. the 8th IEEE International Workshop on Advanced Motion Control, pp.11-19, March 2004

[88] ISO 10218:1992, Manipulating industrial robots – Safety

[89] ISO 10218-1:2011, Robots and robotic devices – Safety requirements for industrial robots – Part 1: Robots

[90] ISO 10218-2:2011, Robots and robotic devices – Safety requirements for industrial robots – Part 2: Robot systems and integration

[91] ISO/CD 18646-1, Robots and robotic devices – Performance criteria and related test methods for service robot – Part 1: Wheeled mobile servant robot

[92] KS B 6939:2006 Test methods of measuring the mobile performance of service robots-part 1: Determination of basic spec

[93] KS B 6940:2006 Test methods of measuring the mobile performance of service robotPart 2 Determination of stability for service robot

[94] C. W. Gadd, “Use of weighted impulse criterion for estimating injury hazard,” Proc. 10th Stapp Car Crash Conference, pp. 164-174, 1966

[95] J. Versace, “A review of the severity index,” Proc. 15th Stapp Car Crash Conference, pp.771-796, 1971

[96] A. Bicchi and G. Tonietti, “Fast and Soft-Arm Tactics,” IEEE Robotics and Automation Magazine, Vol.11, Issue 2, June 2004

[97] N. Kashiri, N. G. Tsagarakis, M. Laffranchi, and D. G. Caldwell, “On the stiffness Design of Intrinsic Compliant Manipulators,” Proc. AIM 2013, pp.1306-1311, 2013

[98] Y. Kim, K. Nam, H. Fujimoto, and Y. Hori, “Realization of steer-by-wire system for electric vehicles using caster wheels and independent driving motors,” Proc. ICPE/ECCE 2011, pp.1688-1695, 2011

Publications

[P1] Yunha Kim, Kanghyun Nam, Hiroshi Fujimoto and Yoichi Hori, "CIMEV: Caster-Wheeled Independent-Motor-Driven Electric Vehicle, its Design and Control as a Future Personal Mobility Solution," International Journal of Mechanical Engineering and Robotics Research, Vol. 3, No. 3, pp. 1-20, 2014

[P2] Yunha Kim and Yoichi Hori, "HUMAN LEG MUSCLE GROUP ACTIVATION ESTIMATION DURING GAIT USING AN EXOSKELETON," International Journal of Robotics and Automation, ACTA Press, 2014 (Under review)

[P3] Yunha Kim and Yoichi Hori, "A novel criterion for evaluation of human-friendliness of robots using lumped compliance and safety velocity," IEEE Transactions on Robotics, 2014 (Being prepared)

[P4] Yunha Kim, Sehoon Oh, and Yoichi Hori, "Road Condition Estimation using Acoustic Method for Electric Vehicles," Proc. FISITA 2010 Student Congress, Budapest, Hungary, June 2010

[P5] Kanghyun Nam, Yunha Kim, Sehoon Oh, and Yoichi Hori, "Steering Angle-Disturbance Observer (SA-DOB) based yaw stability control for electric vehicles with in-wheel motors," Proc. ICCAS 2010, Seoul, Korea, October 2010

[P6] Yunha Kim, Hiroshi Fujimoto, and Yoichi Hori, "Realization of Steer-by-Wire System for Electric Vehicles using Caster Wheels and Independent Driving Motors," Proc. ICPE 2011, Jeju, Korea, May 2011

[P7] Yunha Kim, Shinta Sonokawa, Sehoon Oh, and Yoichi Hori, "JUMPBiE: Jumping Leg with Passive Bi-articular Elements, its Design and Propulsion Control using Equivalent Spring Model," Proc. JIASC 2012, Tokyo, Japan, August 2012

[P8] Yunha Kim, Shinta Sonokawa, Yasuto Kimura, Valerio Salvucci, Sehoon Oh, and Yoichi Hori, "Design and Propulsion Control of a Robotic Leg with Passive Bi-articular Actuators," Proc. The 30th Annual Conference of the Robotics Society of Japan, Sapporo, Japan, September 2012

[P9] Shinta Sonokawa, Yunha Kim, Sehoon Oh, and Yoichi Hori, "Effectiveness of Velocity Control for Walking Assist based on Mono-Bi Configuration with Bi-articular Actuation," Proc. The 30th Annual Conference of the Robotics Society of Japan, Algrve, Portugal, October 2012 (in Japanese)

[P10] Shinta Sonokawa, Yunha Kim, Sehoon Oh, and Yoichi Hori, "Velocity Control for Walk Assistance by End-effector Force in the Leg Coordinate on the Bi-articularly-actuated System," Proc. IROS 2012 WS, Algrve, Portugal, October 2012

[P11] Takahiro Nakamura, Shinta Sonokawa, Motonobu Aoki, Yunha Kim, Hiroshi Fujimoto, and Yoichi Hori, "Walking Assistance Control based on Unswitched Impedance Controller between Swing and Stance phases," Proc. IIC 2013, Chiba, Japan, March 2013 (in Japanese)

[P12] Yunha Kim, Sehoon Oh, and Yoichi Hori, "Simulation study on stabilization of a spring-loaded robotic leg using state feedback," Proc. ISR 2013, Seoul, Korea, 2013

[P13] Yunha Kim, Valerio Salvucci, and Yoichi Hori, "Design and Control of an Underactuated Robot Leg, Using State Feedback and Impulse Shaping," Proc. ICAR 2013, Montevideo, Uruguay, 2013

[P14] Yunha Kim and Yoichi Hori, "Muscle Group Activation Estimation in Human Leg during Gait Using Recursive Least Squares Embodying Hill's Muscle Model," Proc. IEEE/RAS-EMBS BioRob 2014, Sao Paulo, Brazil, August 2014

[P15] Yunha Kim, Sehoon Oh, and Yoichi Hori, "Road Condition Estimation using Acoustic Method for Electric Vehicles," Proc. the 10th SNU-UT Joint Seminar, Seoul, Korea, Mar. 2010

[P16] Yunha Kim, Kanghyun Nam, Hiroshi Fujimoto, and Yoichi Hori, "A Novel Chassis Structure for Advanced EV Motion Control Using Caster Wheels with Disturbance Observer and Independent Driving Motors," Proc. the 11th SNU-UT Joint Seminar, Kashiwa, Japan, Dec. 2011

[P17] Yunha Kim, Sehoon Oh, and Yoichi Hori, "JUMPBiE: A Jumping Robot with Bi-articular Elastic Elements, its Design and Control," Proc. the 12th SNU-UT Joint Seminar, Seoul, Korea, Mar. 2013

Curriculum Vitae

Yunha Kim was born on March 2, 1981 in Seoul, Korea, where he grew up and finished his primary, secondary and university education. He entered Seoul National University, where he graduated with a B.S. in Mechanical Engineering in February 2007. While there, he took a leave of absence and served as an administrative specialist in a medical evacuation helicopter unit of the Republic of Korea Army and the United States Army from May 2002 until June 2004. After receiving his B.S., he joined the Technical Center of Renault Samsung Motors, Co., Ltd. located in Yongin, Korea, where he worked as an Engine Management System engineer for two years until February 2009 when he left for further education.

Since April 2009, Yunha Kim has been with the Graduate School of Engineering of The University of Tokyo in pursuit of master's and Ph.D. degrees, where he has worked on robot mobility platforms, biologically inspired robots, robots working in human environments, and safe human-robot interactions. From The University of Tokyo, he received an M.E. in Electrical Engineering in September 2011, and will receive a Ph.D. also in Electrical Engineering in September 2014.

Yunha Kim has always felt engineering to be a very fascinating and important field of study, and has been passionate about designing and making things that practically help humankind. After graduation, he is planning to work in a company to acquire experiences of the real world industry.

Permanent point of contact: yunha.kim.direct@gmail.com